Fire Performance of a Novel Concealed Mass Timber Moment-Resisting Connection Utilizing Mechanically-Fastened Steel Rods

by

Cory Hubbard

A thesis
submitted to the Faculty of Graduate Studies
in partial fulfilment of the requirements for the
Degree of Master of Science
in

Civil Engineering

Supervisor
Osama (Sam) Salem, Ph.D., P. Eng.
Associate Professor – Dept. of Civil Engineering

Lakehead University
Thunder Bay, Ontario
October 2020

Author's Declaration Page

I hereby declare that I am the sole author of this thesis. This is a true copy of the thesis, including any required final revisions, as accepted by my examiners. I understand that my thesis may be made electronically available to the public.

Abstract

A major hindrance to more application of engineered-wood products in the Canadian building construction market is the lack of technical documentations and guidelines for the design of timber beam-to-column connections, especially those with moment-resisting capacities. In terms of designing for elevated temperatures, there is very limited research done for determining the fire resistance of moment-resisting timber connections. A comprehensive experimental testing program that consisted of thirty-seven full-size tension assemblies and eight novel full-size beam-to-column connection test specimens were subjected to static loading at ambient temperature. In addition, eight beam-to-column connection test specimens identical to those tested at ambient temperature were examined at elevated temperatures of standard fire.

Test variables investigated in this study included rod embedment length and washer size. The effects of these variables on the structural behaviour of the novel concealed glulam beam-to-column moment-resisting connection at both ambient and elevated temperatures were studied. The results of the nine different configurations from the tension tests were used to find the four most ductile and predictable configurations to be used for the newly designed beam-to-column connection configuration. For the tension connections, an embedment length to washer size ratio of about 4:1 provides a more predictable failure of rod pull-out. Accordingly, attention should be taken to ensure that the rod embedment length is to be slightly longer when compared to the washer size to maintain a ratio greater than 4 to 1 to promote for wood crushing failure.

A failure of wood crushing is more consistent and predictable, whereas lesser embedment length to washer size ratio would promote a wood splitting failure which is highly unpredictable. From the beam-to-column connection tests performed, the connections that failed due to the top steel rod yielding were stronger, while the connections that failed due to the wood crushing under the washer had a higher ductility ratio. The results of the four configurations from the ambient beam-to-column connections were used to verify the calculated moment capacities of the test assemblies so they all could be loaded to the full-service design load of the weakest connection assembly before being exposed to CAN/ULC-S101 standard fire in the large-size fire testing furnace accommodated at Lakehead University's Fire Testing and Research Laboratory (LUFTRL). The results showed that using a smaller washer provided more wood cover to protect the steel components from the effects of elevated temperatures. Also, utilizing longer rod embedment length provided more shear resistance. By combining those two parameters, a concealed beam-to-

column timber connection that utilized two mechanically-fastened steel rods can be successfully designed to achieve a one-hour fire resistance with no fire protection.

Acknowledgements

This thesis research project was funded using NSERC- Discovery Grant awarded to Dr. Sam Salem by Natural Sciences and Engineering Research Council of Canada. Any opinions, findings, conclusions, and recommendations are those of the author of this thesis and do not necessarily reflect the views of the funding entity.

The successful completion of this thesis is the outcome of consistent guidance and encouragement provided by my graduate supervisor, Dr. Salem throughout the duration of my master's program.

The author would like to thank Conrad Hagstrom and Rob Timoon for their help in the Dept. of Civil Engineering Structures Laboratory.

Most importantly, I could not have finished this thesis without the support of my wonderful wife, Jessica Hubbard. You are the kite who guides me through life and keeps me soaring through our many goals.

Table of Contents

List of Tables

List of Equations

List of Figures

Nomenclature

Roman

A	cross-sectional area being compressed
a	compression block height
b	compression block width
d	distance from midpoint of tension force to bottom of beam
F_c	factored strength in compression parallel to grain
f_c	specified strength in compression parallel to grain
f_v	specified shear strength
K_C	slenderness factor
K_D	load duration factor
K_H	system factor
K_{Sc}	service condition factor for compression parallel to grain
K_{Sv}	service condition factor for shear
K_T	treatment factor
K_{Zcg}	size factor
l	rod embedment length
M_r	beam-to-column connection moment resistance
p	washer perimeter
P_r	compressive resistance parallel to grain
PR	pull-out resistance of threaded rod in glulam

T tension force in top rod of beam-to-column connection

WC_r wood crushing resistance under the washer

Z member volume

Greek

ϕ_c resistance factor for brittle failure in compression (wood design)

Chapter 1 Introduction

1.1 Background

The use of wood as the main construction material in industrial buildings is an uncommon concept that provides a unique visual aesthetic. Wooden buildings are cost effective, quicker to build, and a more sustainable choice when compared to more traditionally used concrete and steel materials (Ramage, et al., 2017). Wood is a renewable resource that stores carbon during growth and retains it indefinitely after it has been harvested. In the lifecycle of a wooden building, it will produce less air and water pollution, use less energy, and emit less greenhouse gases compared to structural steel or concrete buildings. Traditional sawn lumber can be easily attained, but it has size limitations which can restrict designers when larger sections are required. Thus, engineered-wood products fill the gap in construction demands, such as glued-laminated timber (glulam) and cross-laminated timber (CLT), which have opened new possibilities to further utilize wood in engineering design and construction. Glulam members are structural mass timber members manufactured from smaller sections of wood known as laminations. The manufacturing process can utilize trees that were previously unusable as a building material due to their small size and/or low mechanical properties but are the perfect size for laminations. When laminations are glued together, they form a final product with a greater length, cross section and greater mechanical properties than those of the individual laminations (Nordic Wood Structures, 2015). Starting in 2009, 2013 and 2015, the provinces of British Columbia, Quebec and Ontario, respectively, made amendments to their provincial building codes facilitating the use of timber as the primary building system for construction of up to six storeys. Prior editions of the National Building Code of Canada (NBCC) restricted the use of wood as the primary building system by limiting its application to buildings with a maximum height of four storeys. The current version of the National Building Code of Canada has increased the height restriction to include buildings up to six storeys (National Research Council of Canada 2015). As mid- and high-rise buildings are expected to undergo loading beyond the capacity of sawn lumber, this presents an ideal application for larger glulam structural components, as they are capable of sustaining considerably larger loads when compared to commercially available sawn lumber. Current technical documentations and design guidelines in Canada have some lack in the design of moment-resisting timber beam-to-column connections, a key requirement for taller buildings expected to resist lateral loads combined with heavy vertical

loads. In this context, the primary concern of using timber moment-resisting frames is its capability to resist moments without undergoing brittle failure modes. In terms of designing for elevated temperatures, there is lack of supporting framework for determining the fire resistance rating of moment-resisting connections, and extremely limited research on the behaviour of moment-resisting connections at elevated temperatures. The fire performance of wood structures is a primary concern of the public and regulatory bodies overseeing building codes, especially in the context of safety and designing buildings to withstand fire and needs to be addressed in order to further the use of wood as the primary building system in mid- and high-rise buildings.

1.2 Problem Statement

The primary concern of using timber in structural applications at ambient temperature is the formation of brittle failure. This concern is important in the design of taller timber buildings due to the increased vertical height carrying a wind load when compared to low-rise buildings, as well as the increased load expected during an earthquake. The use of metal connectors promote heavy timber connections to behave in a relatively ductile manner by providing a source of energy dissipation and designing the connection to fail in the steel components instead of the wood (Murty et al., 2008; Andreolli et al., 2011). However, brittle failure can be developed before the connection can experience any possible ductile behaviour (Humbert et al., 2014). An additional consideration for optimizing glulam for practical construction use, is its behaviour as a rotationally-restrained member in framed structures. Such studies have been conducted on the behaviour of heavy-timber connections used in frames subjected to axially-applied compressive and tensile loads (Gattesco, 2004). Very few research projects, such as the work done by (Quenneville, 2014; Xu et al., 2015), have been undertaken to study the behaviour and moment resistance of heavy-timber connections as part of a frame, especially in the context of frames lateral resistance (Xiong et al., 2016).

Most guidelines in North America for fire design are prescriptive; however, the general trend has been to adopt a performance-based methodology for structural fire design (Hadjisophocleous and Benichou, 1999; Barber, 2017). The trend has been supported by extensive testing of building materials as: individual components, sub-assemblies, assemblies, and even entire structures. However, the focus of the fire safety field has predominantly been on steel and concrete components, not glulam or other timber products (Bisby et al., 2013). Specifically, there is considerable lack in the available literature on the fire behaviour of heavy-timber moment-resisting

connections either as individual components or as part of a structural frame. Primarily, the focus has been on axially loaded connections (Racher et al., 2010), under compressive or tensile loading, parallel to the grain (Peng. et al., 2010) or perpendicular to the grain (Audebert et al., 2012). At elevated temperatures, the studies showed that timber connections either fail due to brittle failure in the wood, such as splitting, and row shear-out or due to ductile failure modes, such as hole elongation and wood crushing, or yielding in the steel components at elevated temperatures.

1.3 Scope and Objectives

The results presented in this thesis show an experimental study of a novel concealed glulam beam-to-column moment-resisting connection. The connection was evaluated based on the failure modes, maximum tension capacity, maximum moment capacity, stiffness, ductility, and fire resistance. A comprehensive experimental testing program consisted of thirty-seven full-size tension assemblies and eight full-size beam-to-column test connections subjected to static loading at ambient temperature, and eight test connections at elevated temperatures. Test variables investigated in this research project included rod embedment length and washer size, and the effect of these variables on the normal and elevated temperatures performance of the newly-designed concealed glulam beam-to-column moment-resisting connection. The results of the nine configurations from the tension tests as explored in Chapter 3 were used to find the four most ductile and predictable configurations to be used for the beam-to-column connections as discussed in Chapter 4. The results of the four configurations from the ambient beam-to-column test assemblies in Chapter 4 were used to verify the calculated moment capacities of the test assemblies so they all can be loaded to the full-service design load of the weakest connection assembly before being exposed to CAN/ULC-S101 standard fire in the large-size fire testing furnace accommodated at Lakehead University's Fire Testing and Research Laboratory (LUFTRL) as discussed in Chapter 5.

A few objectives of this research are listed below:

1. Create a new concealed glulam beam-to-column connection configuration using mechanically fastened steel rods that can surpass 60 minutes in standard fire exposure.
2. Develop a simple design guideline for the new concealed glulam beam-to column connection.

3. Experimentally investigate the effects of various parameters, i.e., rod embedment length, and washer size, on the strength and stiffness of the newly-developed glulam beam-to-column connection.

Chapter 2 Literature Review

2.1 Glulam

Larger sawn lumber members are becoming increasingly difficult to obtain for heavy-timber construction because trees are limited in the sizes sometimes required. A way to negate this issue is to use glued-laminated timber (glulam) sections. Glulam is manufactured by gluing together small sections of wood, known as lamina, to form a larger wood section. The laminas used are varied in size depending upon the manufacturer with common sizes used from traditional lumber such as 2.0 inches by 4.0 inches, or smaller. Some manufacturers are using laminas as small as 25 mm x 50 mm (1" x 2") from wood that is normally wasted such as wood sourced from the crown of trees, side cuts, and small branches (Nordic Wood Structures, 2015). These wood sections were previously ignored as a building material due to their small size or low mechanical properties individually. When these laminas are glued together, they can form a larger and stronger member than that from sawn lumber of the same species.

Glulam has been used in Canada in the construction of industrial, commercial, and institutional buildings. Recently, amendments were made to the National Building Code of Canada (National Research Council of Canada, 2015) and several provincial building codes that allowed wood to be the primary building material in mid-rise buildings up to six storeys. These changes have increased the potential scope for glulam sections in Canadian construction as glulam members can be made with much larger cross-sections, lengths, and even be curved in order to support greater loads than sawn lumber members. As these changes have been recently made to the building code, there is little technical design documentation providing adequate design guidelines for mass timber beam-to-column connections.

2.2 Timber Moment Connections

The most lacking areas in the available design guidelines are embedded-rod connections (Hunger et al., 2016) and moment-resisting connections (Petrycki & Salem, 2020). Moment frames as lateral force resisting systems are favoured over other conventional frame systems such as concentrically braced frames, crossed braced systems, or chevron brace frames because of their ability to provide an open, uninterrupted system (Metten, 2012). There are clauses in the Canadian

steel design standard (Canadian Standards Association, 2019) and concrete design standard (Canadian Standards Association, 2014), and the National Building Code of Canada (National Research Council of Canada, 2015) that allow for the design of moment frames in steel or concrete, but as of date, no conventional regulation or guidelines exist for moment frames constructed from timber. This is mainly because ductility is required for moment frames, which cannot be achieved with timber members alone.

The primary focus on research into the capacity of glulam beam-to-column moment-resisting connections is the reduction, control, and prediction of brittle failure modes. Ductile failure modes are well understood and can be designed for, while brittle failure modes are often unpredictable; both in their development and effect on the capacity of the connection. To ensure the safety of occupants in taller buildings made of wood, every effort must be made to either avoid brittle failure modes or ensure that failure is ductile, this reduces any chance of a catastrophic collapse. The limited research on moment-resisting connections has focused on the effect of connections' parameters, such as type of fastener and their locations, as well as the capacity, rotational behaviour, and failure modes in the glulam beams.

Gehloff et al. (2010) increased the ductility and moment capacity of a bolted beam-to-column connection by inserting long threaded screws in between the bolt lines. Canadian glulam 24f-E Douglas fir was used with 9.5 mm thick steel plates. The steel plates were slotted into a 130 mm x 304 mm beam, sandwiched between two 130 mm x 304 mm columns and bolted together with 25.4 mm bolts. An example of one connection bolt and screw layout is presented in Figures 2.1(a) and 2.1(b) respectively. The perpendicular reinforcement provided by the long screws prevented early splitting of the member, but could not fully prevent it as shown in Figure 2.2. Tests, where the screws were closer to the bolt holes, could not significantly increase the connection capacity but did reduce the standard deviation. With the reduction in edge distance of bolts in the column and larger diameter bolts used, the tendency for splitting increased greatly, but the use of the reinforcing long screws were very effective in reducing this tendency. The decrease in edge distance from 94.5 mm to 49.5 mm also increased the ultimate moment capacity by a factor of 1.35 to 1.38. The decrease edge distance also had lower rotation values even though the ultimate capacity was increased which would not have been achieved without the use of the long screws to prevent premature splitting.

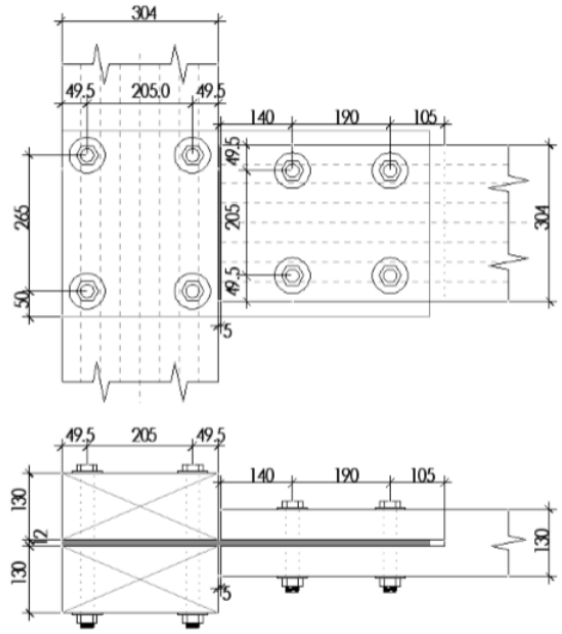

Figure 4: B-CR / C-CR bolt layout

(a)

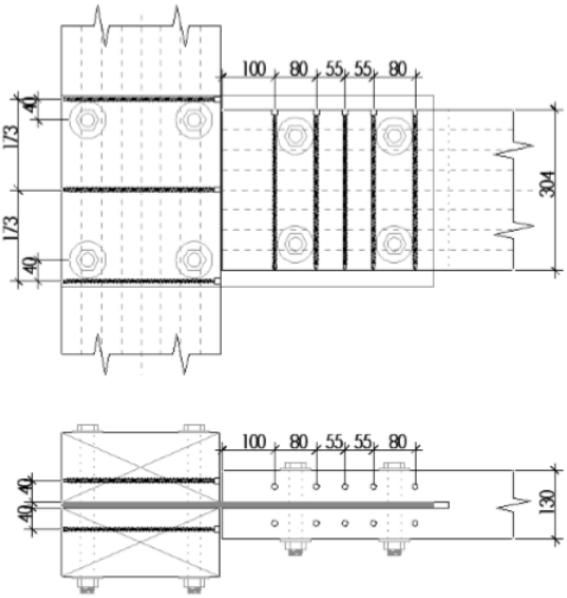

Figure 5: B-CR STS layout

(b)

Figure 2.1. Layout for connection configuration B-CR: (a) bolt layout; (b) STS layout (Gehloff et al., 2010).

Figure 2.2. Typical failure of a bolted connection with STS (Gehloff et al., 2010)

The use of long threaded and large diameter self-tapping screws can be difficult to install, therefore; Wang et al. (2015) used locally cross-laminated glulam instead of long threaded screws to increase the moment capacity. The glulam and steel plates were the same size as Gehloff et al. (2010) and tested in the same configuration. The tests compared normal glulam, glulam with self-tapping screws, and locally cross-laminated glulam bolted connections. The glulam with self-tapping screws failed similar to the unreinforced glulam by splitting with a shear plug, just at higher load and rotation as shown in Figure 2.3(a) reinforced with self-tapping screws and 2.3(b) unreinforced. The locally cross-laminated glulam exhibited superior deformability as well with no substantial load drop. There was a large amount of bearing deformation in the bolt holes, but no tensile splitting was observed in the outer laminas as shown in Figure 2.3(c).

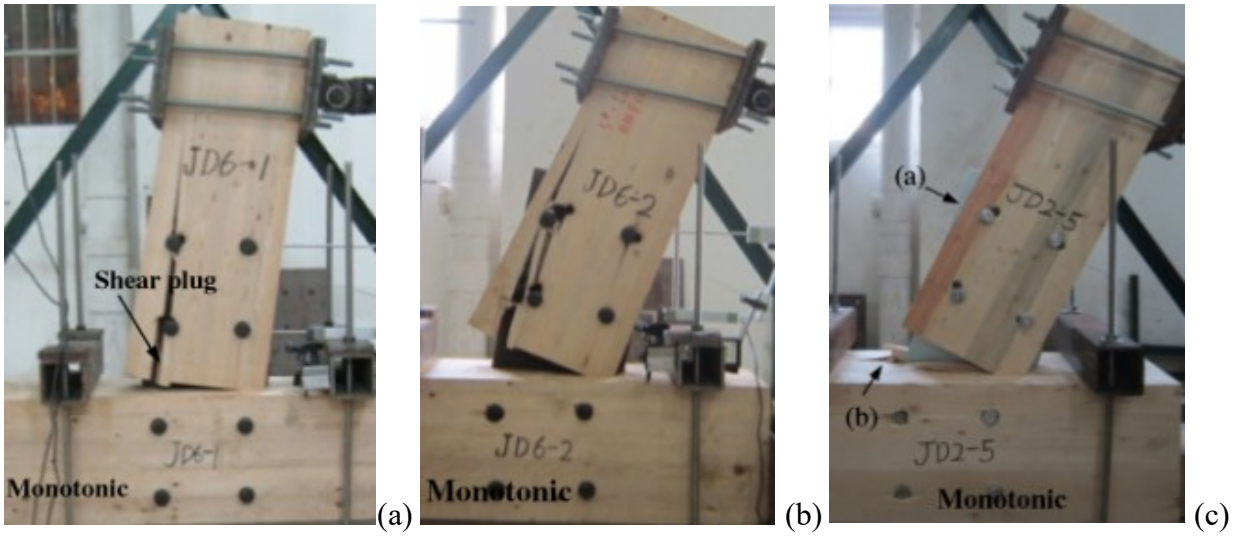

Figure 2.3. Failure modes of bolted glulam beam-to-column connections: (a) failure mode of unreinforced glulam; (b) failure mode of STS reinforced glulam; (c) failure mode of locally cross-laminated glulam (Wang et al., 2015).

Table 2.1 shows the average yielding and maximum moments with their corresponding rotations for each connection configuration. The self-tapping screws increased the yielding moment capacity by 70% while the locally cross-laminated only increased the yielding moment by 5%. The locally cross-laminated did have a larger gain for maximum moment by 52%, but the self-tapping screws were still better with a gain of 80%. Even though the self-tapping screws performed better than the locally cross-laminated, the prefabrication of the locally cross-laminated glulam could make up for savings in construction time installing the self-tapping screws.

Table 2.1. Results of bolted glulam beam-to-column test configurations (Wang et al., 2015)

Connection configuration	Yielding moment (kN.m)	Maximum moment (kN.m)	Yielding rotation (°)	Maximum rotation (°)
Unreinforced	33.9	38.4	5.9	10.4
Self-tapping screws	57.8	69.3	8.2	27.3
Locally cross-laminated	35.6	58.3	6.1	21.1

Closen and Lam (2012) used tension and compression plates attached with self-tapping screws inclined at 30 degrees as the primary fastener instead of bolts to increase the moment capacity. The glulam was of the same type and size and tested in the same configuration as the tests performed by Gehloff et al. (2010). The steel shoes were also made of 9.5 mm thick steel similar to Gehloff et al. (2010). The general test layout and testing equipment are shown in Figure 2.4.

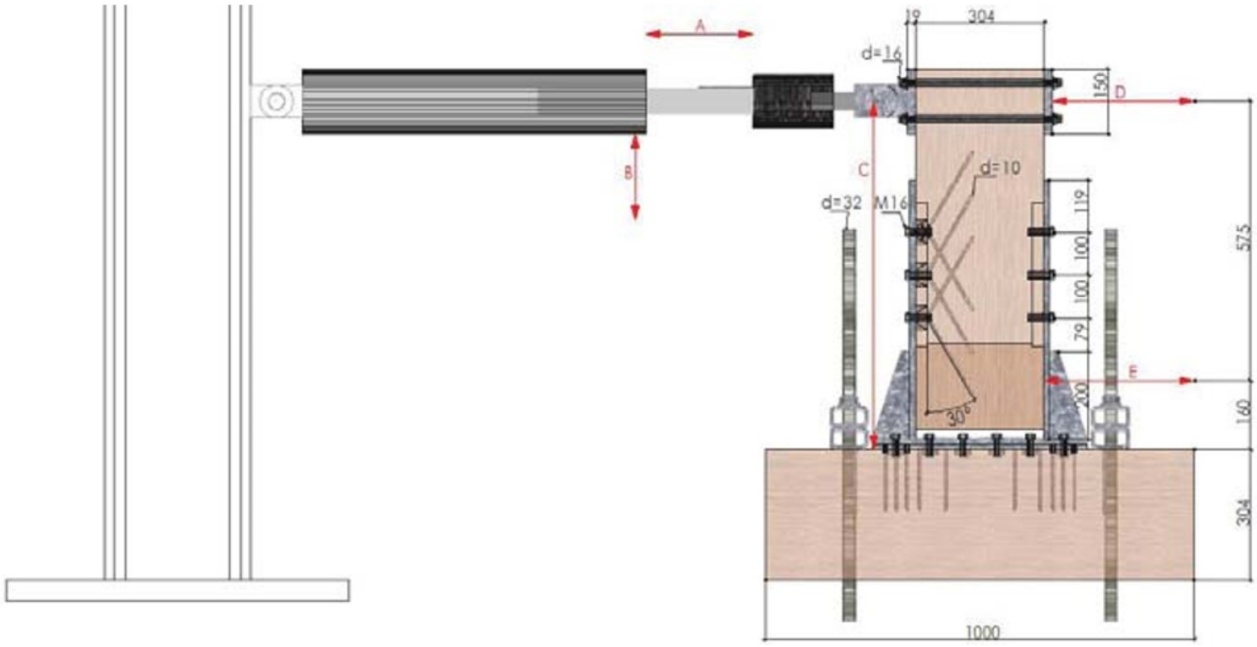

Figure 2.4. General test layout and testing equipment for self-tapping screw fastening beam-to-column connection (Closen & Lam, 2012)

The average ultimate moment resisting capacity exceeded the design moment capacity of the glulam section by a factor of 2. The main failure modes were tension fracture and withdrawal of screws as shown in Figure 2.5. Even though the connection had a high moment capacity, the

ductility of the connection was relatively low. By changing the details of the steel shoe one could design the connection to promote steel shoe to yield instead of failing with the screws.


(a)

(b)

(c)

Figure 2.5. Failure modes of self-tapping screw fastening beam-to-column connection: (a) disassembled ZD-plate with compression screws bending and tension screws fractured removed from beam section; (b) disassembled ZD-plate with compression screws bending and tension screws fractured attached to beam section; (c) Screw withdrawal in bottom member (Closen and Lam, 2012).

While several researchers focused on the interaction between wood members and steel connectors, such as plates, bolts, and screws, other researchers have focused on developing novel connections to promote ductile failure modes. In experimental studies conducted by Andreolli et al. (2011)

(Tomasi et al., 2008), a unique connection configuration that focused on providing deformation capability and energy dissipation in the steel components of the connection to limit brittle failure in the wood was developed as shown in Figure 2.6. It has been found that the connections could be designed to behave in a semi-rigid fashion without a reduction in its moment-resisting capacity and that it could be designed to yield in the steel components before any failure occurred in the wood section. The versatility of the connection configuration and potential for prefabricating most of the components highlighted the need to conduct further experiments on the connection in the context of a full-frame assembly.

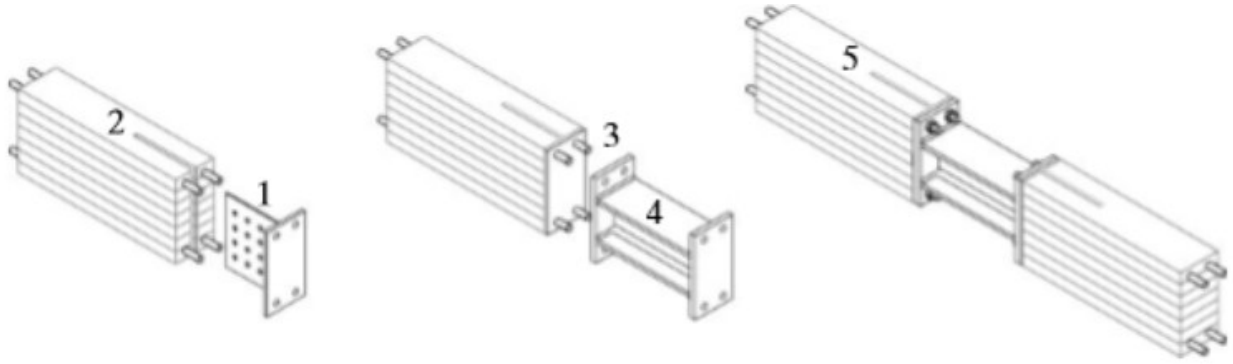

Figure 2.6. End-plate joint in the steel-timber structure (Tomasi et al., 2008)

Similar conclusions were drawn by Humbert et al. (2014) during their experimental study on the mechanical behaviour of post and beam joints secured with metal fasteners. In their study, they found that although the connection capacity could be increased by increasing the stiffness in the connection steel components, this resulted in brittle failure modes in the wood section before the steel yielded in plastic failure as shown in Figure 2.7. A steel cross plate (+) was inserted into the end of 180 mm x 180 mm Japanese larch glulam posts. The plates that were 6 mm thick had deformation in the steel while the 8 mm thick plates, although did increase moment resistance, had the wood section split. This requires good optimization of the connection design to increase the thickness and stiffness of the steel connecting components enough to just provide sufficient moment resistance without promoting the formation of brittle failure in the wood section before failure occurs in the steel components.

Figure 2.7. Post base joint with concealed connector (Humbert et al., 2014)

2.3 Embedded Rod Connections

Glued-in threaded steel rods have been in use and experimentally tested in timber connections since the late 1980s, but there are no consistent design procedures for their application (Barillas, 2014; Fragiacomo and Batchelar, 2012). Some design approaches and code models have been published; however, there are some discrepancies and even partial contradictions between the different models (Steiger et al., 2006). Experimental work has shown that threaded steel rods inserted into wood can provide the connection with a certain degree of ductility, preventing brittle failures from developing in the wood section (Tomasi et al., 2008). As these connections are composed of several materials, they are considered a hybrid connection. The interaction between wood, adhesive, and metal introduces several variables that need to be considered, which have made it difficult to predict the connection's failure mode (Oh, 2016). Factors that have been found to affect the connection strength are the rod embedment length, the size of the hole compared to the rod diameter, the type of adhesive used, and the species of wood (Hunger et al., 2016; Steiger et al., 2006).

Steel rods can be epoxied into one member and secured with a nut and washer to the other member, or the same rod can be glued into two separate members making a permanent connection (Fragiacomo and Batchelar, 2012). A critical issue with connections composed of steel rods glued in both members is that the connection has to be made on site, which has been shown to carry a high risk of being improperly bonded since the effectiveness of the grouting operation cannot be visually checked (Batchelar & McIntosh, 1998). Therefore, it is highly recommended that the

gluing process be done in a controlled environment where skilled workers can check their work and ensure a proper bond.

Steiger et al. (2006) completed a glued-in rod tension testing program using a variety of parameters to try and find some consistency between all of the parameters. Norway spruce glulam was used consisting of low and high density samples. Three different rod diameters; M12, M16, and M20; were selected using a class 8.8 steel rod to promote a timber shear failure rather than a steel yielding failure. Each rod diameter had four different rod embedment lengths as well in relation to the timber and steel, and their corresponding area and modulus of elasticity to give the joints an optimal performance. The results of all of the tests are presented in Figure 2.8.

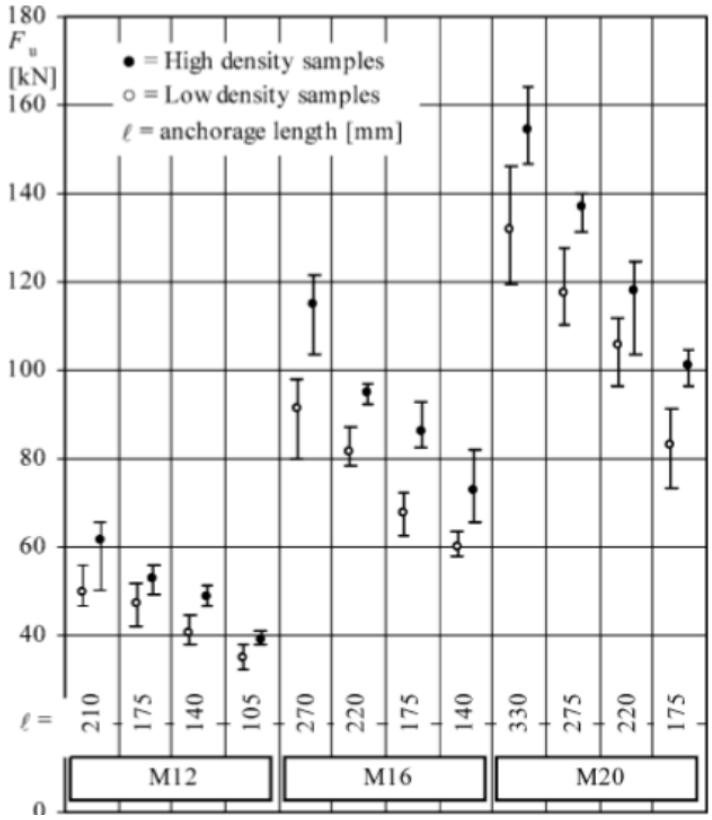

Figure 2.8. Ultimate tension loads for single glued in rod tests (Steiger et al., 2006)

The smallest rod diameter had the smallest standard deviations and the highest load transfer between the wood and steel, while the largest rod diameter had the largest standard deviations and the lowest load transfer between the wood and steel. The density of the wood clearly shows that the high density wood has a higher pull-out resistance compared to the low density wood. Even though the largest rod diameter and embedment length gave the strongest connection, preference

should be given to the smaller rod diameter since it has the highest load transfer as shown in Table 2.2.

Table 2.2. Mean ultimate tensile strength and stress of tension assemblies (adopted from Steiger et al., 2006)

Rods	M12	M16	M20
Mean $F_{u,mean}$ (kN)	43.8	77.2	110
$\sigma_{t,0}$ (N/mm^2)	14.5	13.7	12.2

Hunger et al. (2016) completed a tension testing program as well, similar to Steiger et al. (2006), but with different parameters. The cross-sections were consistent at 120 mm x 120 mm, the steel rod was M12 and embedded at an anchorage depth of 90 mm. The timber tested was Norway spruce glulam and LVL, European ash and European beech glulam, and European beech LVL. The two types of adhesives tested were a two-component epoxy resin and a two-component polyurethane casting resin. The results of the ultimate load versus ductility are shown in Figure 2.9. The higher modulus of rigidity of the hardwoods led to higher shear stress in the timber when compared to the softwood Norway spruce. This also led to higher ductility values for the hardwood glulams. There was no noticeable difference between the types of adhesives used. The beech glulam showed higher strength values than the LVL, while the Norway spruce showed no noticeable differences.

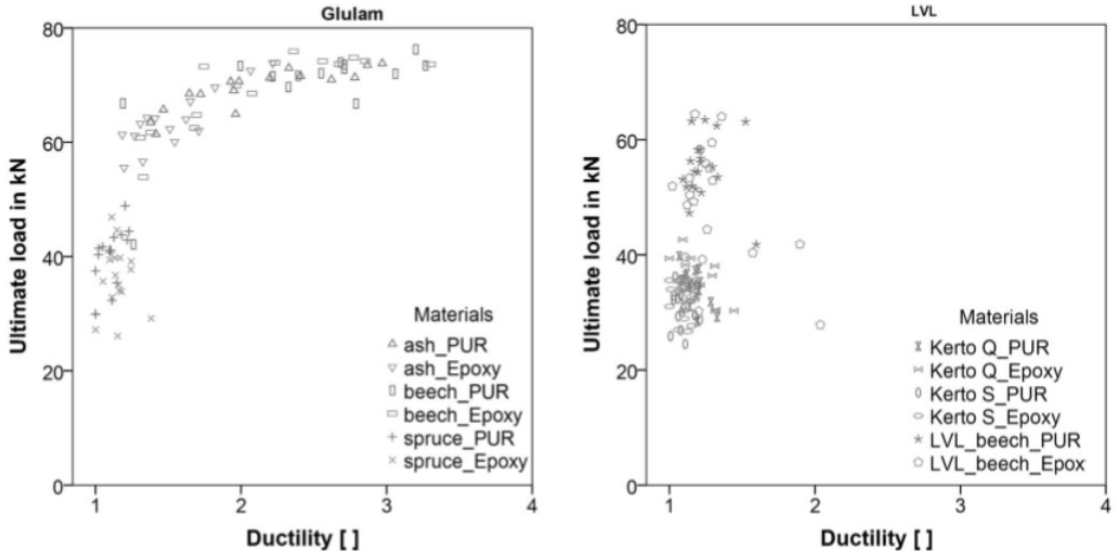

Figure 2.9. Ultimate load versus ductility for glulam and LVL glued in rod tension tests (Hunger et al., 2016)

An extensive study was done by Oh (2016) at UBC testing glued-in rod moment resisting connections. Douglas fir glulam beams were used with 12.7 mm diameter mild steel rods glued in using polyurethane based adhesives. Multiple rod layouts were tested to determine its effect on the connections moment capacity. It was found that ductile failure in the steel rods is achieved when the shear force induced into the connection is less than 25% of the axial rod strength. Multiple failure modes to be observed include splitting of the wood, shear failure in the glue line, rod pull-out, group tear out for multiple glued-in rods, and tensile failure of the timber at the end of the rod. Recommendations have been suggested to prevent each brittle failure mode and promote the ductile failure mode.

To prevent wood splitting and group tear-out, the most stringent recommendation comes from the German regulation (DIN 1052:2004-08). It is recommended that an edge distance of two and a half times the rod diameter and a bar spacing of five times the bar diameter be used (Oh, 2016). Another measure to prevent wood splitting is the use of self-tapping screws as previously explored in section 2.2. To prevent rod pull-out failures and shear failure within the glue line, the glued-in rod connection should be designed so that the capacity of those failures is greater than the capacity of all other failure modes. One way to ensure adequate capacity of rod pull-out failure is to ensure sufficient embedment length and rod diameter which will increase the surface area resisting shear along the adhesive timber interface. The problem with that solution though is that the relationship between the pull-out strength of the rods and their embedment length in complex and challenging to define as discussed earlier by Steiger et al. (2006). The pull-out capacity increases with embedment length, but at a certain point, the increase in capacity reduces significantly, indicating a non-linear relationship between the capacity and embedment length. To prevent shear concentration at the end of the glued-in rods it is recommended that the steel rod and timber member have a similar tensile stiffness for a smooth load transfer as discussed earlier by Steiger et al. (2006). To ensure a ductile failure in the steel rods it is recommended that mild steel be used with a smaller diameter as opposed to high strength steel rods with a larger diameter. This recommendation will promote the yielding of the steel rods providing a more ductile and predictable failure. Figure 2.10 and Table 2.3 show the specimen layouts that were tested following these recommendations. Table 2.4 shows the results of the monotonic testing of those connections.

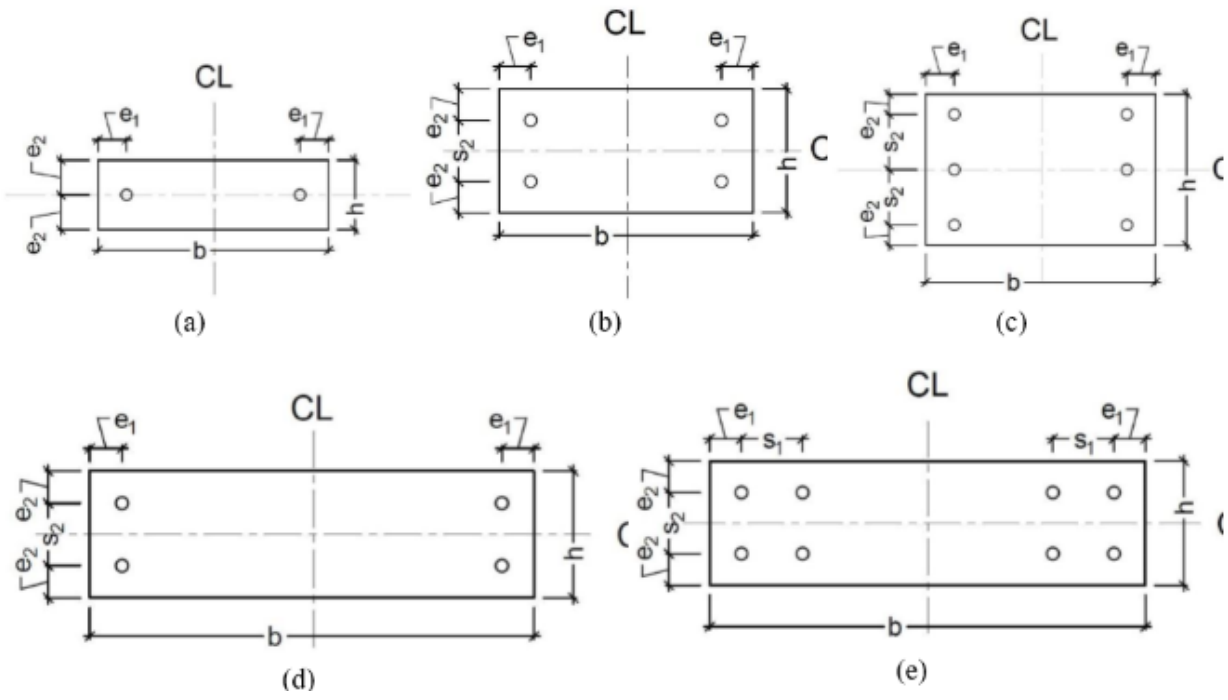

Figure 2.10. Layouts of glued-in rod moment resisting connections: (a) A1; (b) B2; (c) C3; (d) D2; (e) D4 (Oh, 2016).

Table 2.3. Specimen layouts of glued-in rod moment resisting connections (Oh, 2016)

Label	Base, b (mm)	Height, h (mm)	Length, l (mm)	Edge Dist., $e_1^{(1)}$ (mm)	Rod Spac., $s_1^{(1)}$ (mm)	Edge Dist., $e_2^{(2)}$ (mm)	Rod Spac., $s_2^{(2)}$ (mm)	Embed. Length (mm)	Testing	
									Mon.	Cyclic
A1(a)	80	266	1400	33	0	40	0	203 (16d)	4	4
A1(b)	80	266	1400	33	0	40	0	102 (8d)	4	0
B2(a)	130	266	1400	33	0	33	64	203 (16d)	4	3
C3(a)	175	266	1400	33	0	23.5	64	203 (16d)	4	3
C3(b)	175	266	1400	33	0	23.5	64	102 (8d)	4	0
D2(a)	130	456	1400	33	0	33	64	203 (16d)	4	4
D2(b)	130	456	1400	33	0	33	64	102 (8d)	4	0
D4(a)	130	456	1400	33	64	33	64	203 (16d)	3	3

(1) Denotes in the direction of loading

(2) Denotes perpendicular to the direction of loading

Table 2.4. Results of glued-in rod moment resisting monotonic testing (Oh, 2016)

Specimen	Measured Moment Arm (m)	Maximum Load (kN)	Maximum Displacement (mm)	Type of Failure Observed
A1(a)-1 (1)	1.250	8.77	44.83	Steel - Tension
A1(a)-1 (2)	1.250	9.04	41.44	Steel - Tension
A1(a)-1 (3)	1.240	9.01	43.78	Steel - Tension
A1(a)-1 (4)	1.240	8.67	45.33	Steel - Tension
B2(a)-1 (1)	1.240	20.02	47.80	Steel - Tension
B2(a)-1 (2)	1.250	17.07	44.39	Wood - Splitting
B2(a)-1 (3)	1.250	18.01	50.00	Steel - Tension
B2(a)-1 (4)	1.245	16.38	47.16	Steel - Tension
C3(a)-2 (1)	1.210	29.19	49.76	No Failure
C3(a)-2 (2)	1.250	23.27	52.46	Steel - Tension
C3(a)-2 (3)	1.240	29.06	54.29	Steel - Tension
C3(a)-2 (4)	1.240	24.97	54.80	Steel - Tension
D2(a)-1(1)	1.240	33.04	35.46	Steel - Tension
D2(a)-1(2)	1.260	29.10	22.72	Wood - Splitting
D2(a)-1(3)	1.260	29.61	33.77	Steel - Tension
D2(a)-1(4)	1.270	33.81	39.59	Steel - Tension
D4(a)-1(1)	1.270	65.10	51.62	Steel - Tension & Pullout
D4(a)-1(2)	1.255	47.48	50.64	Steel - Tension & Pullout
D4(a)-2(3)	1.265	40.07	45.47	Steel - Tension & Pullout
A1(b)-1(1)	1.240	9.15	22.28	Pullout
A1(b)-1(2)	1.240	8.07	18.15	Pullout
A1(b)-1(3)	1.240	8.04	13.76	Pullout
A1(b)-1(4)	1.235	7.42	14.10	Pullout
C3(b)-1 (1)	1.210	18.84	18.19	Pullout
C3(b)-1 (2)	1.240	20.37	26.81	Pullout
C3(b)-1 (3)	1.240	21.29	27.69	Pullout
C3(b)-1 (4)	1.240	17.37	20.28	Pullout
D2(b)-1(1)	1.260	15.79	12.03	Pullout
D2(b)-1(2)	1.270	21.49	16.97	Pullout
D2(b)-1(3)	1.260	24.50	17.92	Pullout
D2(b)-1(4)	1.260	23.66	16.90	Pullout

As predicted from the recommendations, all of the tests with the shorter embedment length experienced rod pull-out, while the tests with the longer embedment length mainly experienced tension failure in the steel. Figure 2.11 shows the ductile failures that were observed by every configuration with the longer embedment length.

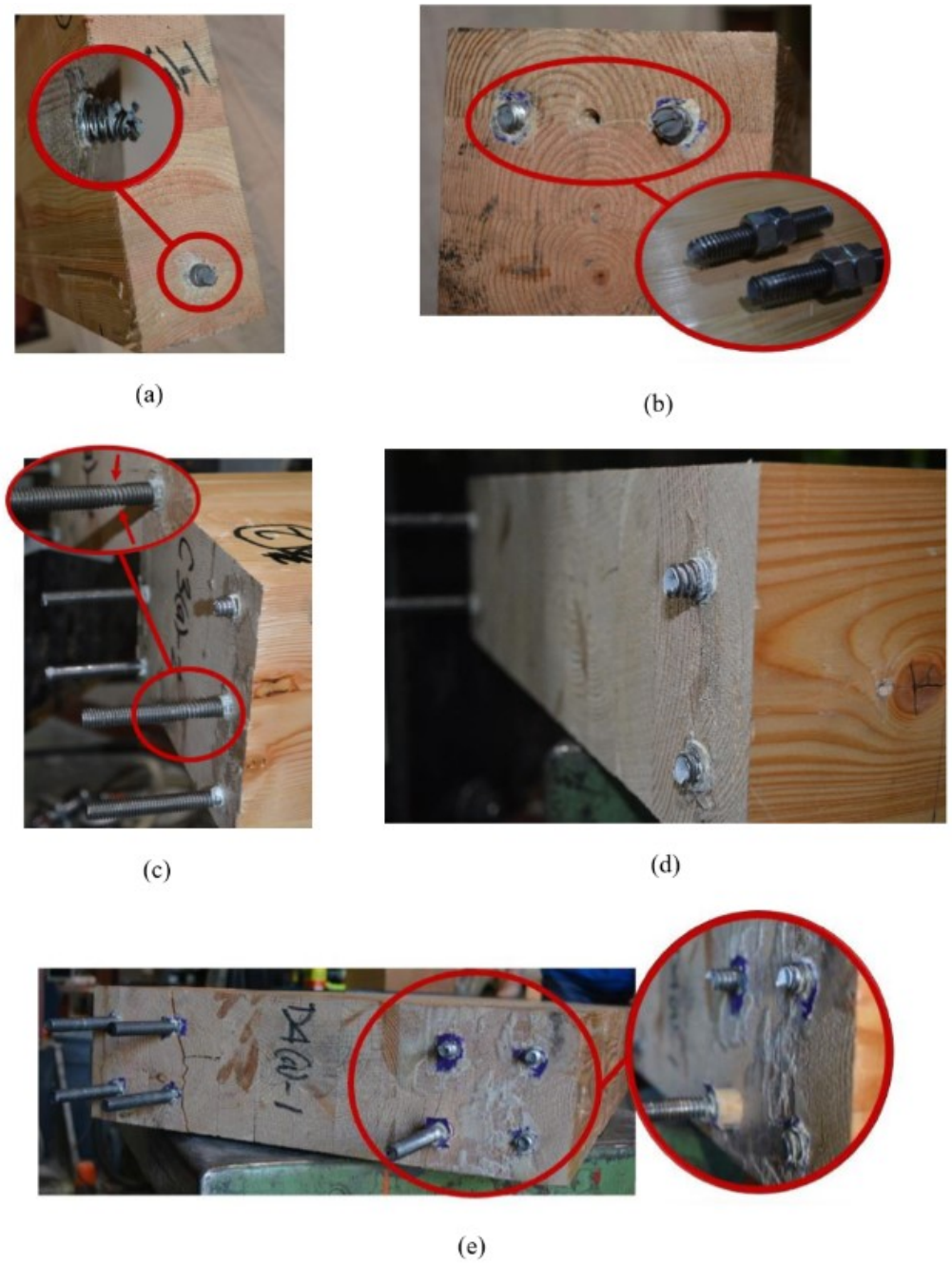

Figure 2.11. Ductile failures of glued-in rod moment connections: (a) A1(a); (b) B2(a); (c) C3(a); (d) D2(a); (e) D4(a) (Oh, 2016).

Figure 2.12 shows the brittle splitting failures that occurred for two of the tests. Even though they were not common, it shows how unpredictable timber can be when using this hybrid connection of steel, wood, and glue.

Figure 2.12. Brittle splitting failures of glued-in rod moment connections: (a) B2(a)-1(2); (b) D2(a)-1(2) (Oh, 2016).

2.4 Fire Performance of Timber Connections

Most guidelines in North America for fire design are prescriptive; however, the general trend has been to adopt a performance-based methodology for structural fire design (Hadjisophocleous and Benichou, 1999; Barber, 2017). The trend has been supported by extensive testing of individual components, sub-assemblies, assemblies, and even entire structures. However, the focus of the fire safety field has predominantly been on steel and concrete components, not glulam or other timber products (Bisby et al., 2013). Specifically, there is almost no available literature on the fire behaviour of heavy-timber moment-resisting connections either as individual components or as part of a structural frame. Primarily, the focus has been on axially loaded connections (Racher et al., 2010), under compressive or tensile loading, parallel to the grain (Peng. et al., 2010) or perpendicular to the grain (Audebert et al., 2012). At elevated temperatures, the studies showed that timber connections either fail due to brittle failure modes in the wood, such as hole elongation, splitting, row shear-out, crushing or due to ductile failure modes caused by yielding in the steel components at elevated temperatures.

A study was done on the structural fire performance of wood-steel-wood bolted connections with and without perpendicular-to-wood grain reinforcement by Petrycki and Salem (2019) using the same type and cross-section of glulam presented in this thesis. The connection had a slotted cut to accommodate a T-stub steel connector and was connected with bolts forming a wood-steel-wood concealed glulam beam connection as shown in Figure 2.13(a). There were also long screws placed in between the bolt rows for half of the connections tested to try and increase the connections fire resistance time. The long screws prevented the connection from splitting and added on average 2 minutes of fire resistance time, but the metal bolts still charred the holes at an accelerated rate causing the holes to become elongated as shown in Figure 2.13(b). The connection was subjected to similar design loads as the connection presented in this thesis, but the strongest connection was only able to achieve 19 minutes till failure in standard fire condition.

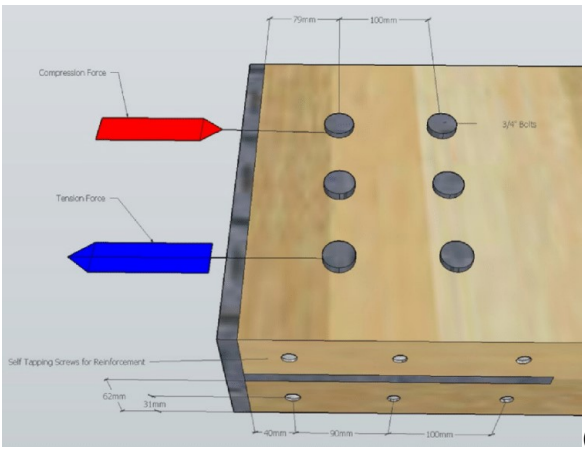

(a)

(b)

Figure 2.13. Bolted moment resisting connection reinforced with self-tapping screws exposed to fire: (a) bolted connection configuration with self-tapping screws; (b) connection after fire with char layer removed (Petrycki & Salem, 2019).

The use of embedded rods has the advantage of being superior in fire performance compared to other connections because the steel components are completely concealed inside the wood section. Even a connection where only a slight portion of the steel rod is exposed still has a considerably high charring rate because steel components quickly conduct heat into the connection (Barber, 2017). One setback though is that issues with epoxy at elevated temperatures still need to be further investigated. A study done by Di Maria et al. (2017) shows that epoxy deteriorates at elevated temperatures as shown in Figure 2.15, and thus, the connection can easily fail when the temperature reaches only 40 to 60°C in the epoxy. An epoxy resin with two different viscosities was used for

testing a single steel rod under tension in the end of spruce glulam and solid sawn Douglas fir. Half the shear strength at ambient temperature testing was chosen as the design load for the elevated temperature testing. Figure 2.14 shows the connections failing at temperatures between 40 and 60°C in the epoxy for the two different viscosities.

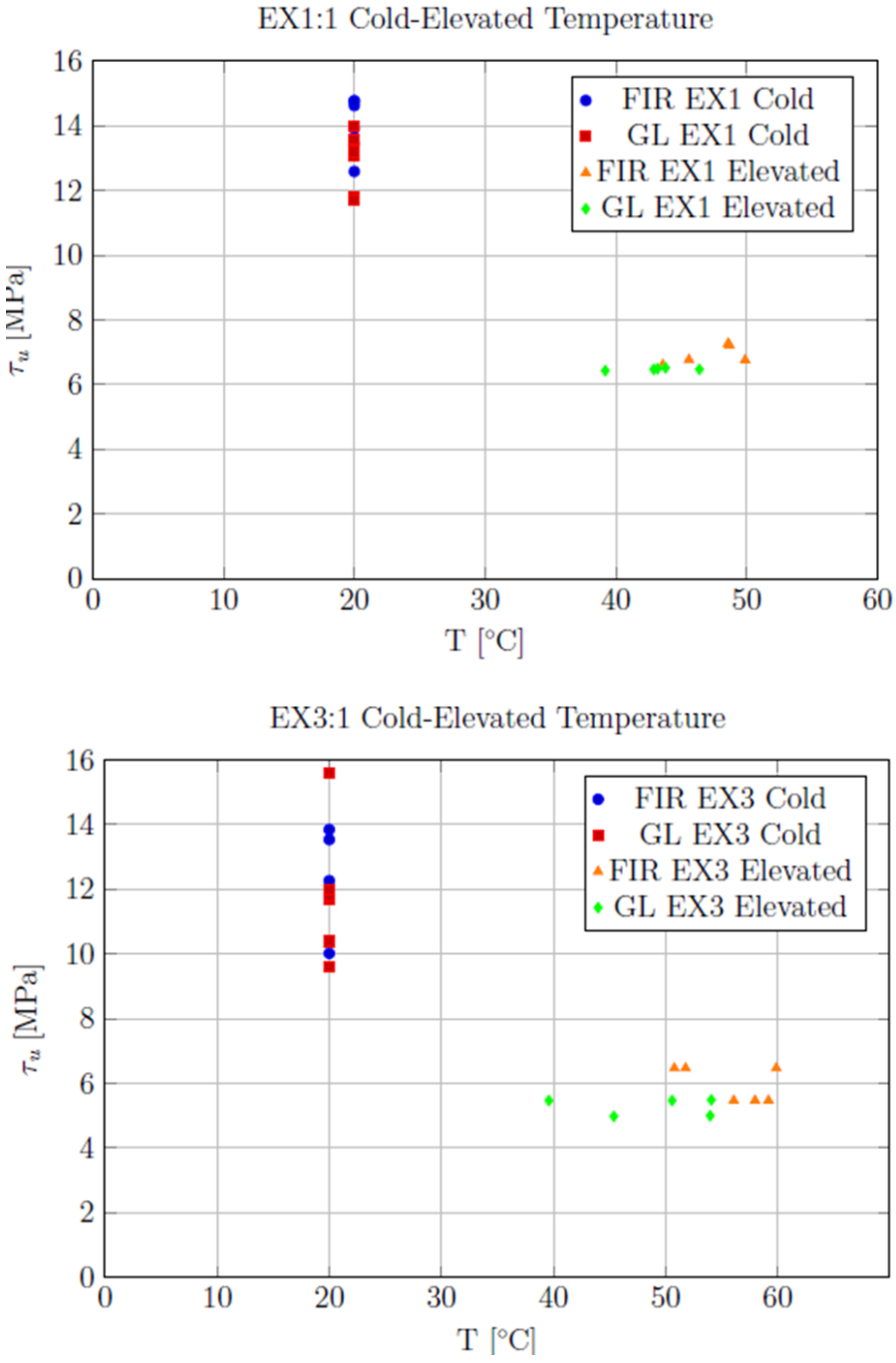

Figure 2.14. Shear strength versus temperature of tension connections at ambient and elevated temperatures (Di Maria et al., 2017)

Figure 2.15. Crumbling effect of epoxy resin after being exposed to elevated temperatures (Di Maria et al., 2017)

2.5 Summary

Section 2.2 shows that there have been many attempts to create a moment resisting timber connection that is strong yet ductile using a variety of configurations, additions, and completely innovative solutions. The problem with such connections is that even though they are strong and ductile, there is little research in regard to their fire performance. Section 2.3 shows moment resisting connections that utilize embedded glued-in steel rods. The connections can provide great strength with the possibility of a ductile failure. The glued-in rod connections flaw is that it must be assembled in the factory under controlled conditions to ensure a quality bond with the glue and is therefore not recommended for assembly in situ. Section 2.4 shows that connections with any exposed steel have poor fire performance due to the steel conducting the heat into the connection and char the wood at an accelerated rate. The concealed glued-in rod connection also needs more research as the deterioration of the epoxy at elevated temperatures is not fully understood. A practical solution to the epoxy problem at elevated temperatures is to mechanically fasten the steel rods instead. The fastening can be done by cutting a small hole in one side of the beam section to meet the end of the rod, then a nut and washer can be utilized to mechanically fasten the steel rod. Once the beam is connected, a small wood plug can be glued into the hole, covering the nut and washer, which will provide a fully concealed connection just like the bonded-in rod connection. Such a connection can be easily assembled in the field as well, which eliminates the risk of bond failure of the glued-in rods done in the field.

Chapter 3 Rod Pull-out Experimental Testing

3.1 Introduction

Thirty-seven full-size test assemblies were examined in the preliminary experimental study presented in this chapter. Nine configurations were used for the embedded rod in glulam connections with each configuration tested four times (A, B, C, D). The 37th connection assembly was tested using the strongest configuration and a weaker steel rod to prove that the wood can cause the steel rod to fail due to yielding. Using the collected load-displacement data, the connections' strength and stiffness were determined, and failure modes were observed and documented.

3.1.1 Materials

3.1.1.1 Glulam sections

The glulam beam sections (135 mm x 314 mm) used in all test assemblies were made of S-P-F, comprised of 90% black spruce (Nordic Wood Structures, 2015). A picture of the glulam beam cross-section is shown in Figure 3.1. The beam sections were manufactured to meet the 24F-ES/NPG (Canadian Standards Association, 2014) stress grade with architectural appearance grade. The individual lamina stocks that were used to build up the beam sections measured approximately 25 mm x 50 mm. The lamina stocks were finger jointed at their ends and glued together in horizontal and vertical layers. Since the laminas are glued along their faces and edges, and the beam section has a homogeneous layup, the strength properties are the same along the cross-section regardless of orientation. With the laminas being of the same quality throughout the beam cross-section the strength properties of the beam section are the same no matter where the rods of the connection are placed. The principle mechanical design properties of the glulam sections are listed in Table 3.1.

Figure 3.1. 135 mm x 314 mm glulam beam cross-section

Table 3.1. Mechanical properties of glulam sections (Nordic Wood Structures, 2015)

Property	Unit (MPa)
Bending moment, f_b	30.7
Longitudinal shear, f_v	2.5
Compression perpendicular to grain, f_{cp}	7.5
Compression parallel to grain, f_c	33.0
Tension parallel to grain, f_t	20.4
Tension perpendicular to grain, f_{tp}	0.51
Modulus of elasticity, E	13100

3.1.1.2 Threaded rods

The threaded rods used for all test assemblies had a nominal diameter of 19.05 mm (3/4"), and original length of 910 mm. The steel rods were of two different stress grades to guarantee the connection failure to occur in the wood section, not in the steel rod: SAE J429-Grade 5 and Class 10.9. Using a horizontal band saw the rods were cut to the desired lengths to allow the required rod embedment lengths into the glulam section. Any remaining cut-off lengths of the steel rods were utilized as tension coupons to confirm the stress grade of the rods.

3.1.1.3 Washers

The washers used for all test assemblies were fabricated from steel flat bar with a stress grade of 300W, as specified by CSA G40.20-04/G40.21-13 (Canadian Standards Association, 2013). Three different washer sizes were fabricated: 38.1 mm x 38.1 mm (1.5” x 1.5”); 50.8 mm x 50.8 mm (2.0” x 2.0”) and 63.5 mm x 63.5 mm (2.5” x 2.5”). The washers were cut to rough length with a horizontal band saw, and then they were trimmed to final dimensions using a milling machine. A 19.05-mm (3/4") diameter hole was drilled at the centre of each washer. Also, two different thicknesses, 8.0 mm and 12.7 mm were used for the different washers.

3.1.2 Test assembly details and fabrication process

Nine different configurations of threaded rod in glulam beam connections were tested with each configuration tested four times (A, B, C, D). The matrix of the test configurations is shown in Table 3.2. The four configurations of the weaker test assemblies were: a rod embedment length of 150 mm with a 38.1 mm (1.5”) square washer; a rod embedment length of 150 mm with a 50.8 mm (2.0”) square washer; a rod embedment length of 200 mm with a 38.1 mm (1.5”) square washer; and a rod embedment length of 200 mm with a 50.8 mm (2.0”) square washer. Three replicates of each connection configuration were tested with the SAE J429-Grade 5 steel rods and the 8-mm thick washers. Also, each connection configuration was tested an additional time with the Class 10.9 steel rod and the 12.7-mm thick washers to ensure that the connection failure occurred in the wood section.

The five configurations of the stronger test assemblies were: a rod embedment length of 150 mm with a 63.5 mm (2.5”) square washer; a rod embedment length of 200 mm with a 63.5 mm (2.5”) square washer; a rod embedment length of 250 mm with a 38.1 mm (1.5”) square washer; a rod embedment length of 250 mm with a 50.8 mm (2.0”) square washer; and a rod embedment length of 250 mm with a 63.5 mm (2.5”) square washer. Four replicates of each of these five configurations were tested with the Class 10.9 steel rods and the 12.7-mm thick washers. The connection configuration with rod embedment length of 250 mm and a 50.8 mm (2.0”) square washer was tested an additional time with a grade 2 steel rod and a 12.7-mm thick washer to prove that with an understanding of the wood sections strength a weaker steel rod can be selected to cause the rod to fail due to yielding with little to no damage to the wood section as shown in section 3.6.

Table 3.2. Threaded rod in glulam sections tests matrix

Test configuration ID	Test Replicates	Rod embedment length (mm)	Washer size (mm)
Test 150-1.5	4	150	38.1
Test 150-2.0	4	150	50.8
Test 150-2.5	4	150	63.5
Test 200-1.5	4	200	38.1
Test 200-2.0	4	200	50.8
Test 200-2.5	4	200	63.5
Test 250-1.5	4	250	38.1
Test 250-2.0	5	250	50.8
Test 250-2.5	4	250	63.5

Notes: For the test configuration ID; 150, 200, and 250 are the rod embedment lengths in (mm); 1.5, 2.0, and 2.5 are the square washer size in (inches).

The glulam beam sections with an embedment length of 150 mm were cut to a minimum length of 450 mm, while the beam sections with an embedment length of 200 mm were cut to a minimum length of 500 mm, and the beam sections with an embedment length of 250 mm were cut to a minimum length of 550 mm using a horizontal band saw. The length of each beam section ensured that there was enough space separating the connection end to be tested from the end where the tension attachment would be which would keep the failure contained in the tested connection end. A 20.6-mm (13/16”) diameter hole was then drilled at the centre of one of the ends of the beam section to the required embedment length using a precise portable drilling station. Every beam section had a line marked perpendicular to the wood grain at the required embedment length, and a line marked parallel to the wood grain down the centre of the widest face. A little rectangle was marked directly below the embedment length line and vertically centred on the beam’s front face. Rectangles measured 41.3 mm (1 5/8”) wide for the 38.1 mm (1.5”) washer, 54.0 mm (2 1/8”) wide for the 50.8 mm (2.0”) washer, and 66.7 mm (2 5/8”) wide for the 63.5 mm (2.5”) washer with all measuring 30-mm high were marked on the beam’s front face to accommodate the washer and nut thicknesses. All rectangles were then carved out into a rectangular prism using wood chisels to a depth where the centre of the washer hole would line up with the centre of the hole made through the end of the beam section. The depth of the hole chiselled out was approximately 88 mm for the 38.1 mm (1.5”) washer, 94 mm for the 50.8 mm (2.0”) washer, and 100 mm for the 63.5 mm (2.5”) washer. The opposite end of the beam section had six 20.6-mm (13/16”) holes drilled on the beam’s front face to match the holes in the tension steel attachment fabricated to

support the test assembly in the Universal Testing Machine (UTM) which was utilized to apply the tensile forces. The design of the tension attachment had at least doubled the expected maximum load of the strongest connection; therefore, there should be no noticeable deformation or slippage in the bolts for the bottom half of the beam section. An example of a prepared beam section is shown in Figure 3.2(a), and the tension steel attachment used in experiments is shown in Figure 3.2(b).

(a)

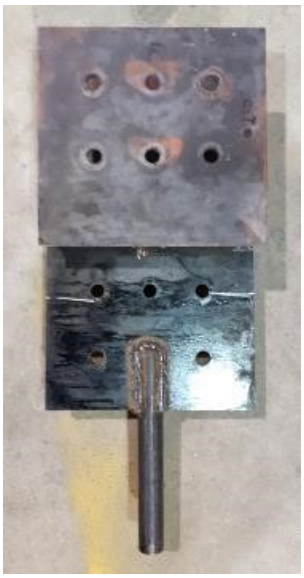
(b)

Figure 3.2. Components of a general test assembly: (a) prepared beam section; (b) tension steel attachment.

3.1.3 Test assembly design

The purpose of this preliminary study as part of the research project was to experimentally determine the maximum strength of the glulam section itself when it fails in the threaded-rod-in-glulam-beam connection configuration; therefore a sufficient strong threaded steel rod and thick washer were selected for each respective connection configuration to ensure that the failure would happen in the wood section and not in any of the steel connecting components. The final test was the only exception as a grade 2 steel rod was utilized in the connection configuration with a rod embedment length of 250 mm and a washer size of 50.8 mm (2.0”) to prove that the utilized glulam section was strong enough to make a lower grade steel rod yields without any damage to the wood section as shown in section 3.6. The anticipated failure of the glulam beam section was rod pull-out, similar to the failure in the case of glued-in rods connections. Since there was no clause for

glued in rods or rod pull-out parallel to the grain in the CSA O86-19 Engineering design in wood (Canadian Standards Association, 2014) or guidelines in the current version of the Canadian Wood Design Manual (Canadian Wood Council, 2018), a simple shear equation was adapted to fit the parameters of this connection. Similar to the failure of a glued-in threaded rod pull-out, the strength of the connection is in the area of wood to be sheared. The glued-in threaded rod area to be sheared is the circumference of the rod multiplied by the embedment length (Muciaccia, 2017). The area to be sheared by the mechanically fastened rod is the perimeter of the square washer multiplied by the rod embedment length.

According to Clause 12.2.1 in the CSA O86-14 standard (Canadian Standards Association, 2014), all connection design formulas must consider certain modification reduction factors (K factors) to accurately predict their true strength values. These K factors include the load duration factor, K_D, the service condition factor, K_S, and the treatment factor, K_T. The glulam beam sections were tested under short duration loading till failure (less than seven days), therefore, the load duration factor, K_D, equals 1.15 as per Clause 12.2.1.6 in the CSA O86-14 standard (Canadian Standards Association, 2014). The beam sections were under dry service condition and were untreated; therefore, the service condition factor, K_S, and the treatment factor, K_T, both equal 1.0 as per Clause 12.2.1.5 and Clause 12.2.1.7, respectively.

The specified shear strength for the glulam beam section, f_v, equals 2.5 MPa according to a technical note published by Nordic Structures (Nordic Wood Structures, 2015). Combining all these values gives Equation 1, as shown below.

Equation 3.1 Rod pull-out failure formula:

$$PR = f_v (K_D K_{Sv} K_T) p l \qquad \text{Eqn. (3.1)}$$

Where; PR = Pull-out resistance of threaded rod in glulam section (N), f_v = specified shear strength (MPa), K_D = load duration factor, K_{Sv} = service condition factor for shear, K_T = treatment factor, p = washer perimeter (mm), and l = rod embedment length (mm)

Using Equation 3.1, the expected ultimate pull-out strength values were calculated as shown in Table 3.3. For the first half of the weaker experiments, the maximum expected pull-out tensile force of the glulam beam section for the strongest connection configuration was 116.8 kN, while the tested yielding tensile force resisted by the grade 5 threaded steel rod was 150 kN; therefore, all failures should occur in the wood section, not in any of the steel connectors.

For the second half of the stronger experiments, the maximum expected pull-out tensile force of the glulam beam section for the strongest configuration was 182.6 kN, while the tested yielding stress of the class 10.9 threaded steel rod was 960 MPa. When the stress is multiplied by the rod cross-sectional area, the yield tensile force was calculated at 200 kN; therefore, all failures should be wood failures, not steel failures.

Table 3.3. Threaded rod in glulam section tests expected tensile force

Test configuration ID	Test Replicates	Rod embedment length (mm)	Washer size (mm)	Expected tensile force (kN)
Test 150-1.5	4	150	38.1	65.7
Test 150-2.0	4	150	50.8	87.6
Test 150-2.5	4	150	63.5	109.5
Test 200-1.5	4	200	38.1	87.6
Test 200-2.0	4	200	50.8	116.8
Test 200-2.5	4	200	63.5	146.1
Test 250-1.5	4	250	38.1	109.5
Test 250-2.0	5	250	50.8	146.1
Test 250-2.5	4	250	63.5	182.6

3.1.4 Tests setup

A schematic of the test assembly is shown in Figure 3.3. The tension steel attachment for the beam section was placed in the bottom gripping jaws of the UTM accommodated in the Civil Engineering's Structures Laboratory at Lakehead University. A small steel plate was attached to the end of the beam, and an attachment for a Linear Variable Differential Transducer (LVDT) was secured to the side of the beam section near the end, both of which were used to help with measuring the displacement using two LVDTs. The glulam beam section then had the threaded rod inserted through the end hole and was secured using a washer and nut through the small rectangular hole carved out of the beam front face. The beam section was then placed on the tension steel attachment and secured using six A325M bolts, while the threaded rod was slipped up into the top assembly of the UTM. The top assembly used gripping jaws for the tests using the 600 mm grade 5 rod, and a fixed assembly for the tests using the 750 mm class 10.9 rods. Both jaws were drawn tight for the 600 mm rod, and just the bottom jaws were drawn tight for the 750 mm rod, while a minimal initial load was applied to the test assembly to secure the machine jaws.

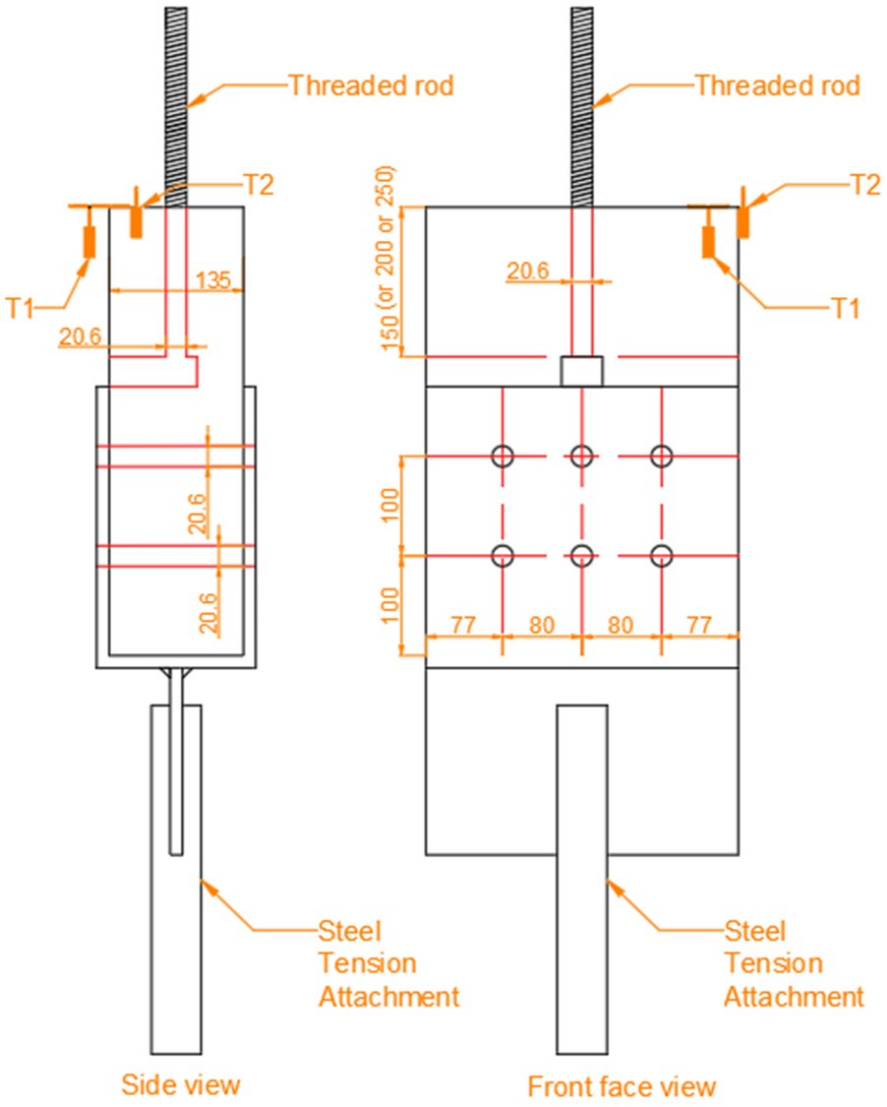

Figure 3.3. Tension assembly diagram

One draw-wire displacement transducer was attached to the UTM head block and the stationary block to measure the displacements of the entire system: including possible slippage in the top and bottom sets of jaws, as shown in Figure 3.4(a). The two installed LVDTs were attached at the top end of the beam section, as shown in Figure 3.4(b); one was attached to a metal pole next to the small plate to measure the displacement between the pole and the small plate; while the other was attached to the side of the glulam section to measure the displacement between the beam section and the UTM head block. Both were measuring the displacement between the beam section and the UTM head block, therefore, the obtained results from both LVDTs shall be the same. It is important to mention that the measurements of the two LVDTs accounted for the displacements

of the beam section and any potential slippage of the machine's top jaws. Once the displacement measuring instruments were in place and zeroed, the initially applied load was recorded, then the test assembly was loaded at a rate of 8.0 kN per minute. The slow rate of loading was chosen to prevent premature brittle failure that might be caused from loading too fast. Also, the loading rate of force per time versus displacement per time was chosen due to the same preventative measure of not loading too quickly. The test was terminated when the glulam beam section developed a wood failure with no additional load gain. The full test setup with the top gripping jaws is shown in Figure 3.4(c). The fixed top assembly used is shown in Figure 3.4(d).

(a)

(b)

(c)

(d)

Figure 3.4. Full test setup of a general tension test assembly: (a) Draw-wire displacement transducer; (b) Two LVDTs installed; (c) Test setup of a general assembly; (d) Fixed top assembly.

3.2 Experimental Results and Discussion

The measurements of the two LVDTs were nearly identical, which confirmed the displacement between the UTM head block and the glulam beam section, as well as any potential slippage that might developed in the top assembly. However, the draw-wire displacement transducer showed an increase in displacements by an average of 3.0 mm and up to 5.0 mm compared to the two LVDTs' measurements, which indicate that there was a slight slippage in the bottom jaws. There was no noticeable deformation in the six bolts of the bottom connection and the bolts where tightly fitted into the tension assembly; therefore, the slight slippage in the bottom half of the assembly was not caused by slippage in the six bolts. Also, when the 600-mm long rod was removed from the top jaws, the threads were bent in the direction of the pulling jaws, which confirms that there was slight slippage in the top jaws as well. Accordingly, the results showed slightly more displacements occurred in the pull-out of the rod than what it should be. However, the exact slippage cannot be proven, therefore, the obtained displacement measurements are more on the conservative side. When the 750 mm rods were used with the fixed top assembly, there was no slippage noticed. The

extra tests done on the first four assemblies with the 750 mm rod and fixed top assembly show an enhanced stiffness since there was no slippage when compared to the 600 mm rod and gripping top jaws. A summary of the maximum load sustained is shown in Table 3.4 below.

Table 3.4. Maximum load results of all test replicates, A through D

Test configuration ID	Expected load (kN)	Test A load (kN)	Test B load (kN)	Test C load (kN)	Test D load (kN)
150-1.5	65.7	66.6	64.5	67.5	82.2
150-2.0	87.6	75.6	93.8	73.5	67.9
150-2.5	109.5	69.7	76.4	82.3	90.1
200-1.5	87.6	80.3	74.6	67.6	65.0
200-2.0	116.8	114.6	105.0	109.5	83.7
200-2.5	146.1	142.0	115.6	101.8	132.4
250-1.5	109.5	76.9	79.0	80.5	87.3
250-2.0	146.1	138.0	146.3	135.4	133.9
250-2.5	182.6	217.9	136.9	127.9	125.8

The failure modes of every test are presented in Table 3.5 below. The short forms for each failure are: rod pull-out (RPO), wood crushing (WC), and splitting (S). For the tests that had two failures, the first one listed is the first one observed.

Table 3.5. Failure mode of all test replicates, A through D

Test configuration ID	Test A load (kN)	Failure mode A	Test B load (kN)	Failure mode B	Test C load (kN)	Failure mode C	Test D load (kN)	Failure mode D
150-1.5	66.6	RPO	64.5	RPO	67.5	WC:RPO	82.2	RPO
150-2.0	75.6	S:RPO	93.8	S:RPO	73.5	S:RPO	67.9	S:RPO
150-2.5	69.7	S:RPO	76.4	S:RPO	82.3	S:RPO	90.1	S:RPO
200-1.5	80.3	WC:RPO	74.6	WC:RPO	67.6	WC:RPO	65.0	WC:RPO
200-2.0	114.6	RPO:S	105.0	RPO:S	109.5	RPO:S	83.7	S:RPO
200-2.5	142.0	RPO:S	115.6	S:RPO	101.8	S:RPO	132.4	S:RPO
250-1.5	76.9	WC:S	79.0	WC:S	80.5	WC:S	87.3	WC:RPO
250-2.0	138.0	WC:RPO	146.3	RPO	135.4	RPO:S	133.9	WC:RPO
250-2.5	217.9	RPO:S	136.9	S:RPO	127.9	S:RPO	125.8	S:RPO

3.2.1 Failure modes

The desirable failure mode was rod pull-out as shown in Figure 3.5. In Figure 3.5(a), the failure was a rod pull-out of a square area of a similar size of the utilized washer. In Figure 3.5(b), the failure was similar to that shown in Figure 3.5(a) except that instead of shearing along the fourth side of the washer closest to the small hole, the wood surrounding the rod sheared along the three walls of the small hole that was chiselled out. In Figure 3.5(c), the failure was similar to that shown in Figure 3.5(b), except that one or two 45-degree cracks also formed on the end surface at approximately where the washer corners were.

(a)

(c)

(b)

Figure 3.5. Rod pull-out failures: (a) Rod pull-out shearing along washer edges; (b) Rod pull-out shearing along carved out hole edges; (c) Rod pull-out shearing along carved out hole edges with 45 degree crack.

As shown in Figure 3.6(a), Test 200-2.0 had a rod pull-out failure with partial wood splitting. The rod pull-out failure occurred like that shown in Figure 3.6(c); in addition, the beam section had a clear split down the middle on the back side of the small hole, which did not form until the end, during the last 5.0 kN before rod pull-out failure. The connection configurations of Test 200-2.0 were strong enough to cause the 8.0-mm washer to yield slightly, as shown in Figure 3.6(b). Since most of the yielding occurred at the corners of the washer, therefore it can be assumed that more stresses happened at the corners to cause the 45-degree cracks to form at the end of the beam section. For the additional test and all other stronger connection configurations, the 8.0-mm thick washer was replaced with a 12.7-mm thick washer.

(a)


(b)

Figure 3.6. Failure mode of Test 200-2.0 replicates: (a) Rod pull-out shearing along carved out hole with 45-degree cracks and beam splitting; (b) Yielded 8-mm thick washer.

As shown in Figure 3.7(a), the first replicate of Test 250-2.5 had a rod pull-out failure with a split happening at the back of the connection simultaneously. Also, the wood section showed no noticeable cracks or damage until the very end when the connection sheared. The test replicate A was strong enough to cause the washer to yield slightly, as shown in Figure 3.7(b). The strength of this replicate of Test 250-2.5 went well beyond the maximum expected load and only happened once; therefore, the same washer type was used for the other tests.

(a)

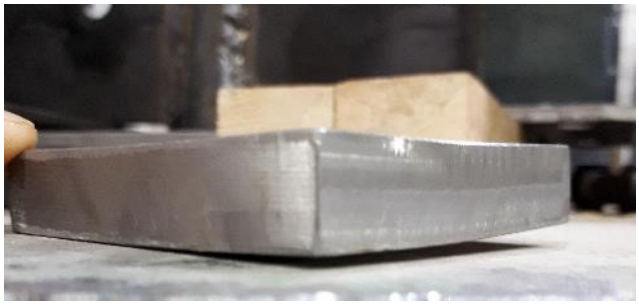
(b)

Figure 3.7. Failure mode of the first replicate of Test 250-2.5: (a) Rod pull-out failure; (b) Yielded 12.7-mm thick washer.

The next desirable failure mode was wood crushing as shown in Figure 3.8. The wood crushing failure happens first and can displace into the wood section a large amount, e.g., 50 mm, as shown in Figure 3.8(a). The final failure of the beam section after the wood was done crushing was either wood splitting failure as shown in Figure 3.8(b), or rod pull-out failure as shown in Figure 3.8(c).

(a)


(b)


(c)

Figure 3.8. Wood crushing failure with associated failures at the end of the tests: (a) Wood crushing failure; (b) Wood splitting failure; (c) Rod pull-out failure.

The final failure mode experienced was wood splitting as shown in Figure 3.9. The wood would either partially or fully split in half first, as shown in Figure 3.9(a). Next, the wood would experience a rod pull-out failure, as shown in Figure 3.9(b). In some specimens, the two failures

would happen simultaneously, but usually, the wood would split first then the test specimen would experience rod pull-out failure.


(a)


(b)

Figure 3.9. Wood splitting failure: (a) Wood splitting before final failure; (b) Rod pull-out failure after wood splitting.

3.2.2 Load-displacement relationships

The displacements used to develop the load-displacement curves were those measured by the LVDT attached to the metal pole. The displacement measurements of the LVDT attached to the glulam section were very similar to those of the other LVDT except for the end of the test when the glulam section failed under rod pull-out. The sudden jerk of the rod pull-out would slightly move the sensor and give a higher displacement value than what the actual value should be.

Figures 3.10 through 3.18 show the load-displacement relationships of the nine different connection configurations. For Figures 3.10, 3.11, 3.13, 3.14, replicates A, B, and C were tested using the machine's top gripping jaws, whereas replicate D was tested using the top fixed assembly. Test replicate D exhibited the greatest initial stiffness, which proves that the top gripping jaws exhibited slippage while the top fixed assembly had no slippage. Also, Figures 3.12, 3.15-3.17 were tested using the top fixed assembly and there graphs show the initial stiffness's of each test configuration very close proving that there was no slippage in the top fixed assembly.

Figure 3.10 show the load-displacement relationship for Test 150-1.5. All tests show a steady increase in load sustained before a sharp drop, except Test C, which follows the trend of a rod pull-out failure. Test C experienced a few millimeters of wood crushing before experiencing the final rod pull-out failure.

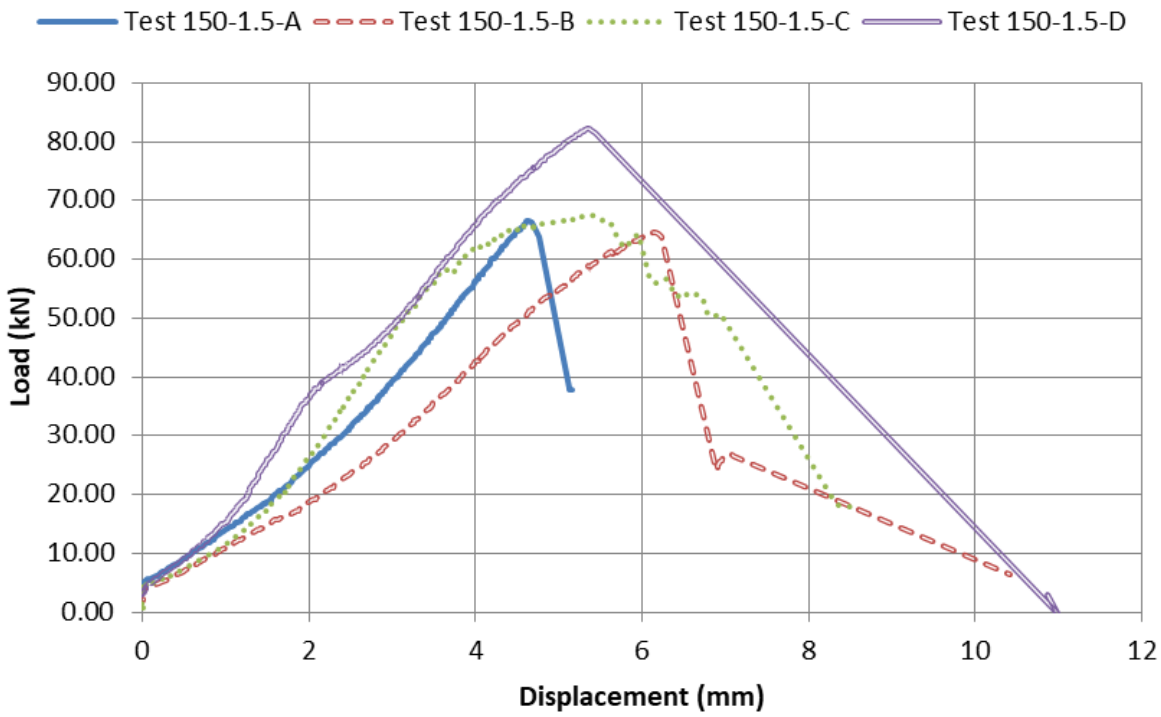

Figure 3.10. Load-displacement relationships for Test 150-1.5 connections

Figure 3.11 shows the load-displacement relationships of the connection configurations of Test 200-1.5. Only test replicate A experienced sudden failure of rod pull-out, similar to the failure developed in the connection configurations of Test 150-1.5. The other test replicates experienced crushing of the wood section, similar to the failure developed in the connection replicate C of Test 150-1.5, and at around the same failure load of 65.0 kN. Also, the wood crushing was experienced for much deeper in the wood section compared to the 3.0 mm experienced in the connection replicate C of Test 150-1.5, by up to 15.0 mm. This extended crushing is because the connection configuration of Test 200-1.5 has an extra 50 mm of length to hold the wood at this failure load before experiencing rod pull-out failure.

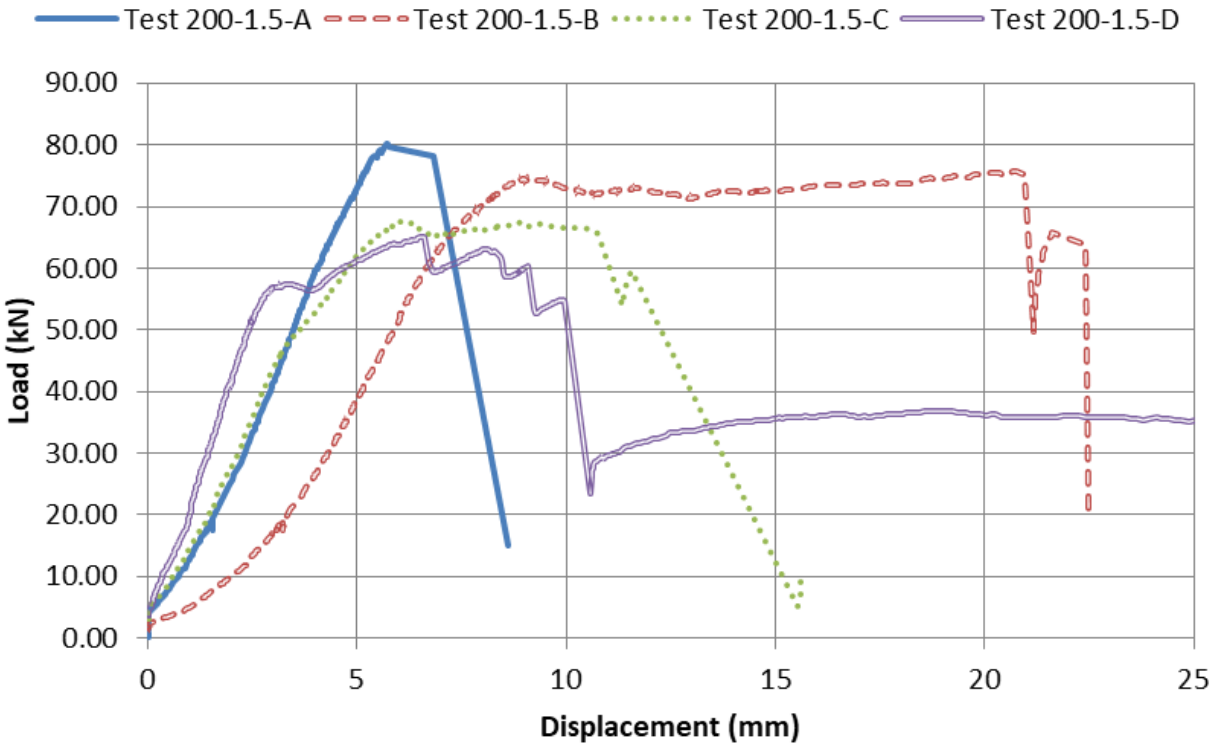

Figure 3.11. Load-displacement relationships for Test 200-1.5 connections

Figure 3.12 shows the load-displacement relationships of the connection configurations of Test 250-1.5. All four test replicates experienced crushing of the wood to some degree before experiencing a splitting or rod pull-out failure. These four replicates of Test 250-1.5 experienced wood crushing at a slightly greater load of about 70.0 kN compared to that of Test 200-1.5 replicates. The extra 50 mm of length in Test 200-1.5 replicates helps the wood section to hold this crushing failure for even longer, by up to 50 mm before experiencing the final failure.

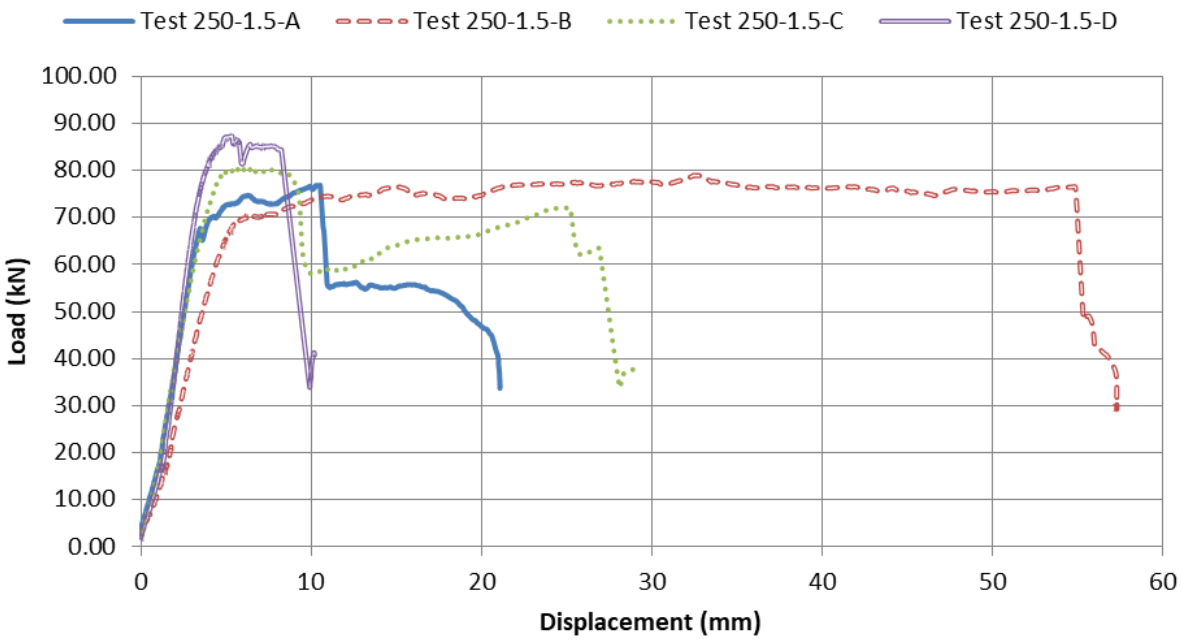

Figure 3.12. Load-displacement relationships for Test 250-1.5 connections

The displacement before wood crushing failure and rod pull-out failure for the three connection configurations using a 38.1 mm (1.5”) wide washer were all around 5.0 mm.

Figure 3.13 shows the load-displacement relationships of the connection configurations of Test 150-2.0. All test replicates had the wood section split partially to fully in half from the hole in the front to the back side before experiencing rod pull-out failure. The split happened around the last 5.0 kN before rod pull-out failure. The split is believed to happen due to uneven bearing on one side of the washer causing a slight lateral force in the section, or due to the compression under the larger washer which disperses some of the load laterally and the short embedment length of 150 mm wasn't strong enough to resist the lateral tension load perpendicular to the wood grain, which is the wood weakest load orientation.

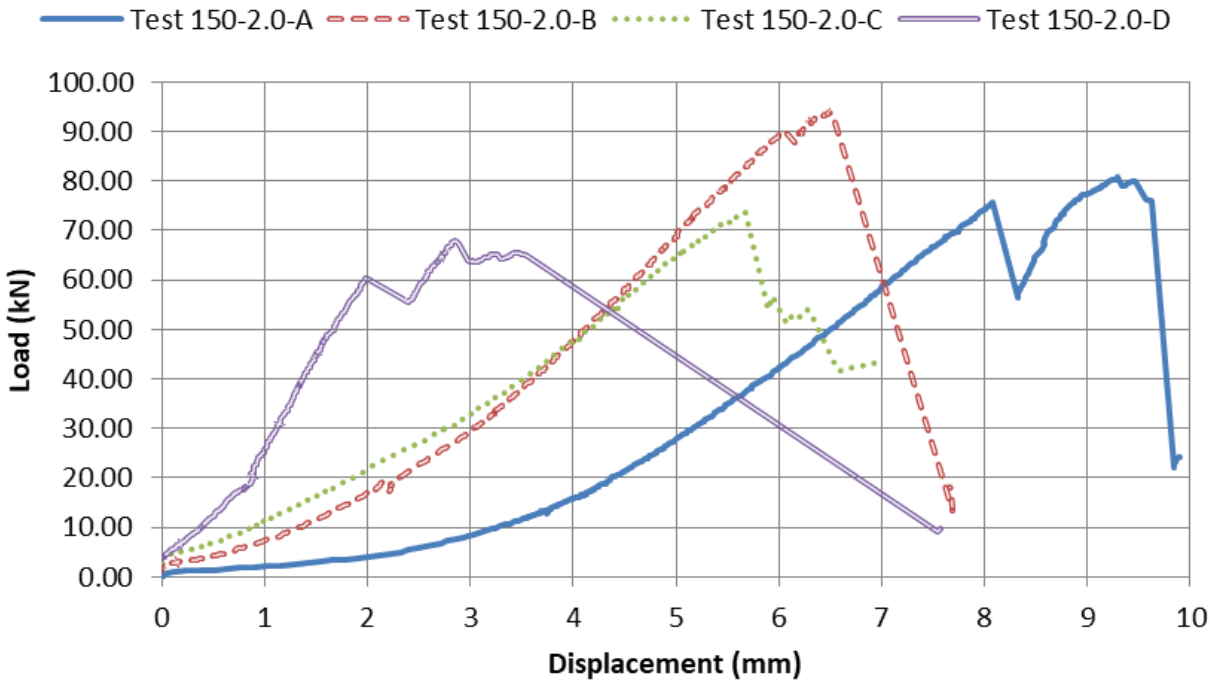

Figure 3.13. Load-displacement relationships for Test 150-2.0 connections

Figure 3.14 shows the load-displacement relationships of the connection configurations of Test 200-2.0. All four test replicates experienced very slight splitting before experiencing rod pull-out failure and major splitting. The first failure happened within the last 5.0 kN before rod pull-out failure. However, the slight drop in load during the final 5.0 kN before ultimate failure was not experienced for the connection configurations of Test 200-2.0 when compared to Test 150-2.0 configurations. The longer embedment length of 50 mm extra provided enough resistance to the lateral tensile force acting perpendicular to the wood grain so that even though the wood was starting to split, there were enough fibres to hold the section together until rod pull-out failure developed.

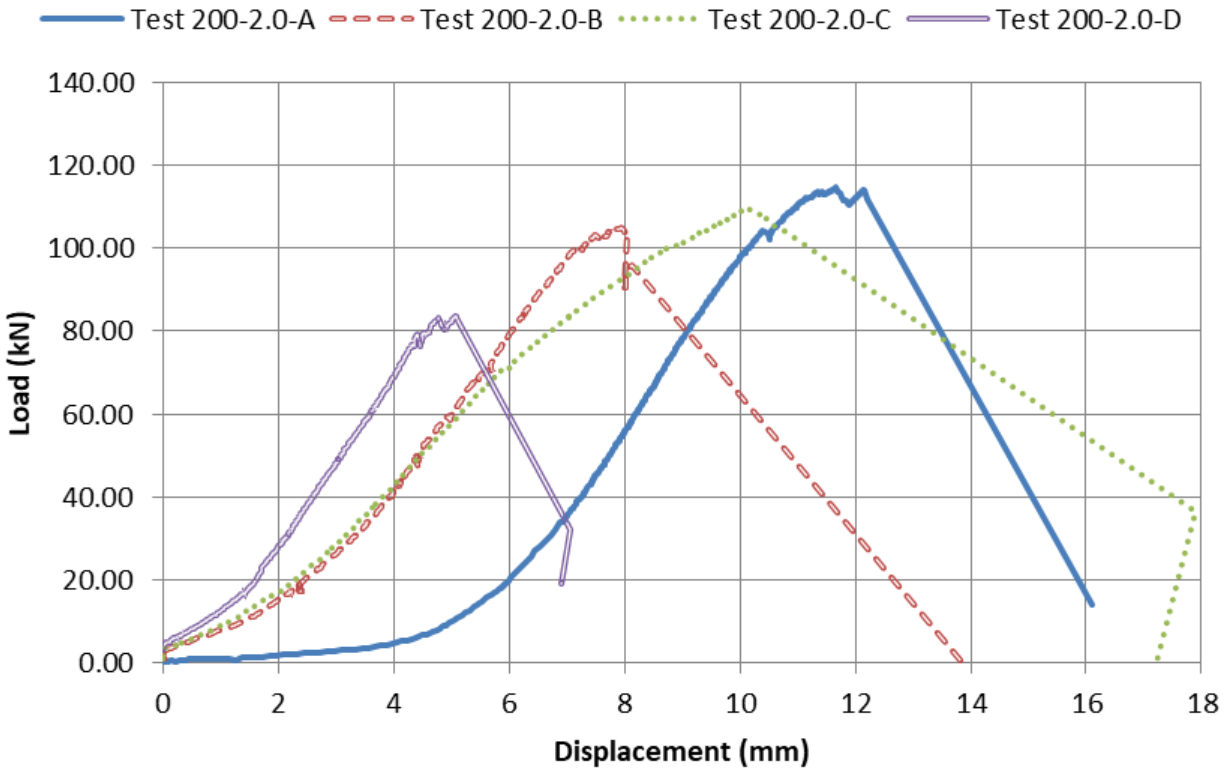

Figure 3.14. Load-displacement relationships for Test 200-2.0 connections

Figure 3.15 shows the load-displacement relationships of the connection configurations of Test 250-2.0. Test replicates B and C experienced a sudden rod pull-out failure. However, test replicate D experienced slight wood crushing before having a rod pull-out failure, whereas test replicate A experienced a long wood crushing failure before having a rod pull-out failure. The displacement of test replicate A during the wood crushing failure was about 12.0 mm.

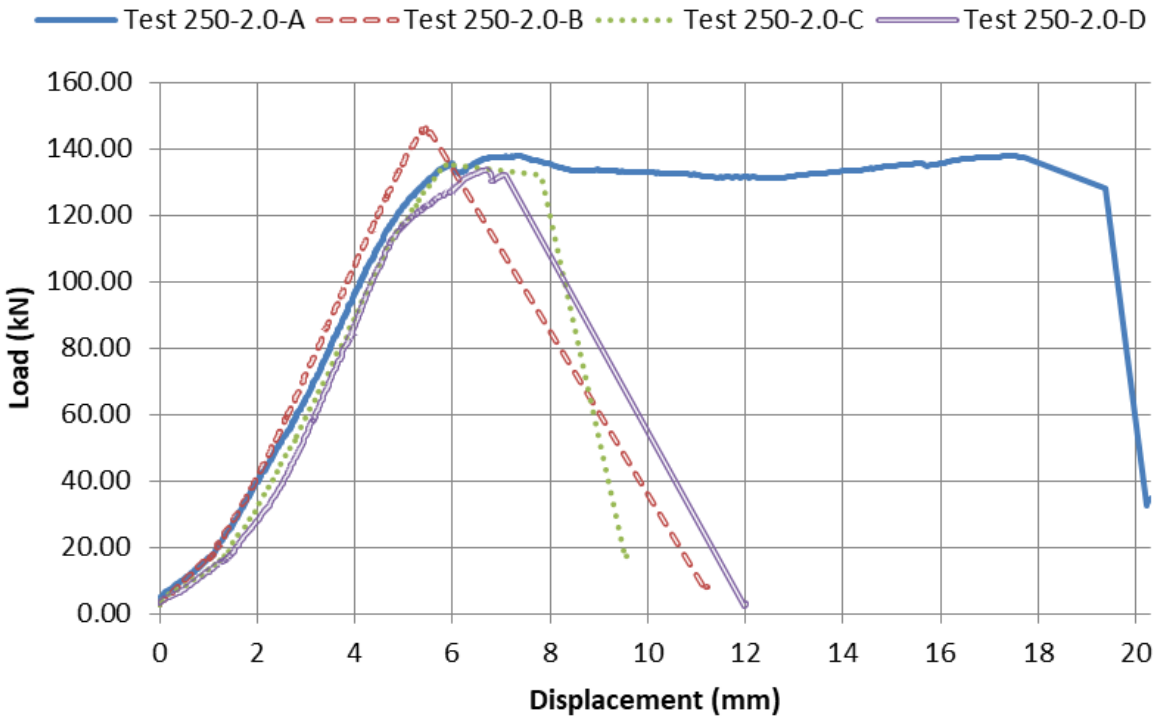

Figure 3.15. Load-displacement relationships for Test 250-2.0 connections

The displacements measured before the wood crushing failure and rod pull-out failure for the connection configurations using a 50.8-mm (2.0”) wide washer and the top fixed assembly with the three different rod embedment lengths were all between 5.0 and 6.0 mm.

Figure 3.16 shows the load-displacement of the connection configurations of Test 150-2.5. All test replicates had the wood section split fully in half from the hole in the front to the back side before experiencing rod pull-out failure. The split happened at the maximum load and then rod pull-out failure happened shortly after. Since the split happened across the entire section, there was not enough area of wood to be sheared by the washer for the rod pull-out failure to gain a higher load. The split is believed to happen due to uneven bearing on one side of the washer causing a slight lateral force in the wood section. Also, the split is believed to happen due to the compression under the larger washer which disperses some of the load laterally and the short embedment length of 150 mm is not strong enough to resist the lateral tension load perpendicular to the wood grain.

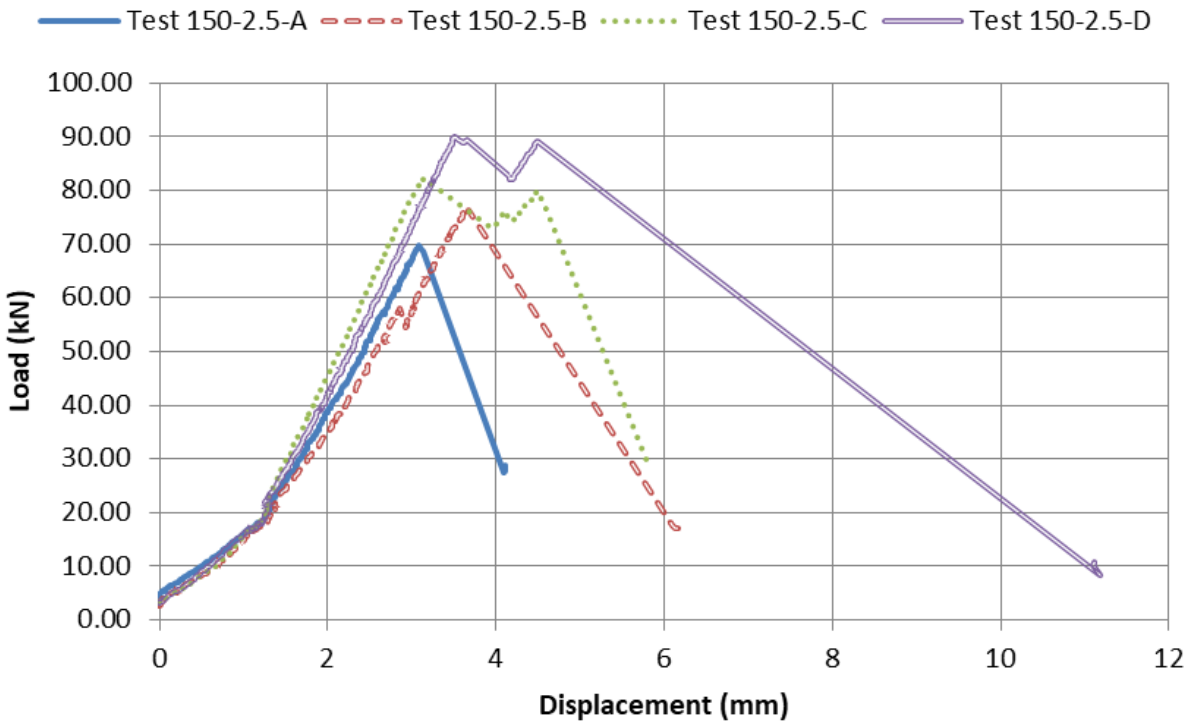

Figure 3.16. Load-displacement relationships for Test 150-2.5 connections

Figure 3.17 shows the load-displacement relationships of the connection configurations of Test 200-2.5. All test replicates experienced rod pull-out failure and splitting at the same time except for test replicate C which had the wood section split before experiencing rod pull-out failure. The connection configurations of Test 200-2.5 experienced similar wood section splitting as those of Test 150-2.5; however, because of the extra 50 mm of embedment length in the preceding configurations, the wood section was able to resist the lateral tension force developed perpendicular to the wood grain for longer. Similar comparison is valid for the connection configurations of Test 150-2.0 versus those of Test 200-2.0.

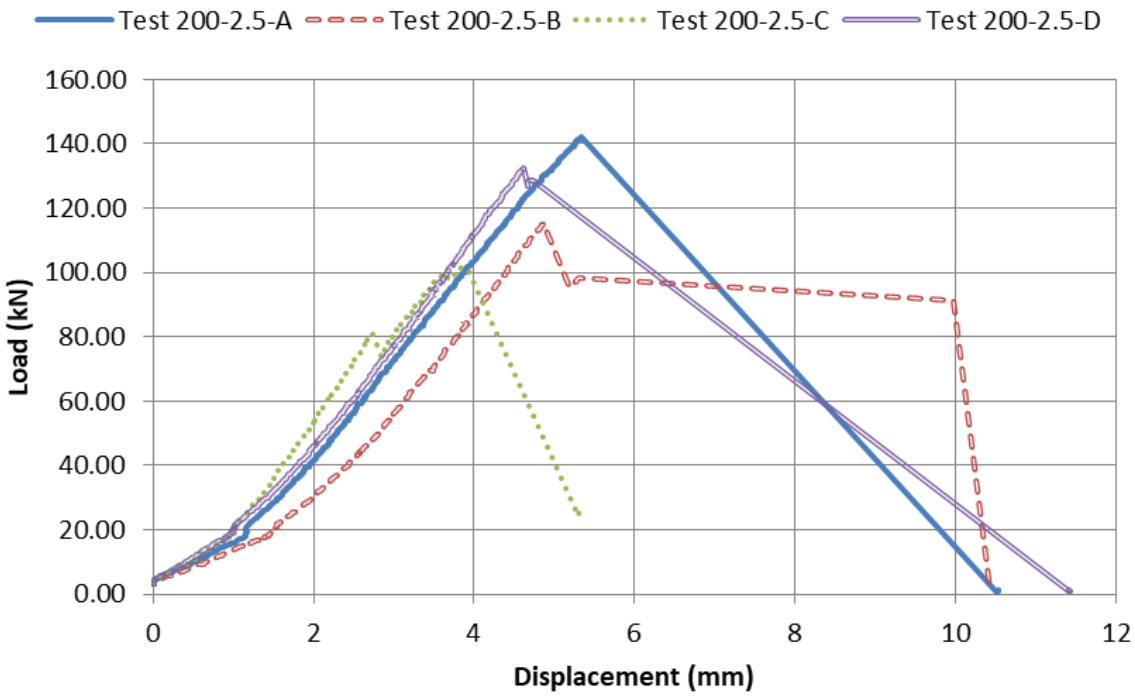

Figure 3.17. Load-displacement relationships for Test 200-2.5 connections

Figure 3.18 shows the load-displacement of the connection configurations of Test 250-2.5. Test replicate A experienced rod pull-out failure, whereas test replicate B had the wood section split at maximum load before experiencing rod pull-out failure. While test replicates C and D had their sections split but were still able to sustain more load until rod pull-out failure. The connection configurations of Test 250-2.5 experienced splitting at a slightly higher loads than those of Test 200-2.5 connection configurations, except for replicate A of Test 250-2.5, as the maximum loads obtained for the connection configurations of both test groups were in the range of 120.0 to 140.0 kN. Also, since test replicate A of Test 250-2.5 experienced no splitting until the end, it was able to achieve a simultaneous rod pull-out and splitting failure which provided the highest tensile resistance force when compared to all other sections that experienced splitting beforehand.

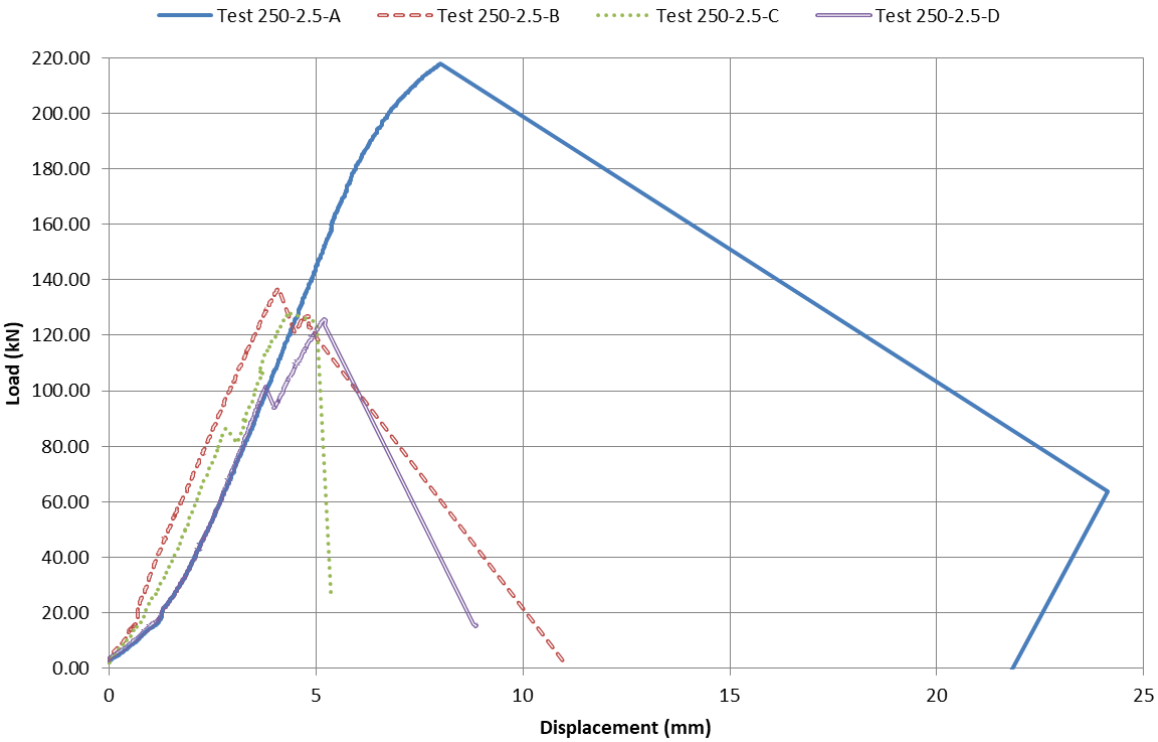

Figure 3.18. Load-displacement relationships for Test 250-2.5 connections

The displacements measured before wood section splitting failure developed in all three connection configurations using a 63.5-mm (2.5”) wide washer and the top fixed assembly were all between 3.0 and 5.0 mm, and about 5.0 mm before rod pull-out failure.

3.2.3 Maximum load comparison

Shown in Figure 3.19 are the expected maximum and the actual maximum loads of the test replicates of each connection configuration grouped by washer size. The expected maximum load was calculated from Equation 1. Results of all test replicates are either within the expected range or above the expected maximum load value. Also, all test replicates that experienced pure rod pull-out failure had their maximum load close to, or above, the maximum load value predicted from Equation 1, without the use of the resistance factor. Therefore, for test replicates predicting pure rod pull-out failure, Equation 1 fits this failure mode the best. Replicates of Test 150-1.5 and Test 250-2.0 show the best fit for pure rod pull-out failure.

The connection configurations with the 38.1-mm (1.5") wide washer experienced a longer wood crushing failure as embedment length increased. Connection configurations of Test 150-1.5 had one replicate experienced slight wood crushing failure while the rest experienced pure rod pull-out failure. The other two configurations with the same washer size experienced mainly wood crushing failure which happened due to the wood under the small washer acted like a small fully supported column crushing. Since the 38.1-mm (1.5") wide washer's bearing area is small, the wood under the washer behaved like a fully-supported short column and crushed before experiencing large enough load to experience a splitting or rod pull-out failure. As the rod embedment length increased, the displacement before final failure increased as well. The increase in displacements with embedment length suggests that the wood would crush, and thus reduces the area to be sheared until the strength of such area to be sheared is equal to the strength of the wood crushing. Therefore, the connection would fail under shear from rod pull-out until the increase in resistance from rod embedment length is greater than the resistance of wood crushing, and then the connection would fail due to wood crushing. The transition from rod pull-out to wood crushing failure is between the 150- and 200-mm embedment lengths. The maximum load only increases slightly with the increase in embedment length for the 38.1-mm (1.5") wide washer, therefore there is a strong correlation of wood crushing with washer size and a weaker correlation of wood crushing with embedment length.

The connection configurations with the 50.8-mm (2.0") wide washer experienced wood splitting failure, rod pull-out failure, and wood crushing failure. Test 150-2.0 had three replicates that experienced wood splitting failures which are shown in between the maximum and minimum

expected loads. The second replicate, test B, experienced a rod pull-out failure with wood splitting failure and is shown slightly above the maximum expected load. Test 200-2.0 had three replicates that experienced rod pull-out failures which are shown to be close to the maximum expected load. The fourth replicate, test D, experienced a wood splitting failure and is shown in between the maximum and minimum expected loads. Test 250-2.0 had two replicates that experienced wood crushing failures, and all test replicates experienced eventual rod pull-out failures close to the maximum load of the wood crushing failures which are shown to be close to the maximum expected load. The connection configurations with the 50.8-mm (2.0") wide washer show the best spread of failure types. The wood splitting failure happens with a larger washer versus a smaller embedment length as shown for Test 150-2.0 replicates. The wood crushing failure happened with a smaller washer versus a larger embedment length as shown for Test 250-2.0 replicates. The rod pull-out failure happened when the washer size and embedment lengths were in a certain proportion to each other in between wood splitting and wood crushing failure. Results of the replicates of Test 200-2.0 and Test 250-2.0 showed that Equation 1 without the resistance factor is a reliable equation when predicting a pure rod pull-out failure.

The connection configurations with the 63.5-mm (2.5") wide washer experienced mainly wood splitting failure. Test 150-2.5 had all replicates experienced wood splitting failure, and their maximum load ranged wide in between the maximum and minimum expected loads. Test 200-2.5 replicates were the strongest connection configurations that exhibited combined wood splitting and rod pull-out failure at the same time, with its weaker replicate experienced a wood splitting failure earlier on. The stronger test replicates that experienced the combined failure modes were close to the maximum expected load of a pure rod pull-out failure. The range of maximum loads for Test 200-2.5 replicate was very large in between the maximum and minimum expected loads since the wood splitting failures were developed at lower loads compared to the combined failures that were developed at higher loads. Test 250-2.5 four replicates exhibited wood splitting failure except for the first replicate, test A, that experienced a pure rod pull-out failure which is why it experienced a very large maximum failure load. The results of the connection configurations with the 63.5-mm (2.5") wide washer showed that there is a strong correlation of wood splitting with washer size and with rod embedment length. The large washer induced a wood splitting failure which is very brittle and spans a large range of maximum loads between the test replicates, as shown in Figure 3.17. The range of wood splitting failures gets smaller for Test 250-2.5 replicates

as it gets closer to the likely hood of a rod pull-out failure. The maximum load increased linearly from Test 150-2.5 replicates to Test 200-2.5 replicates since connection configurations of both test groups experienced wood splitting failures. From Test 200-2.5 replicates to Test 250-2.5 replicates, the maximum load increased slightly, and the range of wood splitting failures decreased since Test 250-2.5 replicates were close to the transition point of wood splitting failure to rod pull-out failure.

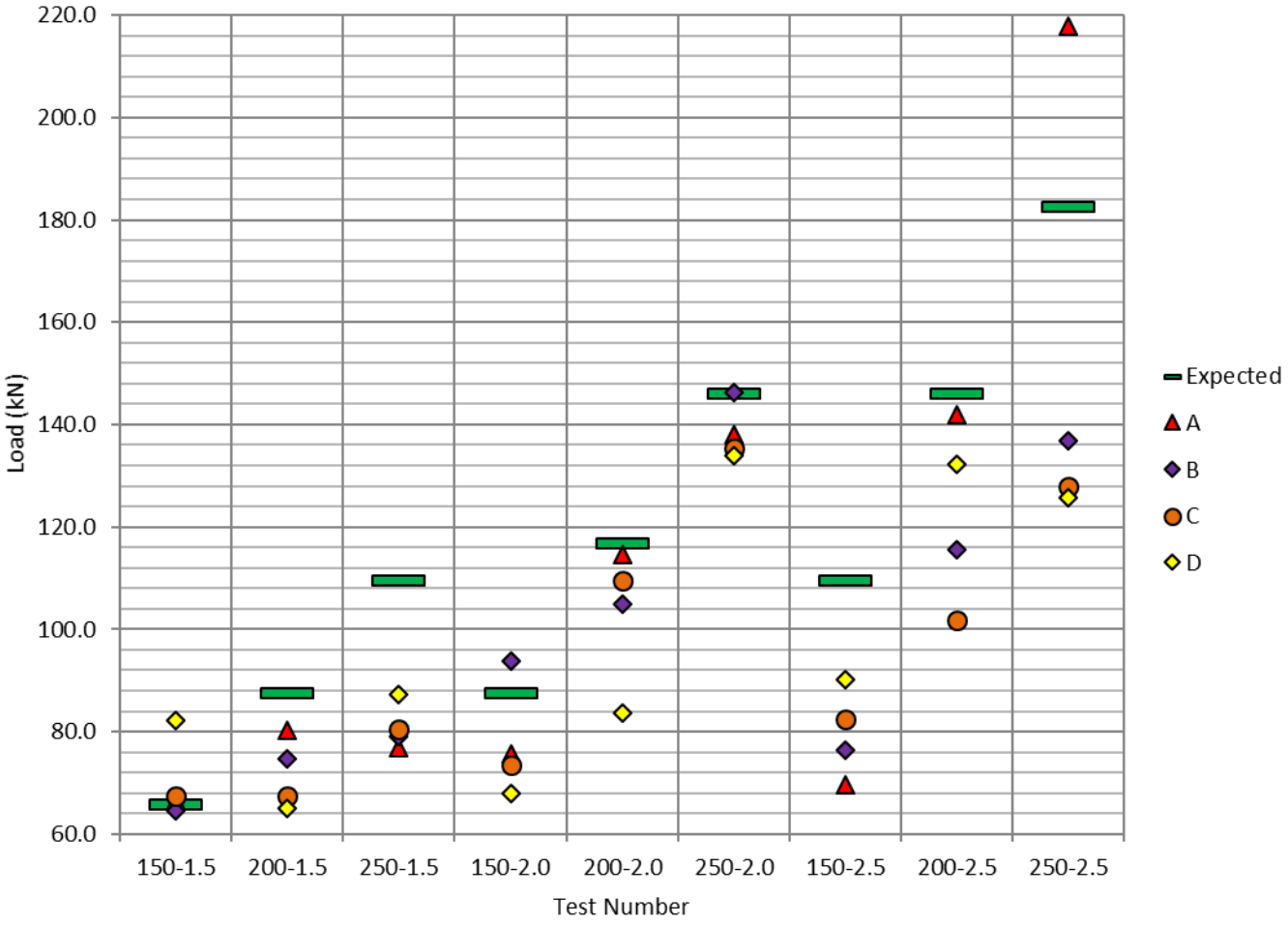

Figure 3.19. Maximum load with changing rod embedment length comparison

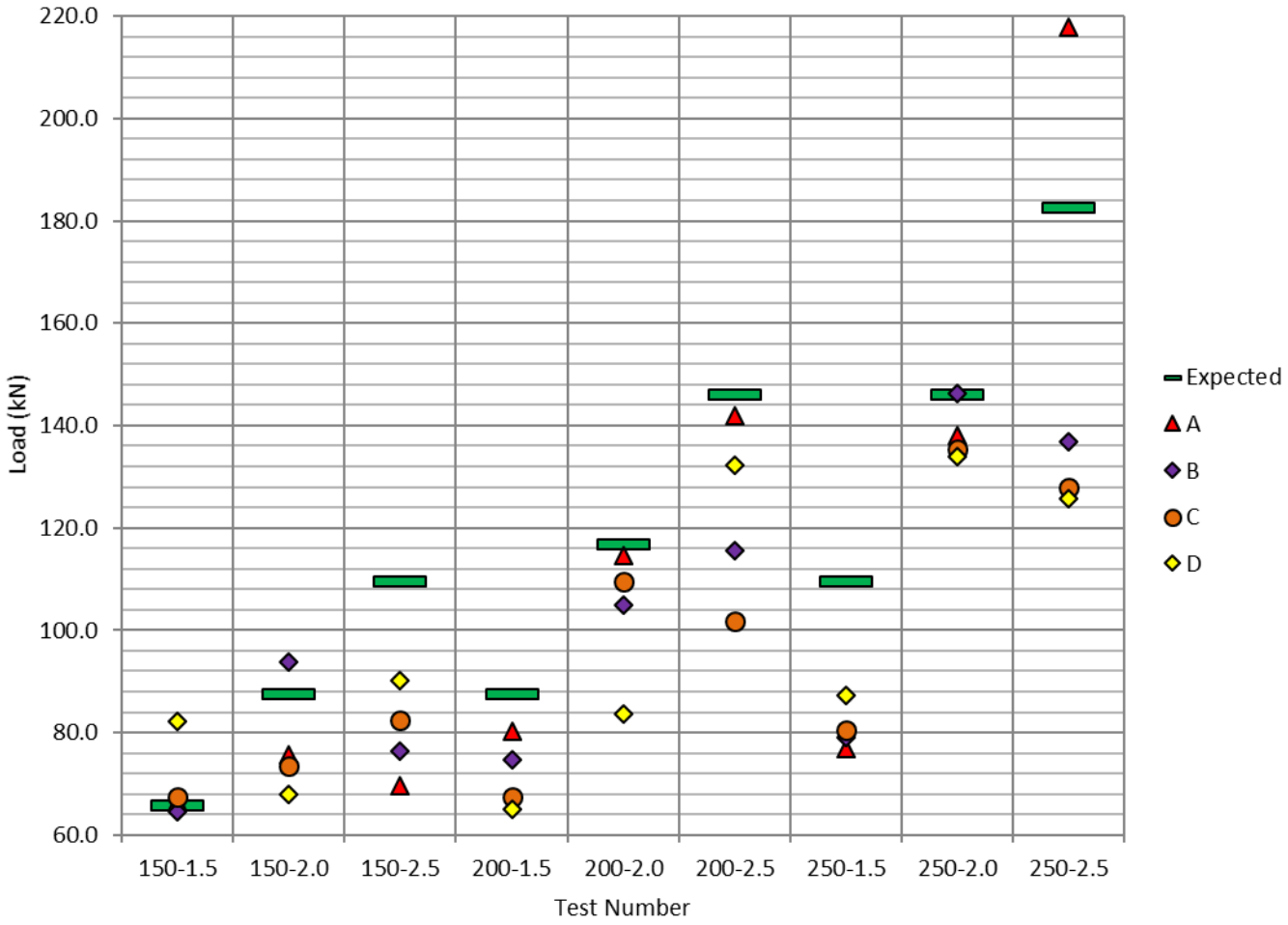

Figure 3.20. Maximum load with changing washer size comparison

Shown in Figure 3.20 are the expected minimum, expected maximum and the actual maximum loads for all tests of each configuration grouped by embedment length. The order of failures with increasing washer size goes from wood crushing to rod pull-out, then to wood splitting failure.

The three different connection configurations with the 150 mm embedment length experienced wood crushing failure, rod pull-out failure, and wood splitting failure. Test 150-1.5 replicates experienced rod pull-out failures with one replicate having a slight signs of wood crushing failure, whereas Test 150-2.0 replicates experienced wood splitting failures with one replicate having a rod pull-out failure. While Test 150-2.5 replicates experienced wood splitting failures. The rod pull-out failure exhibited by the second replicate of Test 150-2.0, test B, occurred at greater maximum load than that of all replicates of Test 150-2.5. This comparison is similar to how the rod pull-out failure of the first replicate of Test 200-2.5, test A, occurred at greater load than that

of all replicates of Test 250-2.5, which experienced wood splitting failures, as shown in Figure 18. The spread in the range of the obtained maximum load for wood splitting failure increases from Test 150-2.0 to Test 150-2.5 since Test 150-2.0 replicates sustained maximum loads that were just greater than that required for the transition from rod pull-out failure to wood splitting failure. This comparison is similar to how the spread in the maximum load range for wood splitting failure increased from Test 250-2.5 to Test 200-2.5, as shown in Figure 3.18.

The connection configurations with the 200 mm embedment length experienced wood crushing failure, rod pull-out failure, and wood splitting failure. Replicates of Test 200-1.5 experienced wood crushing failure, whereas Test 200-2.0 replicates experienced rod pull-out failure except for one replicate which experienced wood splitting failure. While Test 200-2.5 replicates were the strongest and experienced a combined wood splitting and rod pull-out failure at the same time, with the weakest test replicate experienced a wood splitting failure earlier on. There is a slight spread in the range of the obtained maximum load for Test 200-1.5 replicates due to wood crushing, however Test 200-2.5 replicated had a larger spread in the range of the obtained maximum load due to wood splitting being more brittle and unpredictable. The spread in failures highlights again that rod pull-out failure happens when the washer size and rod embedment lengths are in a certain proportion to each other in between wood splitting and wood crushing failures.

The connection configurations with the 250 mm embedment length experienced wood crushing failure, rod pull-out failure, and wood splitting failure. The connection configurations with the 250 mm embedment length showed an excellent spread of failure modes. All replicates of Test 250-1.5 had experienced wood crushing failure, whereas all replicates of Test 250-2.0 had experienced rod pull-out failure except for one replicate which experienced slight wood crushing failure. Test 250-2.5 four replicates had experienced wood splitting failure except for one replicate which experienced rod pull-out failure. The wood crushing failure in Test 250-1.5 replicate shows a slight spread in the range of maximum load between the maximum and minimum expected loads, whereas the rod pull-out failure in Test 250-2.0 replicates shows a sharp increase in maximum load and the spread in the range of the maximum load was very similar to Test 250-1.5 and close to its maximum expected load. The wood splitting failure in Test 250-2.5 shows a slight decrease in the maximum load and the spread in the range of maximum load was very similar to Test 250-2.0. The connection configurations with the 250 mm embedment length showed that the rod pull-out failure is the strongest and has the most consistent maximum failure load.

3.2.4 Summary of test results

Table 3.6 summarizes the results of all experiments using the strong threaded rods. When the average of the closest three replicates of each test with similar failure types was taken into account, Test 150-1.5, Test 200-2.0, and Test 250-2.0 had their maximum loads closest to the maximum expected values. These three connection configurations had experienced rod pull-out failures which explains why their maximum load values are close to the maximum expected loads calculated from Equation 1. The three connection configurations also had on average the smallest standard deviation compared to the other connection configurations. The two connection configurations that experienced mainly wood crushing failure were Test 200-1.5 and Test 250-1.5. The connection configurations that had wood crushing failures had the second closest standard deviation, close to the standard deviation of the configurations that had rod pull-out failures. The other connection configurations that experienced wood splitting failures had the worst standard deviation because wood splitting is brittle and unpredictable. Therefore, a rod pull-out failure is preferred, followed by a wood crushing failure while a wood splitting failure is undesirable.

Table 3.6. Summary of test results for the nine threaded-rod-in-glulam beam configurations

Test configuration ID	Maximum expected load (kN)	Average load (kN)	Average load of closest 3 tests (kN)	Standard deviation (kN)	Standard deviation of closest 3 tests (kN)
150-1.5	65.7	70.18	66.18	7.01	1.24
150-2.0	87.6	77.71	72.34	9.72	3.27
150-2.5	109.5	79.64	76.16	7.50	5.15
200-1.5	87.6	71.86	69.06	5.99	4.05
200-2.0	116.8	103.19	109.69	11.75	3.92
200-2.5	146.1	122.93	129.98	15.45	10.91
250-1.5	109.5	80.92	78.79	3.91	1.47
250-2.0	146.1	138.39	135.76	4.79	1.69
250-2.5	182.6	152.13	130.21	38.20	4.82

3.2.5 Failure modes formula analysis

The splitting failure mode is difficult to express in a formula and unpredictable as shown by the tests with the largest standard deviations of the closest three tests in Table 3.5. More tests will need to be completed to fully understand this failure mode. The wood crushing failure mode has a smaller standard deviation compared to the splitting failure mode and has a similar standard

deviation compared to the rod pull-out failure mode. Therefore, a formula for the wood crushing failure mode is achievable using the data presented in this paper.

The wood directly under the washer is acting as a fully supported column in its resistance to crushing, and the wood along the four edges of the washer are shearing as the wood crushes under the washer. Therefore, a combination of a column formula and the rod pull-out formula were used.

The formula for compressive resistance parallel to the wood grain from the CSA O86-19 standard (Canadian Standards Association, 2014) clause 7.5.8.4.2 is shown in Equation 3.2 below.

Equation 3.2 Compressive resistance parallel to the wood grain:

$$P_r = \phi_c \, F_c \, A K_{Zcg} K_C \qquad \text{Eqn. (3.2)}$$

Where; P_r = Compressive resistance parallel to grain (N), ϕ_c = 0.8 (resistance factor for brittle failure), $F_c = f_c \, (K_D K_H K_{Sc} K_T)$ = factored strength in compression parallel to grain (MPa), f_c = specified strength in compression parallel to grain (MPa), K_D = load duration factor, K_H = system factor, K_{Sc} = service condition factor for compression parallel to grain, K_T = treatment factor, A = cross-sectional area being compressed (mm^2), $K_{Zcg} = 0.68(Z)^{-0.13} \leq 1.0$ = size factor, Z = member volume (m^3), and K_C = slenderness factor.

The formula in Equation 3.2 can be simplified for the special case of the wood crushing failure. The specified strength in compression parallel to grain for the glulam beam, f_c, equals 33.0 MPa according to a technical note published by Nordic Structures (Nordic Wood Structures, 2015). The glulam beam sections were tested under quick loading till failure (less than seven days); therefore, the load duration factor, K_D, equals 1.15 as per Clause 7.4.1 in the CSA O86-14 standard (Canadian Standards Association, 2014). The wood crushing under the washer is only being considered as one column; therefore, the system factor, K_H, equals 1.0 as per Clause 7.4.3. The beam sections were under dry service condition and were untreated; therefore, the service condition factor, K_{Sc}, and the treatment factor, K_T, both equal 1.0 as per Clause 7.4.2 and Clause 7.4.4, respectively. The volume of the column under the washer being considered is always under 0.05 m^3; therefore, K_{Zcg} will always equal 1.0. The column being considered under the washer is fully supported since the washer is bearing in the middle of a section of glulam larger than the washer on all sides of the washer; therefore, the slenderness factor, K_C, equals 1.0 as per Clause 7.5.8.5. The ϕ_c resistance

factor is ignored for the testing comparison. Using all the aforementioned values in Equation 3.2 results in Equation 3.3 as shown below.

Equation 3.3 Simplified compressive resistance parallel to the wood grain:

$$P_r = f_c K_D A \qquad \text{Eqn. (3.3)}$$

The maximum expected values associated with compression parallel to the grain under the washer were calculated as shown in Table 3.7.

Table 3.7. Threaded-rod-in-glulam section expected tensile and compressive forces

Test configuration ID	Washer size (mm)	Maximum expected PR force (kN)	Maximum expected compression force (kN)
Test 150-1.5	38.1	65.7	42.4
Test 150-2.0	50.8	87.6	85.2
Test 150-2.5	63.5	109.5	140.3
Test 200-1.5	38.1	87.6	42.4
Test 200-2.0	50.8	116.8	85.2
Test 200-2.5	63.5	146.1	140.3
Test 250-1.5	38.1	109.5	42.4
Test 250-2.0	50.8	146.1	85.2
Test 250-2.5	63.5	182.6	140.3

The wood crushing failure is being resisted by both compression parallel to the grain and shear along the four edges of the washer; therefore, the strength of the wood crushing failure is a combination of these two resistances. Since the wood under the washer is being crushed, it is assumed that the full value of the compression parallel to the grain is resisting the applied load; therefore, only a fraction of the shear resistance is resisting the load. The formula that best fits the tests that experienced wood crushing failure is shown in Equation 3.4.

Equation 3.4 Wood crushing failure formula:

$$WC_r = P_r + PR \times \frac{3}{8} \qquad \text{Eqn. (3.4)}$$

Where; WC_r = Wood crushing resistance under the washer (N), P_r = Compressive resistance parallel to grain (N), and PR = Pull-out resistance of threaded rod in glulam (N).

The full resistance for compression parallel to the wood grain was used and trying different fraction combinations of the shear resistance found that using 3/8 of the resistance for shear fits best with the connections that failed due to wood crushing, as shown by the grouping of the tests around the maximum expected values, which are shown in Figure 3.21. The results for the expected wood crushing failure are shown in Table 3.8.

Table 3.8. Threaded-rod-in-glulam section expected wood crushing forces

Test configuration ID	Maximum expected PR force (kN)	Maximum expected comp force (kN)	Maximum expected wood crush force (kN)
Test 150-1.5	65.7	42.4	67.0
Test 150-2.0	87.6	85.2	118.1
Test 150-2.5	109.5	140.3	181.4
Test 200-1.5	87.6	42.4	75.3
Test 200-2.0	116.8	85.2	129.1
Test 200-2.5	146.1	140.3	195.1
Test 250-1.5	109.5	42.4	83.5
Test 250-2.0	146.1	85.2	140.0
Test 250-2.5	182.6	140.3	208.8

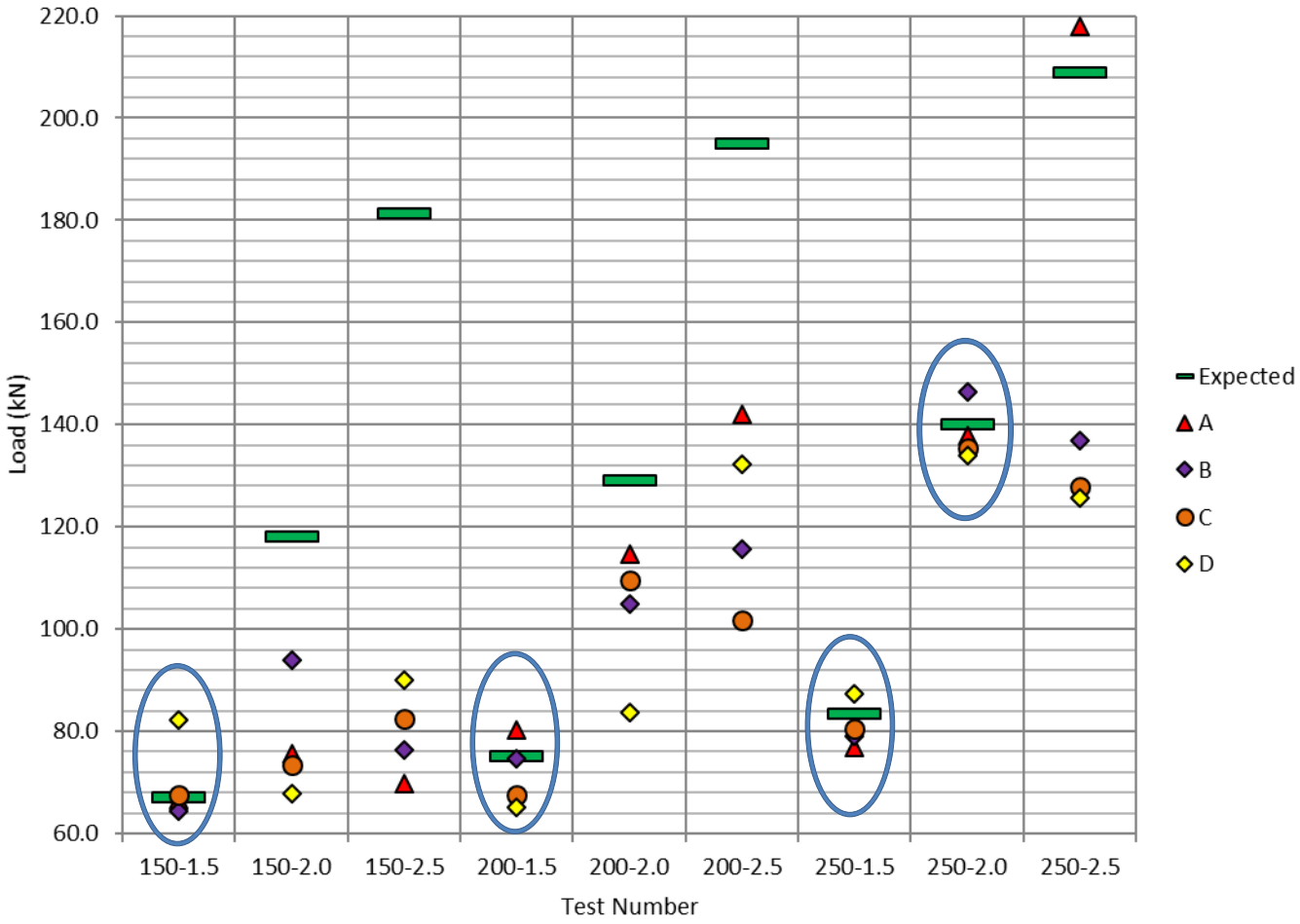

Figure 3.21. Maximum load for expected wood crushing failure

The three tests configurations that utilized the 38.1-mm (1.5") wide washer experienced the wood crushing failure along with one test from Test 250-2.0. The test configurations with the largest washer size of 63.5-mm wide had their expected wood crushing failure well above the actual results since the amount of wood resisting crushing far surpassed its probability to split. From these results, it shows that the formula presented in Equation 3.4 for wood crushing failure is very plausible, but more tests will need to be completed to prove its validity.

3.2.6 Ductile steel failure

From the experimental results of the strength of the wood, a connection could be designed so that the steel component would yield before the wood experiences any deformation. The connection configuration used was Test 250-2.0 which had an average maximum load of 135.76 kN. The steel rod used had a grade of SAE J429-Grade 2 and a yielding tensile force of 90.0 kN. When Test

250-2.0-AR was conducted, only the steel rod deformed and broke while the wood section experienced no noticeable deformation, as shown in Figure 3.22. Figure 3.23 shows the load versus displacement curve for Test 250-2.0-AR, and the curve follows a similar trend to how a steel rod yields during a tension test. Test 250-2.0-AR proves that a predictable failure in the steel can be achieved once the strength and failure mode of the wood is known.


(a)

(b)

Figure 3.22. Yielded steel rod and non-deformed glulam section: (a) Steel rod broken in glulam; (b) Fractured steel rod.

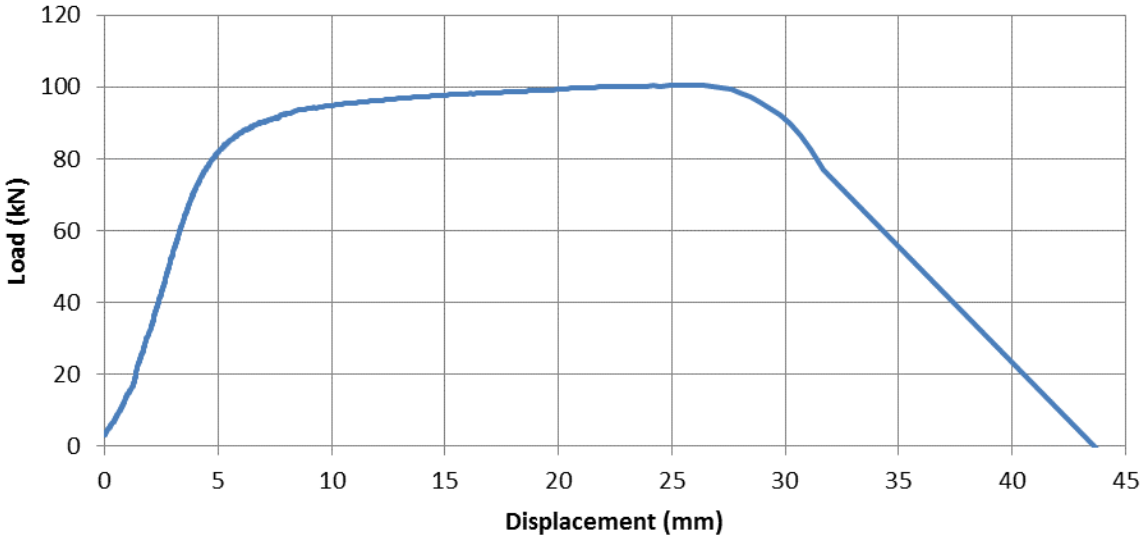

Figure 3.23. Load-displacement relationship for Test 250-2.0-AR

3.3 Conclusions

Based on the obtained experimental results and analysis performed afterwards, the formula shown in Equation 3.1 is highly plausible for pure rod pull-out failures, whereas the formula shown in Equation 3.4 is plausible for wood crushing failures, but more tests need to be performed to confirm their validity. It should be noted that these equations have only been tested on glulam beams with a homogenous layup and tests should be done on other types of glulam beams to confirm their validity. The following conclusions have been drawn:

- Keeping an embedment length versus a washer size ratio of around 100 mm and 125 mm to 25.4 mm (1.0”) provides a more predictable failure mode of rod pull-out and a more predictable failure load with the least amount of deviation.
- Keeping the embedment length slightly larger compared to the washer size will keep the failure mode closer to a wood crushing failure which is more consistent and predictable.
- Having a larger washer size compared to embedment length is not recommended because the failure mode will be closer to a wood splitting failure which is more brittle and unpredictable compared to a wood crushing failure.
- With an understanding of how the wood section would fail, a connection can be designed so that its metal components would yield before the wood experiences any damage as shown in Test 250-2.0-AR.

With the information from the rod pull-out series of tests, the four optimum and predictable configurations were selected to be used for the moment resisting beam-to-column connection. Those four configurations include 200-1.5 and 250-1.5 which failed due to wood-crushing under the washer, and 200-2.0 and 250-2.0 which failed due to rod pull-out.

Chapter 4 Ambient Temperature Moment Connection Testing

4.1 Introduction

Four different connection configurations of mechanically fastened steel rods in glulam sections were experimentally examined, with each test assembly tested twice (A and B) to verify results. Test variables for the connection configurations included rod embedment length and size of the square washer. Using the collected load-displacement data, the connection's strength and stiffness were determined, and the connection failure modes were observed and documented.

4.1.1 Materials

4.1.1.1 Glulam sections

The glulam beam sections used were the exact same as described in section 3.1.1.1 of this thesis.

4.1.1.2 Threaded rods

The threaded rods used in the experiments had a diameter of 19.05 mm (3/4 inch), length of 910 mm, and stress grade of SAE J429-Grade 2 which is the common grade used for wood construction. Using a band saw, the rods were cut into pieces of 470-mm and 520-mm long that were used in the test assemblies of 200 mm and 250 mm embedment lengths, respectively. The remaining cut off rod sections were prepared and used as tension coupons, and thus were tested to confirm the stress grade of the rods. The average yield tensile force exerted by the rods was recorded at 90 kN, confirming the rods stress grade.

4.1.1.3 Washers

The washers used for the experiments were fabricated from a 12.7-mm thick steel flat bar with a stress grade of 300W, as specified by CSA G40.20-04/G40.21-13 (Canadian Standards Association, 2013). There were four washers fabricated: two were 38.1 x 38.1 mm (1.5 x 1.5 inches); and two were 50.8 x 50.8 mm (2.0 x 2.0 inches). A hole of 20.6 mm (13/16 inch) diameter was drilled in the centre of each washer.

4.1.2 Test assembly details and fabrication process

The two threaded rods employed in the glulam beam pilot connection configuration had embedment lengths of either 200 or 250 mm. Every beam section had a line marked perpendicular to the wood grain at the required embedment length, and a line marked parallel to the grain down the centre of the beam wide face. Two lines were then marked parallel to the grain, and each one was offset 80 mm on either side of the centre line. Next, two little rectangles were marked directly below the embedment length line and centred on each of the offset lines. Rectangles measured 41.3 mm (1-5/8 inches) wide for the 38.1 mm square washer and 54.0 mm (2-1/8 inches) wide for the 50.8 mm square washer, and 30 mm thick to accommodate the washer and nut were marked, as shown in Figure 4.1. All rectangles were then carved out into a rectangular prism using wood chisels to a depth of approximately 87 mm for the 38.1 mm square washer and 93 mm for the 50.8 mm washer, as shown in Figure 4.2(a). A 20.6-mm (13/16") diameter hole was then drilled in line and centred of each carved out hole on the 314-mm wide face and centred on the 135-mm wide face at the end of the beam section to the required embedment length using a precise portable drilling station as shown in Figure 4.2(b).

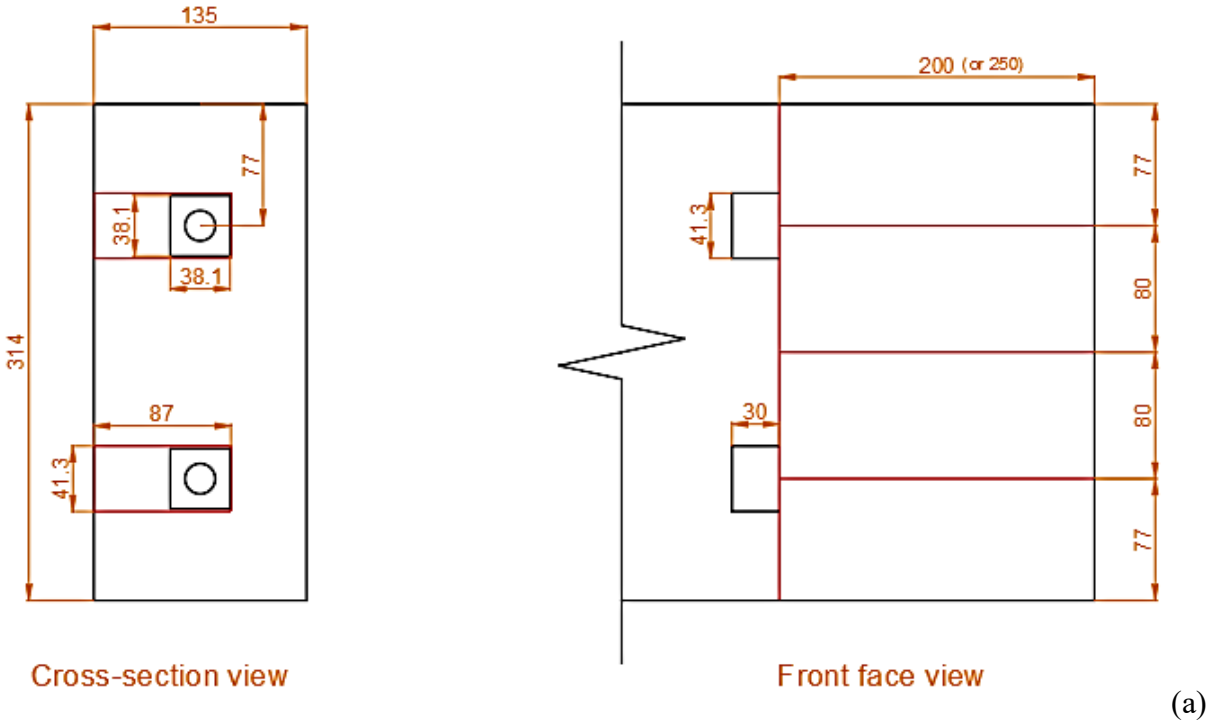

(a)

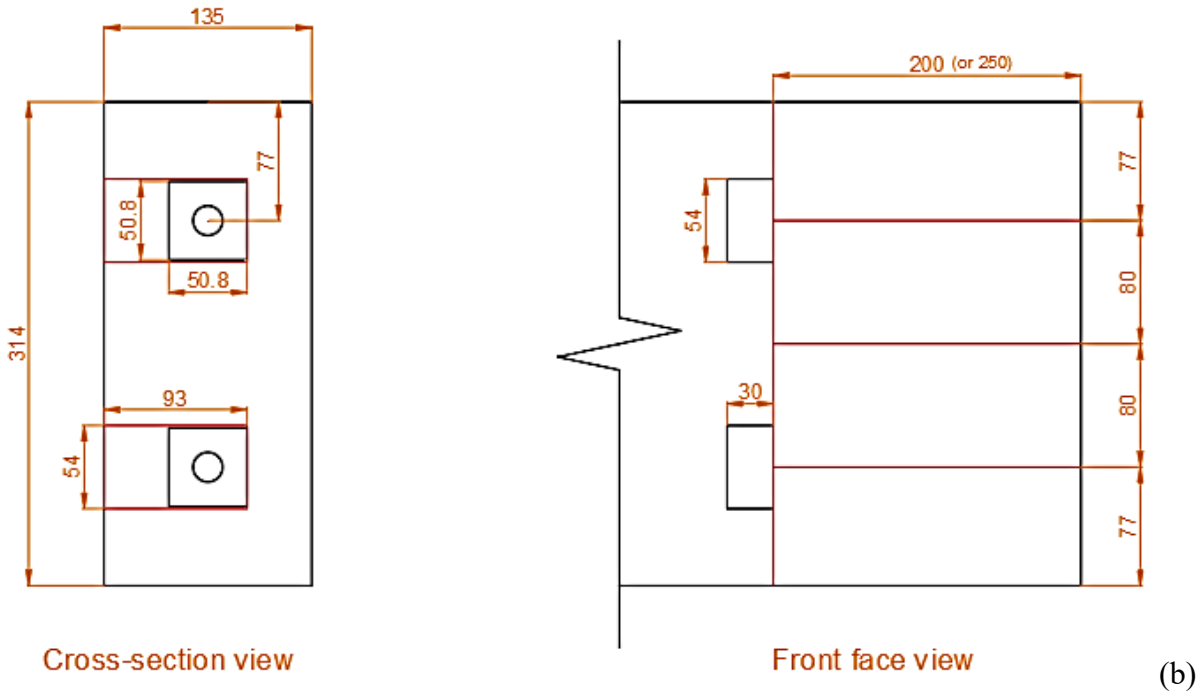

(b)

Figure 4.1. Connection configurations: (a) Connection configuration with 38.1 mm square washer; (b) Connection configuration with 50.8 mm square washer.

(a)

(b)

Figure 4.2. Preparation of beam: (a) A beam section being chiselled; (b) A beam section being drilled.

4.1.3 Test assembly design

The rod pull-out tests performed earlier helped determine the optimal embedment length and washer size configurations to be used. From the individual rod pull-out strength tests, the four configurations that yielded the most predictable results were selected for the beam-to-column connection configurations. With the beam-to-column connection experiencing a bending moment, the top rod in the connection was subjected to tension; a lower portion of the wood section was subjected to compression; and the bottom rod was subjected to minimal tension since it is close to the neutral axis of the connection. Using the results from the rod pull-out tests as the top tension rods strength, the moment-resisting capacity of the connection was possible to be calculated. For ease of calculation, the bottom rod was not included as it would add very little to the connections capacity.

The compression force at the bottom of the connection is calculated based on the factored compression resistance of glulam parallel to grain as per Clause 7.5.8.4 of the CSA O86-14 standard (Canadian Standards Association, 2014). Several modifications factors are applied to the compression resistance formula to accurately determine the actual compression strength, but most of them can be omitted or equal to 1.0 due to the nature of the connection. For example, the size factor, K_{Zcg}, can be omitted because the amount of wood being compressed is very small, and this factor only changes when dealing with large volumes. The slenderness factor, K_C, can be omitted since only a small area of the section is under compression and is fully supported along the connection's neutral axis. The load duration factor, K_D, equals 1.15 as per Clause 12.2.1.6 in the CSA O86-14 standard (Canadian Standards Association, 2014) because the glulam beam sections were tested under quick loading till failure (less than seven days). The system factor, K_H, equals 1.0 since only an individual connection is being tested and not a system. The service condition factor, K_{Sc}, and the treatment factor, K_T, both equal 1.0 as per Clause 12.2.1.5 and Clause 12.2.1.7, respectively because the beam sections were under dry service condition and were untreated.

The specified parallel-to-the grain compressive strength for the glulam beam, f_c, equals 33.0 MPa according to a technical note published by Nordic Structures (Nordic Wood Structures, 2015). The area being compressed (a x b) is the compression block on the bottom of the connection where (a) is the compression block height and (b) is the compression block width which is 135 mm. The final value to account for is the resistance reduction factor, ϕ_c, which equals 0.8 as per Clause

7.5.8.4.2. Combining all the above-mentioned values helped in determining the force that the compression block can resist (C), as shown in Equation 4.1.

Equation 4.1 Compression block resistance:

$$C = \phi_c f_c (K_D K_H K_{Sc} K_T) a \cdot b \qquad \text{Eqn. (4.1)}$$

With the values inserted into Equation 4.1, the formula can be simplified to $C = \phi F_c a.b$; where F_c equals the factored compressive resistance parallel to the grain which equals 37.95 MPa. With the tension force equalling the compression force in the connection, the compression block height, a, can be calculated. Finally, the connection moment resistance, M_r, can be calculated using Equation 4.2 with the assistance of Figure 4.3.

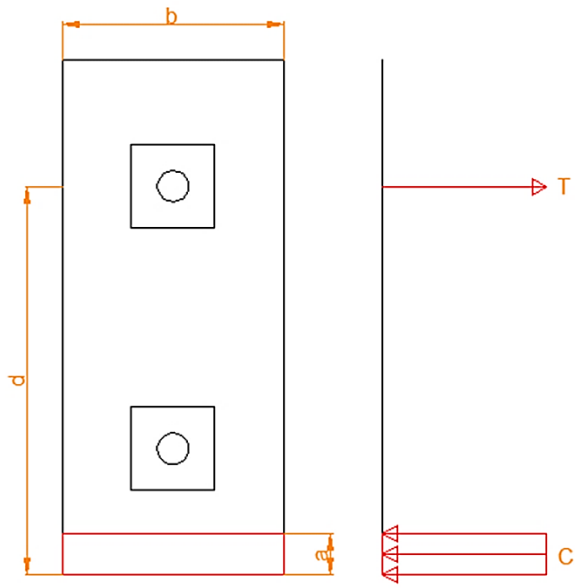

Figure 4.3. Beam end cross section and stress diagram

Equation 4.2 Moment resistance formula:

$$M_r = T (d - 0.5a) \qquad \text{Eqn. (4.2)}$$

Where; M_r = connection moment resistance (N.mm), T = tension force in top rod (N), d = distance from midpoint of tension force to bottom of beam, a = compression block height (mm).

From the previous tension tests done on individual steel rods in glulam sections, the tensile strengths at failure along with the calculated maximum moment resistances are shown in Table

4.1. The failure mode of the tension tests with the 38.1 mm washer was crushing of wood under the washer, which was same as the predicted failure mode for the top rod of the two test configurations with the 38.1 mm washer. The two test configurations with the 50.8 mm washer had their expected tensile forces over 90 kN which was the average yield strength of the steel rods; therefore, the steel strength was used to calculate the connection moment resistance. The steel rods yielding tensile strength were 90 kN and ultimate tensile strength was 104 kN. Also, the predicted failure mode of the top rod was steel rod yielding.

Table 4.1. Concealed beam-to-column connection tests matrix

Test configuration ID	Test replicates	Embedment length (mm)	Washer size (mm)	Average tensile force (kN)	Maximum moment resistance (kN.m)
Test-BC 200-1.5	2	200	38.1	71.9	16.4
Test-BC 200-2.0	2	200	50.8	103.2 (steel 104.0)	23.3 (20.3 yielding)
Test-BC 250-1.5	2	250	38.1	80.9	18.4
Test-BC 250-2.0	2	250	50.8	138.4 (steel 104.0)	23.3 (20.3 yielding)

Notes: For the test configuration ID; 200 and 250 are the rod embedment lengths in (mm); 1.5 and 2.0 are the square washer size in (inches). BC stands for Beam-to-Column.

4.1.4 Tests setup and procedure

The cantilever beam was held in place with a crane so that the beam end could be attached to a strong steel support in a Universal Testing Machine (UTM). The two steel rods were inserted through the column and into the beam end, then each rod end was fastened using a steel nut and square washer desirable for the configuration being tested. A rigid steel strip was attached on the underside of the beam and placed 200 mm from the column face to allow the installment of a Linear Variable Differential Transducer (LVDT), labelled T1, which was then used to measure the beam vertical displacements that were then used to calculate the rotations of the beam. A second steel strip was placed inline and perpendicular to the top tension rod with another LVDT, labelled T2, against that strip to measure the gap between the beam end and the supporting column at the top tension rod. A third steel strip was attached to the underside of the beam but at a distance of 1400 mm from the column face with a Draw-wire Displacement Transducer, labelled T3, attached to it to measure the beam vertical displacements inline with where the load was applied. A pinned steel attachment was placed between the UTM crosshead and the top side of the beam at a distance of 1400 mm from the column face so the load would always be applied at the same spot as the

beam rotated. Once the displacement measuring transducers were in place and zeroed, the test assembly was loaded at a rate of about 8.0 kN per minute. The test was terminated when the glulam beam achieved failure with no additional load gain. The full test setup of a general assembly is shown in Figure 4.4.

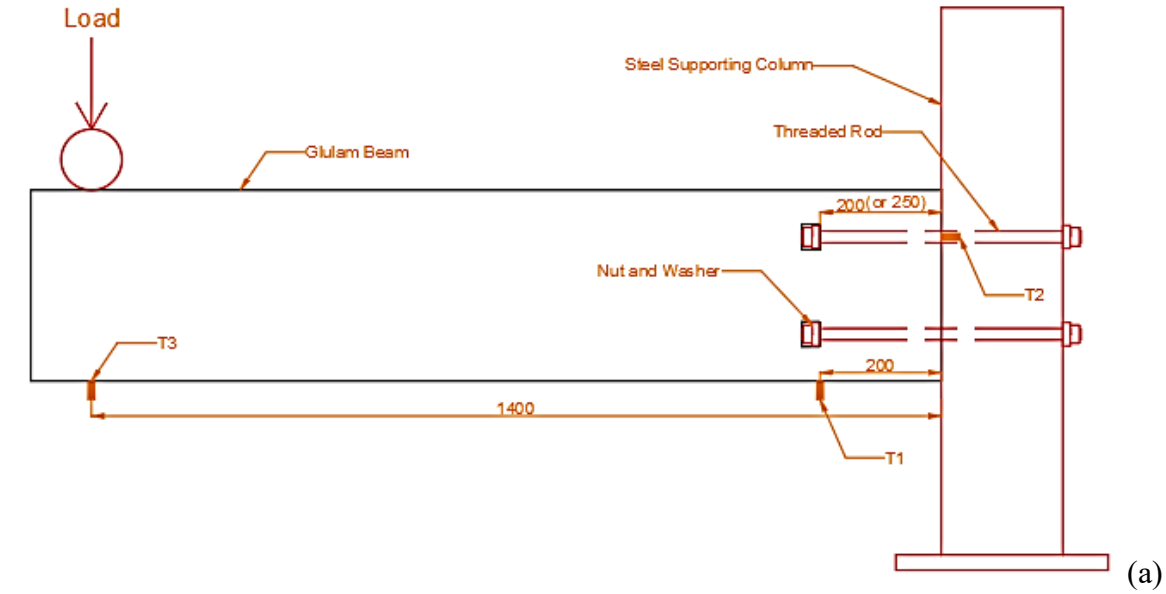

(a)

(b)

(c)

Figure 4.4. Full test setup of a general beam-column connection test assembly: (a) Full test assembly diagram; (b) Front side of assembly setup; (c) Back side of assembly setup.

4.2 Experimental Results and Discussion

The experimental results presented in this chapter were the displacements measured by the LVDT located at 200 mm from the column face, labelled T1, which was used to calculate the beam rotation, and the associated loads that were applied and then were used to calculate the moment magnitudes on the beam end connection.

The initial stiffness's, yielding moments, and maximum moments were determined using the method developed by Yasumura and Kawai (1998) instead of other methods as it was found to provide the most consistent results for different types of timber beam connections. Following this method, the connection initial stiffness, $K_{10\text{-}40}$, is calculated between 10% and 40% of the maximum load. The yielding moment of the connection is estimated based on determining the intersection of the initial stiffness line (the tangent to the moment-rotation curve from the zero point) and the straight line drawn offset and parallel to the secant line plotted between 40% and 90% of the peak load. This point of intersection is then projected horizontally onto the moment-rotation curve to determine the yielding rotation of the connection. Finding the point of intersection is demonstrated in Figure 4.5.

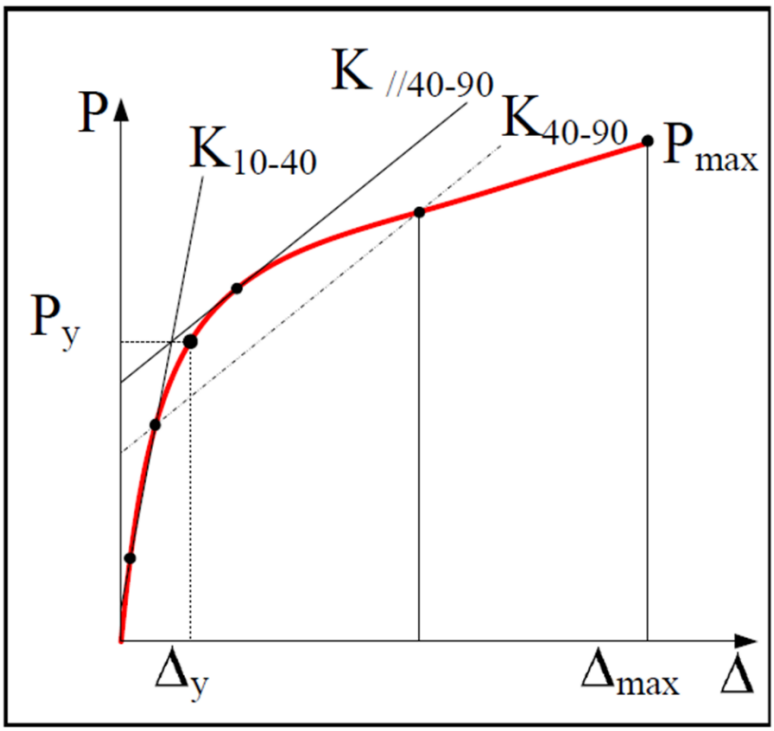

Figure 4.5. Yasumura and Kawai method for finding yielding moment (Muñoz et el., 2008)

The peak moment and rotation of the connection were based on the maximum load sustained by the connection before an appreciable load drop, greater than 5%, occurred in conjunction with observable brittle failure in the wood around the connection. The failure rotation was based on the maximum rotation sustained before either fracture failure in the steel rod or brittle failure in the wood occurred. The ductility ratio was determined using the rotation values measured at the yielding moment and failure rotation as opposed to the deformation ratio which uses the rotation values measured at the yielding and maximum moments. The reason for the use of the ductility ratio instead of the deformation ratio was that the connection did not have a brittle failure in the wood occur once the maximum moment was reached. Instead, some of the connections had the steel rod fail by yielding and some of the connections had the wood under the washer compress into the beam for a significant displacement before a brittle failure occurred.

4.2.1 Failure modes

The primary failure mode for the tests with the 38.1 mm (1.5 inches) washer was wood crushing under the washer of the top steel rod, as shown in Figure 4.6(a), which confirms the prediction from the previous tension tests performed prior to this study. For this failure, the top washer compressed into the wood by an average of 40 mm, whereas the bottom washer compressed into the wood by an average of 10 mm, as shown in Figure 4.6(b). There was no shear rod pull-out or beam splitting observed at the end of the connection, as shown in Figure 4.6(c). The compression block width, a, was observed and measured between 17 to 21 mm for all the tests with the 38.1 mm washer, as shown in Figure 4.6(d).

(a)

(c)

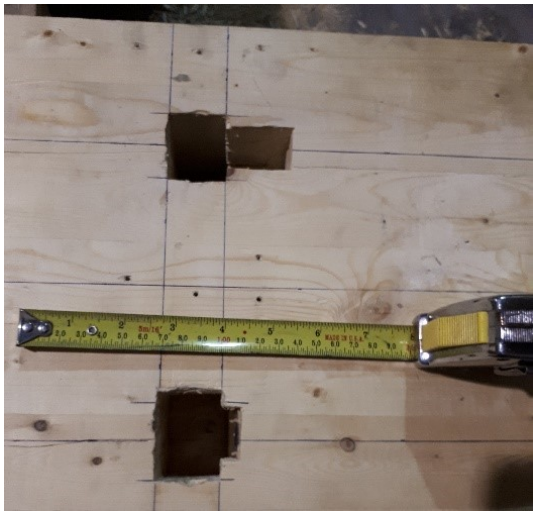

(b)

(d)

Figure 4.6. Test failures of BC with 38.1 mm (1.5 inch) washer: (a) Top and bottom washers after failure; (b) Depth of top and bottom washer compressed into wood; (c) Rotation of beam end; (d) Width of compression block.

Test-BC 200-1.5-A failed similar to the other tests with a 38.1 mm washer, except at the end when the top rod failed by shear rod pull-out as shown in Figure 4.7(a). The reason for the pull-out failure was that the 200 mm embedment length has less wood surrounding it to resist shearing along the edges of the washers compared to the 250 mm embedment length. As a result, test configuration 200-1.5 has a chance for the wood to shear along the washer's edges once compressed into the wood which shortens the embedment length of the amount of wood resisting shear forces. As shown in Figure 4.7(b), the wood under the washer only compressed 20 mm when compared to the 40 mm that the other tests with the 38.1 mm washer experienced.


(a)

(b)

Figure 4.7. Test-BC 200-1.5-A failure: (a) Top rod shear pull-out failure; (b) Compressed depth of top washer into wood.

The primary failure mode for the tests with the 50.8 mm (2.0 inches) washer was yielding of the top steel rod, as shown in Figure 4.8(a), which confirms the prediction from the previous tension tests performed prior to this study. A crack was observed to form along the face of the beam on each side in line with the bottom rod, just above the compression zone, as shown in Figure 4.8(b). Figure 4.8(c) shows the top washer having no noticeable deformation or compression into the wood. Figure 4.8(d) shows the bottom washer having no noticeable deformation, but the washer did compress into the wood slightly along the bottom edge.


(a)


(b)

(c)

(d)

Figure 4.8. Failures of Test-BC connection with 50.8 mm (2.0 inch) washer: (a) Connection end with top rod snapped; (b) Crack along face of beam just above compression zone; (c) Top washer with no deformation to wood, (d) Bottom washer with little deformation to wood.

Test-BC 250-2.0-B failed similar to the other tests with a 50.8 mm washer, except at the end when the top rod had the washer compressed into the wood before the rod snapped as shown in Figure 4.9(a). Figure 4.9(b) shows that the top steel rod yielded at the intersection where the washer was bearing against the wood. Since the steel rod yielded at the washer-wood interface, it could have caused slightly more rotation at that point which would have made the washer apply more pressure along one edge instead of along the entire surface. The uneven pressure would then cause the washer to start compressing into the wood allowing for the beam to endure a greater rotation than the other tests with the 50.8 mm washer. As shown in Figure 4.9(c), the beam experienced no cracks along the face just above the compression zone. Since the beam was allowed to rotate more due to the washer compressing the wood, the force was distributed more towards the steel yielding allowing the wood in the compression zone not to crack. The compression block width, a, was observed and measured between 25 to 30 mm for all the tests with the 50.8 mm washer, as shown in Figure 4.9(d).

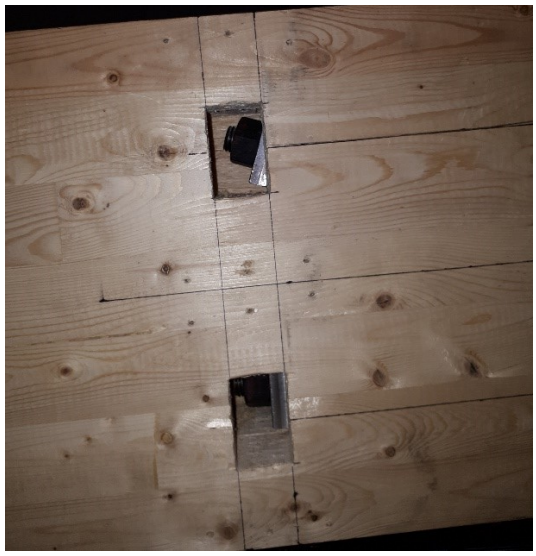

(a)

(b)

(c)

(d)

Figure 4.9. Test-BC 250-2.0-B failure: (a) Top and bottom washers after failure; (b) Top rod snapped at edge of washer; (c) Compression of wood with no cracks in compression zone; (d) Width of compression block.

4.2.2 Moment-rotation relationships

The moment versus rotation relationships shown in Figure 4.10 show that most of the connections have a considerable degree of ductility. The four tests with the 50.8 mm washer failed due to the steel rod yielding, and most of those assemblies failed at a connection rotation over 0.1 radians. Whereas, the four tests with the smaller washer (38.1 mm) failed due to wood crushing under the washer, and all were more ductile than the tests with the steel rod yielding failure with most tests failing over 0.175 radians. The general trend shows the connections with the larger washer (50.8 mm) have greater stiffness and moment resistance compared to those with the smaller washer (38.1

mm), however the connections with the smaller washer have higher ductility ratios. All tests have the yielding moment at around 0.02 radians.

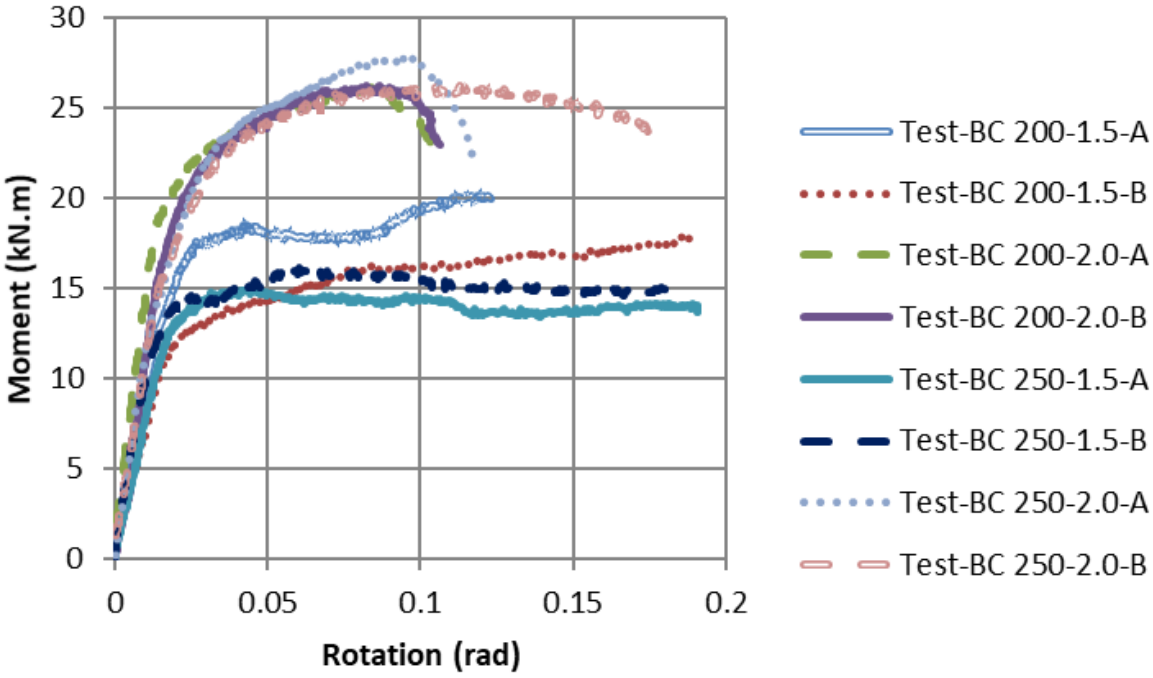

Figure 4.10. Moment versus rotation relationships for all eight tests

Figure 4.11 shows the effect of increasing the washer size from 38.1 mm to 50.8 mm on the moment-rotation relationships for the connections that utilized steel rods of 200 mm embedment length. It was noticed that the increase in the washer size increased the connection yield moment capacity by about 35% (from an average of 12.77 to 17.28 kN.m), and the connection maximum moment by about 38% (from an average of 18.98 to 26.16 kN.m). The failure mode also changed with the increase of the washer size from wood crushing under the washer to steel rod yielding. The average ductility ratio of the connections with the 50.8 mm washers, which failed due to steel rod yielding, was 7.40 while those with the smaller washers (38.1 mm), which failed due to wood crushing, had an average ductility ratio of 8.49. The failure mode for Test-BC 200-2.0 connections was steel rod yielding, which was very predictable and explains why their moment-rotation curves are very similar. While the failure mode for Test-BC 200-1.5 connections was wood crushing under the washer, except for Test-BC 200-1.5-A connection which experienced a shear rod pull-out failure at the end, as shown in Figure 4.7(a). The shear rod pull-out failure explains why Test-BC 200-1.5-A connection had a higher moment resistance and a lesser ductility ratio when compared to Test-BC 200-1.5-B connection.

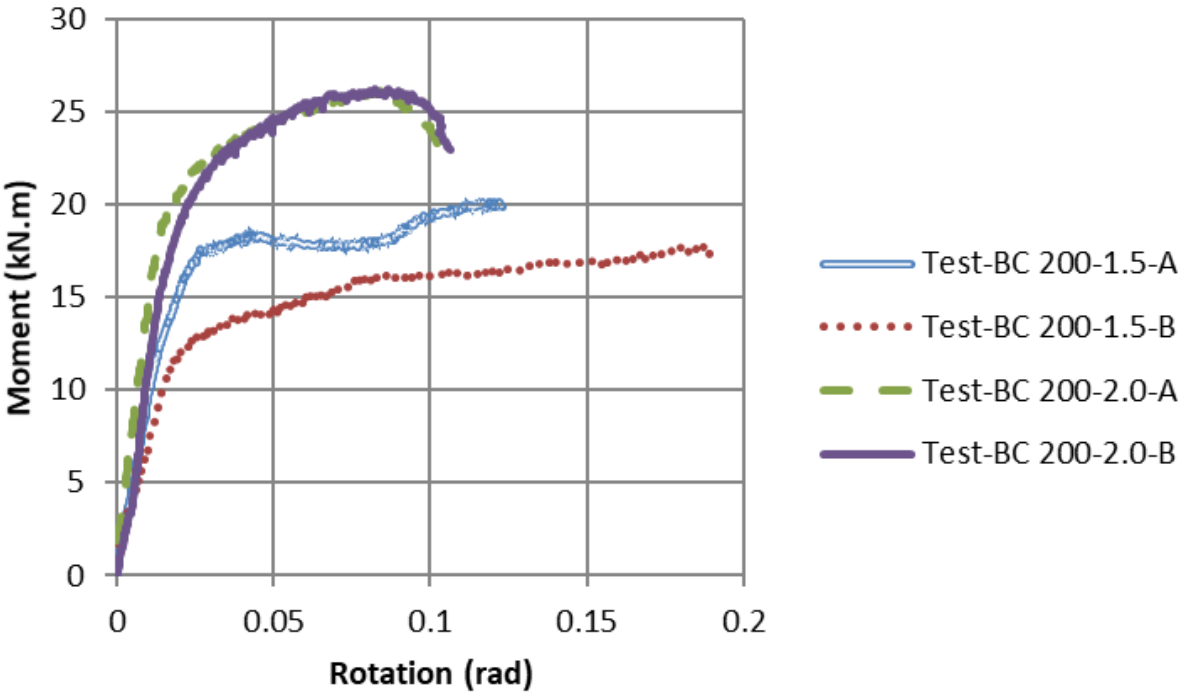

Figure 4.11. Moment-rotation relationships for Test-BC 200-1.5 versus 200-2.0

Figure 4.12 shows the effect of increasing the washer size from 38.1 mm to 50.8 mm on the moment-rotation relationships for the connections utilized steel rods of 250 mm embedment length. It was noticed that the increase in the washer size increased the connection yield moment capacity by about 58% (from an average of 10.51 to 16.60 kN.m), and the connection maximum moment by about 74% (from an average of 15.56 to 27.03 kN.m). Similar to the connections with 200 mm embedment length, the failure mode of the connections with longer rod embedment length changed with the increase of the washer size from wood crushing under the washer to steel rod yielding. The average ductility ratio of the connections with the 50.8 mm washers, which failed due to the steel rod yielding, was 8.25; while the connections with the smaller washers (38.1 mm), which failed due to wood crushing, had an average ductility ratio of 15.17. The failure mode for both Test 250-1.5 connections was wood crushing under the washer, which was why their moment-rotation curves are very similar. The failure mode for Test-BC 250-2.0 connections was steel rod yielding, except for Test-BC 250-2.0-B connection which experienced wood crushing under the washer at the end of the test, as shown in Figure 4.9(a). The wood crushing under washer combined with the rod yielding failure explains why Test-BC 250-2.0-B connection had a similar ductility ratio as the connections of Test-BC 250-1.5, and had higher ductility ratio when compared to Test-BC 250-2.0-A connection.

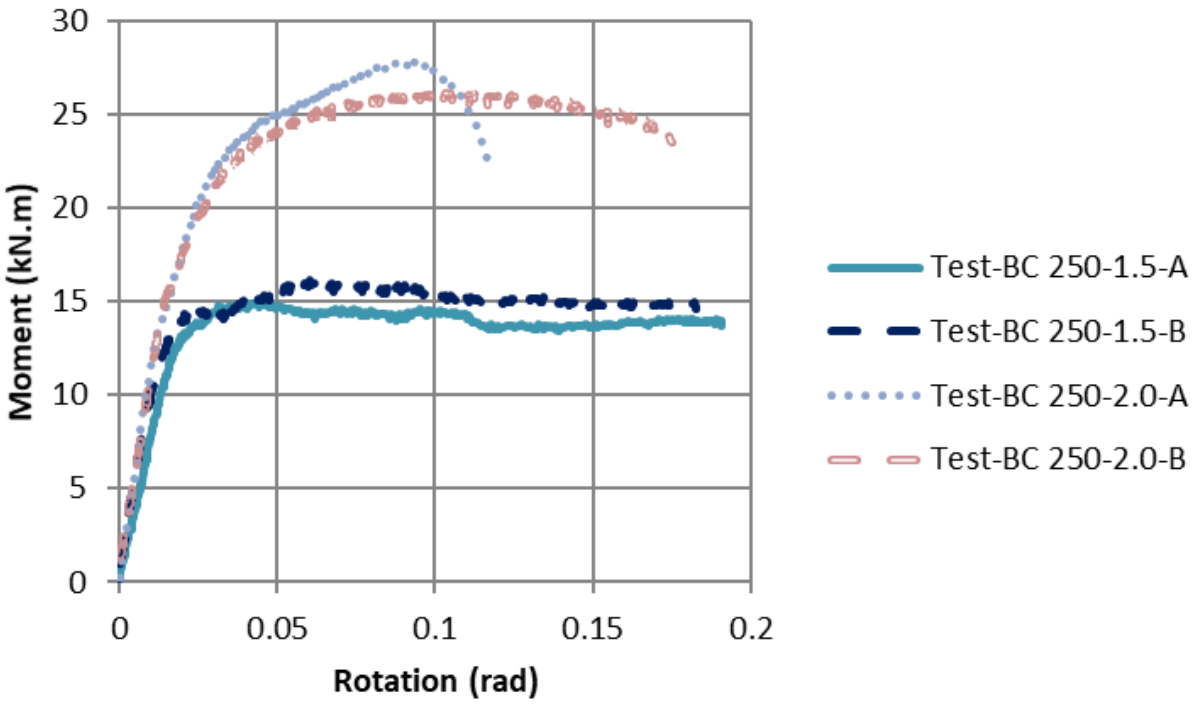

Figure 4.12. Moment-rotation relationships for Test-BC 250-1.5 versus 250-2.0

Figure 4.13 shows the effect of increasing the steel rod embedment length from 200 to 250 mm for the connections that utilized the smaller washers (38.1 mm). It was noticed that increasing the rod embedment length decreased the connection yield moment capacity by about 18% (from an average of 12.77 to 10.51 kN.m). The increase of the rod embedment length also decreased the connection maximum moment by about 18% (from an average of 18.98 to 15.56 kN.m). However, the failure mode stayed the same for connections with both embedment lengths as wood crushing under the washer. The average ductility ratio of the connections with the 200 mm rod embedment length was 8.49, while it was 15.17 for the connections with longer embedment length of 250 mm. The ductility ratios for both connection configurations would had been relatively the same except that Test-BC 200-1.5-A connection failed at the end of the test due to shear rod pull-out which increased the connection strength but decreased its ductility ratio.

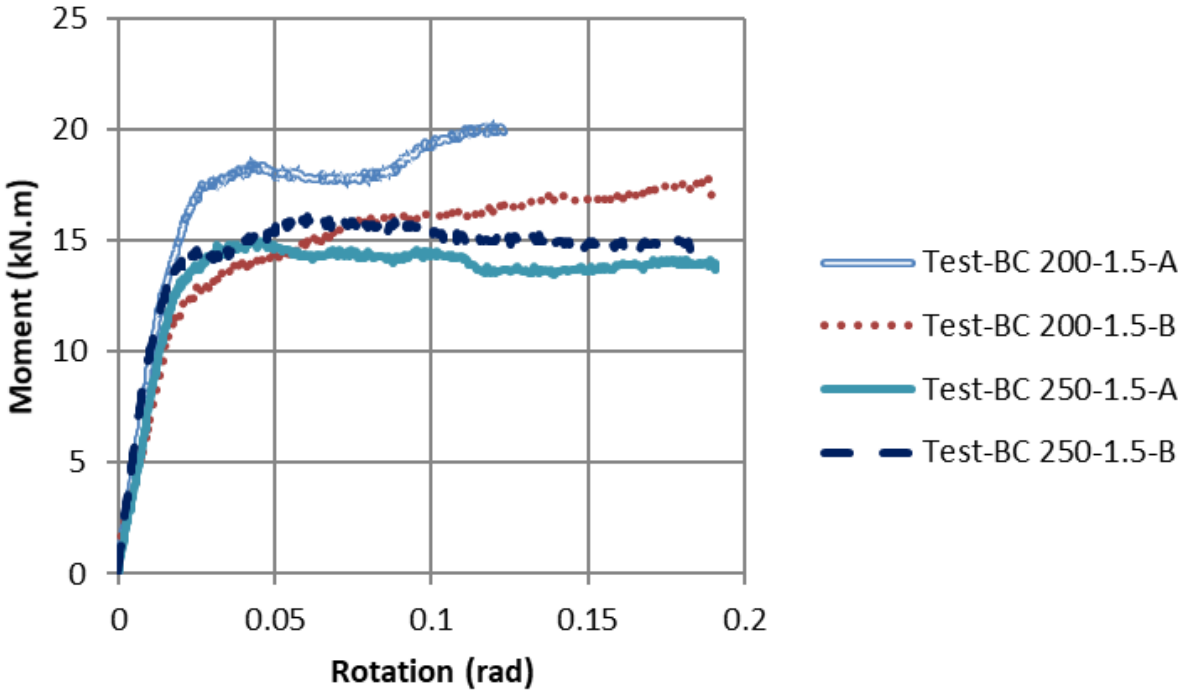

Figure 4.13. Moment-rotation relationships for Test-BC 200-1.5 versus 250-1.5

Figure 4.14 shows the effect of increasing the steel rod embedment length from 200 to 250 mm for the connections that utilized the larger washers (50.8 mm). It was noticed that increasing the rod embedment length had very little effect on the yield moment capacity (from an average of 17.28 to 16.60 kN.m), and the maximum moment capacity (from an average of 26.16 to 27.03 kN.m). Similar to the connections with the smaller washer size, the failure mode stayed the same for the connections with both embedment lengths as yielding of the steel rod. The average ductility ratio of the connections with the 200 mm rod embedment length was 7.40, while for the connections with the 250 mm embedment length the ductility ratio was 8.25. Since the failure mode for the connections with both embedment lengths and the same larger washer size (50.8 mm) was steel rod yielding, it was expected that there would be very little difference in the results because steel material behaviour was more predictable and consistent when it fails. Accordingly, as long as the steel rod was the only component failing in those connection configurations, the connection strength can be predicted with a high degree of certainty.

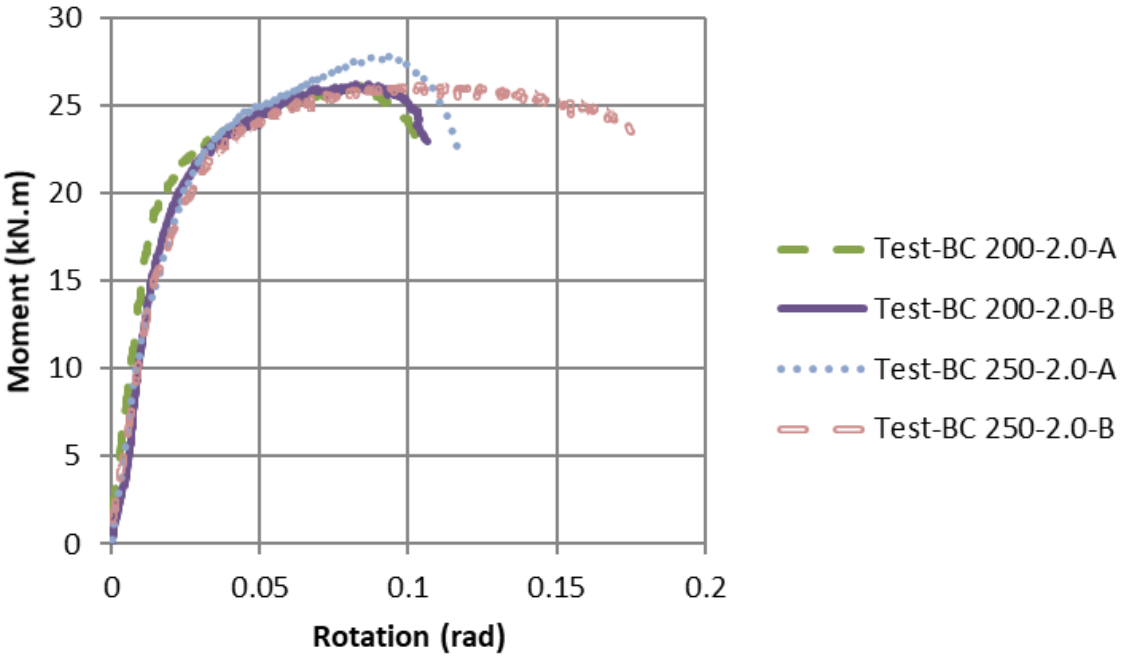

Figure 4.14. Moment-rotation relationships for Test-BC 200-2.0 versus 250-2.0

4.2.3 Summary of test results

Shown in Table 4.2 is a summary of all results including the calculated moment resistance, yielding moment, maximum moment, and ductility ratio for all BC connection configurations experimentally examined in this study.

Table 4.2. Results summary for all BC connection configurations tested

Test-BC ID	Initial stiffness (kN.m/rad)	M_{yield} (kN.m)	Yield Rotation (rad)	M_{max} (kN.m)	Failure Rotation (rad)	Ductility ratio	Estimated M_{max} (kN.m)
200-1.5-A	831.47	13.59	0.0164	20.10	0.1229	7.52	16.4
200-1.5-B	597.24	11.94	0.0200	17.86	0.1894	9.47	16.4
200-2.0-A	1365.08	18.16	0.0133	26.11	0.1058	7.95	23.3 (20.3 yield)
200-2.0-B	1058.63	16.41	0.0155	26.21	0.1062	6.85	23.3 (20.3 yield)
250-1.5-A	749.15	10.41	0.0139	14.97	0.1908	13.72	18.4
250-1.5-B	964.30	10.61	0.0110	16.14	0.1827	16.61	18.4
250-2.0-A	896.63	16.99	0.0189	27.86	0.1166	6.15	23.3 (20.3 yield)
250-2.0-B	959.45	16.21	0.0169	26.21	0.1750	10.36	23.3 (20.3 yield)

The connection configuration Test-BC 200-1.5 had an average maximum moment of 19.0 kN.m which is about 16% greater than the connection maximum moment resistance calculated at 16.4 kN.m. The connection configuration Test-BC 250-1.5 with the small washers but longer embedment length had an average maximum moment of 15.6 kN.m which is 15% less than the connection moment resistance calculated at 18.4 kN.m. The reason why the connection configuration Test-BC 200-1.5 had a higher increase in maximum moment versus the calculated maximum moment as compared the connection configuration Test-BC 250-1.5 could be attributed to two reasons. First, was that the bottom rod was adding a small increase in the moment resistance and second was that a bending factor was added to the calculated predicted moment resistance since the pure tension force was only used in the calculations. The bending force applies slightly more pressure along the top edge of the washer; causing the compression failure to happen slightly earlier than if the washer was under uniform tension, which causes the pressure to be distributed evenly.

The maximum moment of the Test-BC 250-1.5 connections was less than that of the Test-BC 200-1.5 connections because the washer in the connection with the 250 mm embedment length was further from the supporting column than the connection with the 200 mm embedment length; therefore, when the beam was rotating, the further washer travelled a greater vertical distance than the closer washer with the same rotation causing more pressure to develop along the washer's top edge, and thus caused the Test-BC 250-1.5 connections to fail at lesser moments.

One positive result in the longer embedment length comparing the connection configurations with the smaller washer was that the decrease in moment resistance was gained by the increase in ductility ratio. The average ductility ratio for the Test-BC 200-1.5 connection was 8.5 while the average ductility ratio for the Test-BC 250-1.5 connection was increased by about 79% to 15.2. Also, the ductility ratios for both connections with the larger washer were both slightly below 8.5 meaning the wood crushing failures exhibited by the connections with the smaller washer has a higher ductility ratio than the steel rod yielding failures exhibited by the connections with the larger washer.

Regardless of the steel rod embedment length, the connection configurations with the larger washers (50.8 mm) had its maximum moments and yielding moments almost the same. The connections with the larger washer had a yielding moment average of 16.9 kN.m which was about

17% lower than the calculated yielding moment resistance of 20.3 kN.m, while their average maximum moment resistance was 26.6 kN.m which was about 14% greater than the calculated maximum moment resistance of 23.3 kN.m. An explanation for the lower yielding moment compared to the calculated was that the top tension rod was not under pure tension. As shown in Figure 4.8(a) and Figure 4.9(b), both steel rods were bent at the interface between the beam end and the column side. Also, the rotation of the connection caused the top rod to bend at the beam-to-column interface creating a starting point for the rod to start yielding slightly early similar to what happened in the connections with the smaller washers (38.1 mm). The increase in maximum moment compared to the calculated was similar with the smaller washer connections in which the bottom rod adds a slight increase in resistance to the moment resistance.

4.3 Conclusions

Based on the obtained experimental results and analysis performed afterwards, the formulas shown in Equations 4.1 and 4.2 are plausible for the glulam beam end connection configurations experimentally examined in this study. However, more tests need to be performed to calculate the bending factor that caused the connection to fail at slightly smaller moment values than that if the top rod was under uniform tension, instead of being subjected to combined tensile and bending forces. The following conclusions have been drawn:

- Depending on the desired failure, a connection configuration can be designed to promote a steel rod yielding failure which is stronger and also predictable, or a wood crushing failure which can provide the connection with a high ductility ratio.
- The longer steel rod embedment length affects the strength of the connection slightly negative due to the uneven pressure under the washer, but increases the ductility ratio greatly when the failure mode was wood crushing under the washer.
- The increase in washer size was the largest gain in the connection strength as it increases the area of wood to be crushed and increases the area of wood to resist shear rod pull-out failure. Increasing the area of the washer by 63% increased the 200 mm embedment length connections maximum moment resistance by 38% and increased the 250 mm embedment length connections maximum moment resistance by 74%.
- The increase in washer size from 38.1 to 50.8 mm didn’t show any ill effect due to the rotation of the connection, but from previous tension tests, as shown in Chapter 3 of this

thesis, a larger washer of 63.5 mm (2.5 inches) was observed to cause splitting in the wood underneath, and therefore should be avoided.

- For a comparison of a simply supported beam with the same section size, the moment resistance is 70.5 kN.m and the strongest connection had a yielding moment resistance of about 17 kN.m giving the connection an efficiency of 24%.

With the information from the ambient moment resisting beam-to-column connection series of tests, the elevated temperature tests can be performed using the exact same connection configurations. Knowing that the actual results are slightly lower than the expected results, a design moment of 10 kN.m was selected to test each connection at elevated temperatures.

Chapter 5 Elevated Temperatures Moment Connections Testing

5.1 Introduction

The four connection configurations tested as detailed in Chapter 4 were experimentally examined at elevated temperatures, with each test assembly tested twice (A and B) to verify results. Using the collected load, displacement, time, and thermal data, the connection's time to failure and internal temperatures were determined, and the connection failure modes were observed and documented.

5.1.1 Materials

5.1.1.1 Glulam sections

The glulam beam sections used were the exact same as described in section 3.1.1.1 of this thesis.

5.1.1.2 Threaded rods

The threaded rods used were the exact same as described in section 4.1.1.2 of this thesis.

5.1.1.3 Washers

The washers used were the exact same as described in section 4.1.1.3 of this thesis.

5.1.2 Test assembly details and fabrication process

The beam-to-column connections fabrication process and assembly details were the exact same as that described in section 4.1.2 of this thesis.

5.1.3 Test assembly design

The purpose of this stage of the experimental program of this study is to confirm that a fully concealed glulam beam-to-column connection sized at 135 mm x 314 mm high can achieve a one-hour fire resistance rating. From the previous tests done at ambient temperature, as described in Chapter 4 of this thesis, the safe design capacity of the weakest connection configurations was 10.0 kN.m. For consistency to compare how changing the embedment length and washer size affects the time to failure the 10.0 kN.m moment was applied to all four connection configurations.

The nominal char rate of the glulam sections tested at this stage of the experimental program of this study was 0.7 mm/min (Nordic Wood Structures, 2015). Therefore, after one-hour fire exposure, a char layer of about 42 mm is to be formed on the bottom and the two sides of the glulam beam as shown in Figure 5.1. The top surface of the beam will be covered with a layer of insulating ceramic fibre blanket to represent a slab on top of the beam. Therefore, there will be no charring on the top surface of the beam. Considering the width of the 38.1 mm washer located in the centre of the beam width, the beam should still have about 6.5 mm of wood protection at the washers' sides. Considering the width of the 50.8 mm washer located in the centre of the beam width, the beam should still have about 0.1 mm of wood protection at the washers' sides. The tests matrix with the corresponding fire resistance predicted times to failure is presented in Table 5.1.

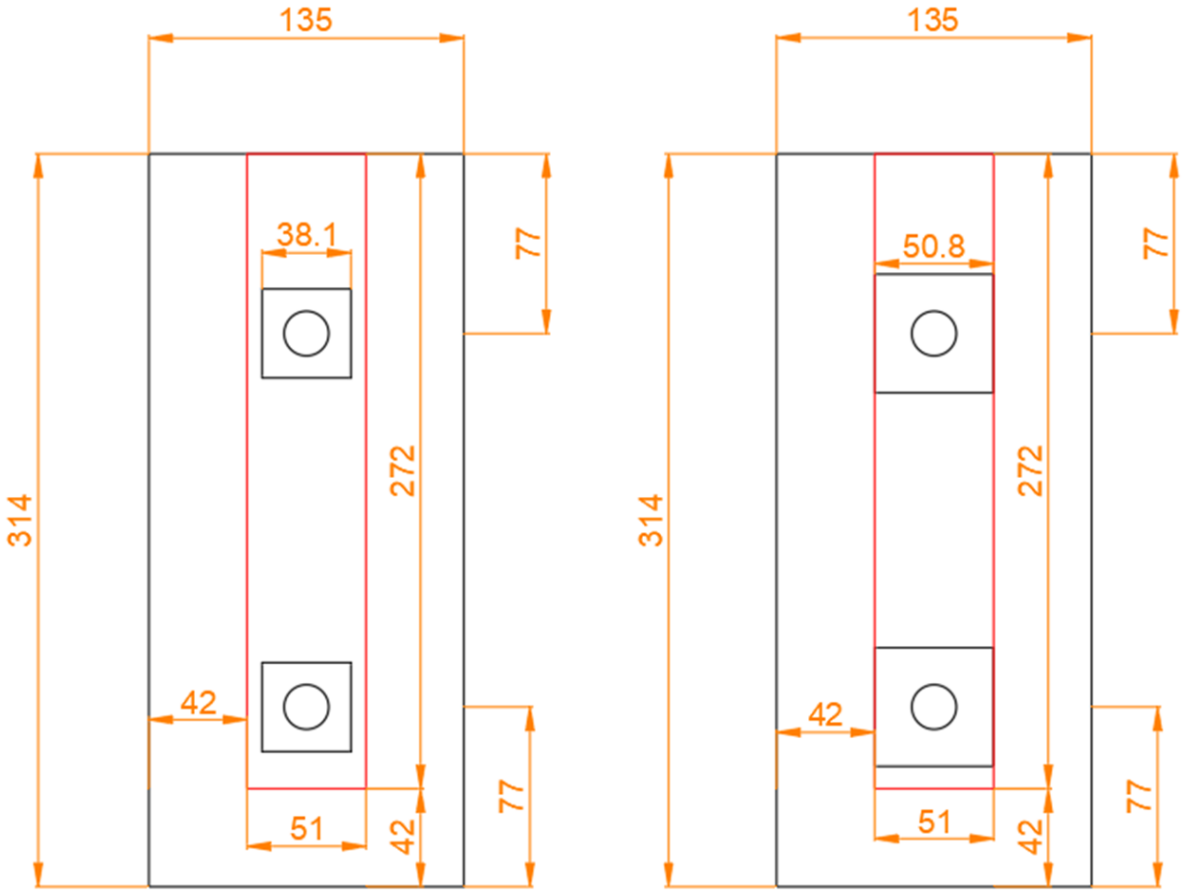

Figure 5.1. Beam-to-column connections' predicted cross section after standard fire exposure

Table 5.1. Threaded rod in glulam beam-to-column connection fire tests matrix

Test configuration ID	Test replicates	Embedment length (mm)	Washer size (mm)	Safe design load applied (kN.m)	Predicted time to failure (min)
Test-BCF 200-1.5	2	200	38.1	10.0	60
Test-BCF 200-2.0	2	200	50.8	10.0	60
Test-BCF 250-1.5	2	250	38.1	10.0	60
Test-BCF 250-2.0	2	250	50.8	10.0	60

Notes: For the test configuration ID; 200 and 250 are the rod embedment lengths in (mm); 1.5 and 2.0 are the square washer size in (inches). BCF stands for Beam-to-Column Fire

5.1.4 Tests setup and procedure

Each test assembly was fixed to a strong steel support using two threaded steel rods. The carved cut offs on the beam face, which accommodated the steel rods' nuts and washers, were then plugged with a small fitting chunk of glulam, which was then glued in place as shown in Figure 5.2(a). Both, the glulam beam and the fire-protected support were placed inside the large-size fire testing furnace accommodated at Lakehead University's Fire Testing and Research Laboratory (LUFTRL), as shown in Figure 5.2(b). The beam top side was fire protected using a 1-inch thick layer of ceramic fibre blanket insulation to simulate the existence of a slab on top of the beam. A hydraulic jack mounted to the strong loading steel structure that surrounded the furnace was used to apply the transverse load on the beam via an insulated steel post which was installed through an opening in the furnace roof.

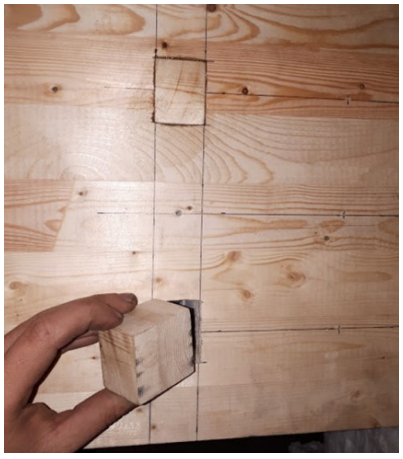
(a)

(b)

Figure 5.2. Fire test setup: (a) Beam section holes being plugged; (b) A general fire resistance test setup.

One draw-wire displacement transducer was installed outside the furnace and attached to a ceramic rod that was inserted through the furnace roof 200 mm from the face of the steel support to capture the vertical displacements of the beam. Another draw-wire displacement transducer was installed outside of the furnace and attached to the insulated steel post to measure the vertical displacements of the beam end. The locations of the transducers are shown in Figure 5.3. The measured displacements from both transducers were used to determine the rotation of the beam-to-column connections. As for thermal measurements of the wood and steel components of the connections during fire tests, twelve metal-shielded K-type thermocouples were placed on each specimen as detailed in Figure 5.4. Six thermocouples were installed in the wood section on the beam front face and the other six mirrored on the back face of the beam. Thermocouples 1, 3, 7, and 9 were installed just at the edge of the cavity where the nut and washer were located. Thermocouples 4, 6, 10, and 12 were installed just at the edge of the cavity where the steel rod was located (57 mm deep). Thermocouples 2, 5, 8, and 11 were placed at a depth similar to thermocouples 1, 3, 7, and 9 (49 mm for the 38.1 mm washer and 43 mm for the 50.8 mm washer). Test beams were loaded to 100% of the calculated design moment-resisting capacity of the weakest connection configuration.

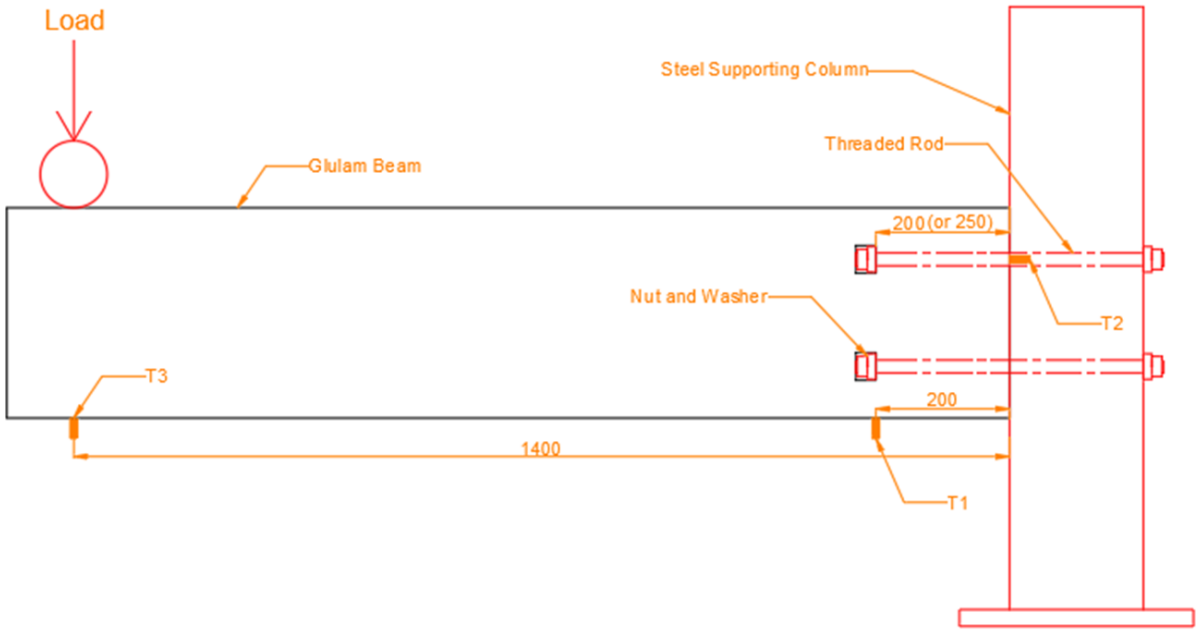

Figure 5.3. Fire test transducer locations

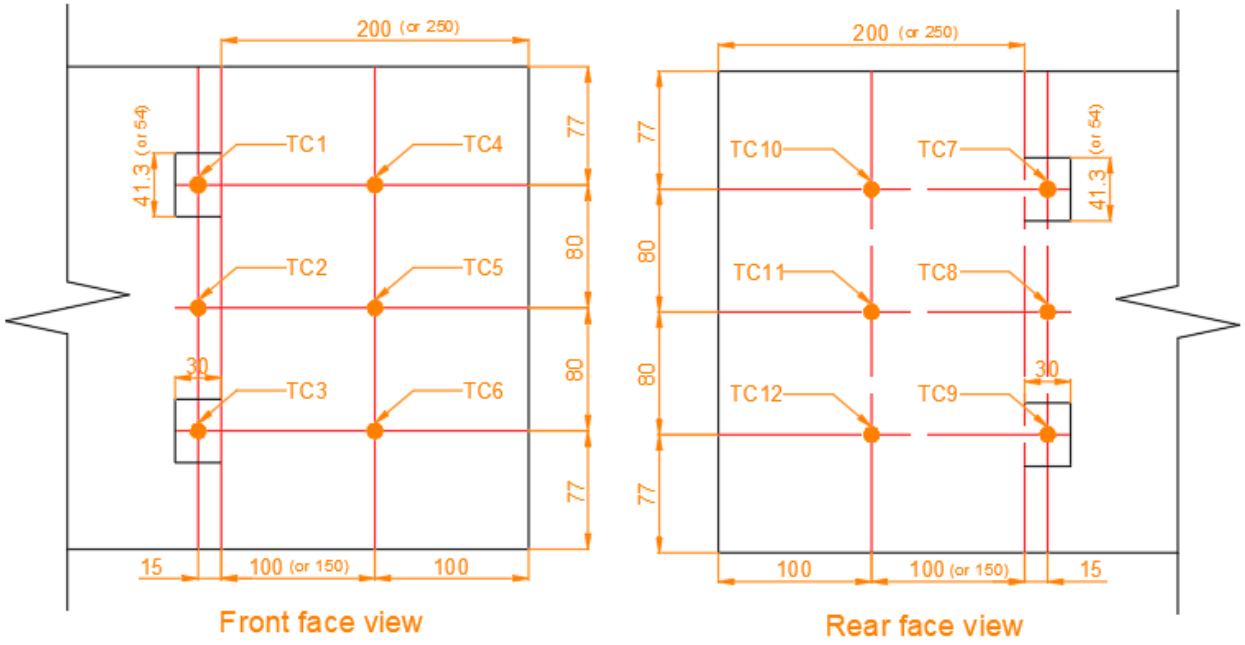

Figure 5.4. Fire test thermocouple locations

As per CAN/CSA-S101, the total transverse load was applied in 25% increments at least 30 minutes before the test assembly was exposed to CAN/ULC-S101 standard fire time-temperature profile. Deflections of each test assembly were measured during fire testing until the test assembly could no longer hold the applied load, or the test assembly reached the maximum measurable amount of deflection, at which the test was terminated. Figure 5.5 shows a general test assembly that underwent fire exposure after about 30 minutes with no noticeable deflection.

Figure 5.5. Beam-to-column connection assembly exposed to 30 minutes of a standard fire

5.2 Experimental Results and Discussion

The experimental results presented in this chapter are mainly the temperatures measured by the thermocouples, and the displacements measured by the draw-wire transducer located at the end of the beam in line with the loading, labelled T2, which was used to calculate the beam rotation. The draw-wire transducer, labelled T1, located at 200 mm from the column face could not be used because when the beam failed it would snap the ceramic rod, as shown in Figure 5.6, and was therefore stopped after the second attempt. Since all of the beams lasted close to an hour there was not much wood left to be salvaged for examination and the residual heat of the furnace during the cool down phase would burn the remaining amount of wood that was left.

Figure 5.6. Fire tested beam upon completion of testing

5.2.1 Failure modes

For all tests, the top rod did not bend due to the wood not bearing on the rod after the test has been terminated. However, the bottom rod experienced varied degrees of bends after the test was terminated due to the wood bearing on the bottom rod and the amount of time the steel rod was exposed to fire.

The pictures shown in Figure 5.7 are in good agreement with the graphed results presented in Figure 5.11; where the failure of the 200-mm embedment length connections was a brittle failure mode due to the wood splitting as shown in Figure 5.7(a). The wood splitting caused the test to be terminated due to the connection not being able to hold the full applied design load. With the wood splitting and the second least fire resistance time, the bottom steel rod experienced slightl deformations as shown in Figure 5.7(b).

(a)

(b)

Figure 5.7. Test-BCF 200-1.5-A after failure: (a) Connection just after failure; (b) Steel rods after failure.

The pictures shown in Figure 5.8 for Test-BCF 200-2.0-B show a similar failure as Test-BCF 200-1.5-A. The failure of the 200-mm embedment length connections was a brittle failure mode due to the wood splitting as shown in Figure 5.8(a). The wood splitting caused the test to be terminated due to the connection not being able to hold the full applied design load. With the wood splitting and the least amount of fire resistance time, the bottom steel rod experienced slightly more deformations as shown in Figure 5.8(b). Due to the 50.8 mm washer having less wood cover than the 38.1 mm, the bottom rod experienced more heat and therefore bent slightly more as shown in Figure 5.8(b) when compared to Figure 5.7(b).

(a)

(b)

Figure 5.8. Test-BCF 200-2.0-B after failure: (a) Connection just after failure; (b) Steel rods after failure.

The pictures shown in Figure 5.9 are in excellent agreement with the graphed results presented in Figure 5.11; where the failure of the 250-mm embedment length connections was a relatively ductile failure mode due to the steel rods deforming as shown in Figure 5.9(a). The steel rods deforming caused the test to be terminated due to the beam reaching the maximum measurable amount of deflection. Also, with the longer embedment length, there was more wood to resist the shear forces imposed by the top steel rod; therefore, allowing the steel rods to be considerably heated causing the bottom rod to deform excessively, as shown in Figure 5.9(b).

(a)

(b)

Figure 5.9. Test-BCF 250-1.5-A after failure: (a) Connection just after failure; (b) Steel rods after failure.

The pictures shown in Figure 5.10 for Test-BCF 250-2.0-B show a similar failure as Test-BCF 250-1.5-A. The failure of the 250-mm embedment length connections was a semi-ductile failure mode due to the steel rods deforming as shown in Figure 5.10(a). The test was terminated due to the connection not being able to hold the full applied design load, but it was not as abrupt as the connection configurations with the 200 mm embedment length. With the longer embedment length, there was more wood to resist the shear forces imposed by the top steel rod; therefore, allowing the steel rods to be considerably heated causing the bottom rod to deform excessively, as shown in Figure 5.10(b). Due to the 50.8 mm washer having less wood cover than the 38.1 mm, the Test-BCF 250-2.0 connections failed sooner than the Test-BCF 250-1.5 connections, but the longer rods allowed the connection to last longer than the shorter rods. The longer rods allowed the bottom rod to experienced more heat and therefore bend slightly more than the shorter rod connections as shown in Figure 5.10(b) when compared to Figure 5.8(b), but not as much as the Test-BCF 250-1.5 connections as shown in Figure 5.10(b) when compared to Figure 5.9(b).

(a)

(b)

Figure 5.10. Test-BCF 250-2.0-B after failure: (a) Connection just after failure; (b) Steel rods after failure.

5.2.2 Time-rotation relationships

The test specimens' failure criterion was determined to be a maximum beam-to-column connection rotation of 0.1 radians or when the connection was not able to hold the full applied design load after a considerable load drop. It was observed that the test assemblies underwent two different trends of increased rotations with time in all four fire resistance test configurations. The connection rotations slightly increased in a linear trend during the first half of the test time (about 30 minutes). For the second half of the test time, the connection rotations increased exponentially over time until failure. Both rotation trends are shown in Figure 5.11. All linear trends of the four fire test configurations are very similar; however, the experimental results show that the connection configurations with 250-mm embedment length were slightly stiffer than those of 200-mm embedment length.

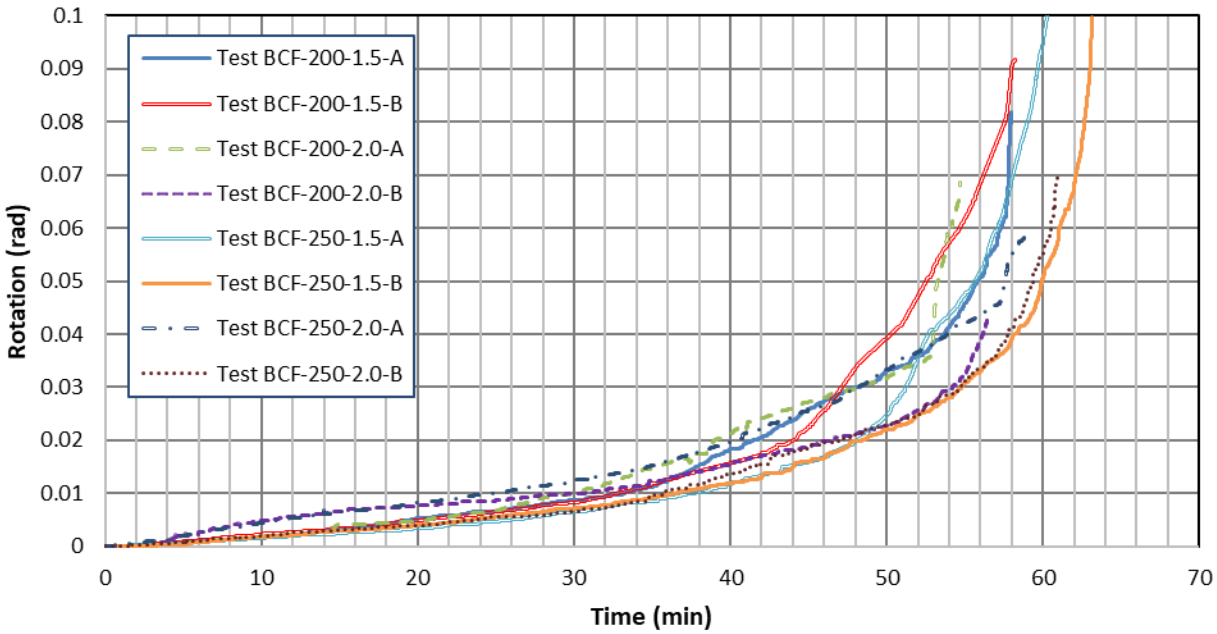

Figure 5.11. Full time-rotation relationships for all fire tests

The last 10 minutes of the fire tests show a better representation of the failure modes and exact fire resistance time, as shown in Figure 5.12. The fire resistance tests showed that the Test-BCF 200-2.0 connections failed the earliest at an average time of about 55.5 min due to the shorter embedment length and the larger washer providing minimal wood cover to the steel components. The connections with the second earliest time of failure was Test-BCF 200-1.5 with an average time of about 58 min. The extra wood cover of the smaller washer gave the connections about a 2.5 min extra resistance time compared to the larger washer configuration Test-BCF 200-2.0. The connections with the second longest time of failure was Test-BCF 250-2.0 with an average time of about 60 min. The longer embedment length of the rods added an additional 4.5 min resistance time when compared to the shorter embedment length configuration Test-BCF 200-2.0. The connections with the longest time of failure was Test-BCF 250-1.5 with an average time of about 61.5 min. The extra wood cover of the smaller washer gave the connections about a 1.5 min extra resistance time compared to the larger washer configuration Test-BCF 250-2.0 and the longer embedment length of the rods added an additional 3.5 min resistance time when compared to the shorter embedment length configuration Test-BCF 200-1.5. Therefore, starting with the weakest configuration Test-BCF 200-2.0, decreasing the washer size adds 2.5 min to the fire resistance and then increasing the embedment length adds 3.5 min to the fire resistance time totalling 6 min of additional fire resistance time for the configuration Test-BCF 250-1.5.

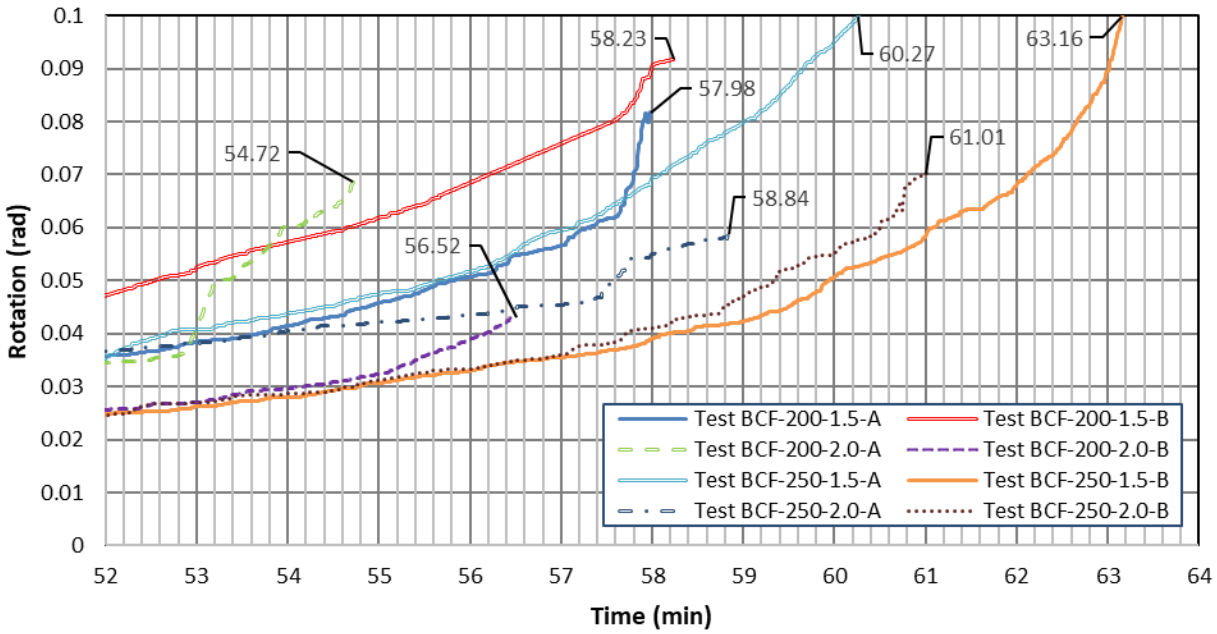

Figure 5.12. Time-rotation relationships for all fire tests throughout the last 10 minutes

When comparing configurations Test-BCF 200-1.5 and Test-BCF 250-1.5, even though the curves are offset from each other in the last 10 minutes, the lines match very well (200-1.5-A with 250-1.5-B and 200-1.5-B with 250-1.5-A) as shown in Figure 5.13. The configuration Test-BCF 200-1.5 looked like it had a ductile failure with its high rotation, but at the end the wood split abruptly and could no longer gain any load. The configuration Test-BCF 250-1.5 had a ductile failure as the tests continued to hold load past the 0.1 rad rotation and maxed out the measurement range of the centre draw-wire transducer. The longer embedment length of the rods allowed for the extra wood resisting shear to add a greater time and rotation to failure. Comparing the curves with the similar trend in the last 10 minutes (200-1.5-A with 250-1.5-B and 200-1.5-B with 250-1.5-A), at the same point of rotation, the additional length of the rod embedment added two to four minutes of fire resistance time.

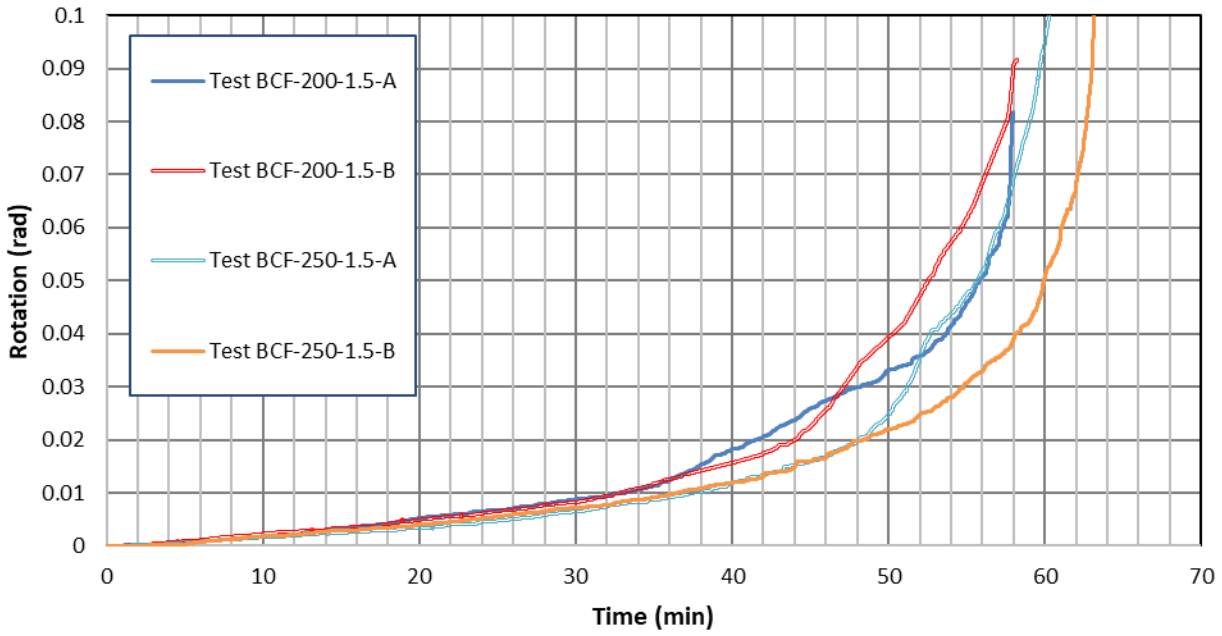

Figure 5.13. Time-rotation relationships for Test-BCF 200-1.5 versus 250-1.5

Similar to Figure 5.13, Figure 5.14 shows the lines match very well when comparing configurations Test-BCF 200-2.0 and Test-BCF 250-2.0, even though the lines are offset from each other in the last five minutes (200-2.0-A with 250-2.0-A and 200-2.0-B with 250-2.0-B). The configuration Test-BCF 200-2.0 had brittle failures as the wood split abruptly and could no longer gain any load. The configuration Test-BCF 250-2.0 had a semi-ductile failure as the tests continued to hold some load after failure, but could no longer hold the design load of 10 kN.m and slowly continued to drop the load over a period of time. The longer rod embedment length allowed for the extra wood resisting shear to add a greater time to failure, but there was no noticeable gain in additional rotation capacity. When comparing the curves with the similar shape in the last five minutes (200-2.0-A with 250-2.0-A and 200-2.0-B with 250-2.0-B) at the same point of rotation, the additional length of the rod embedment added two to four minutes of fire resistance time.

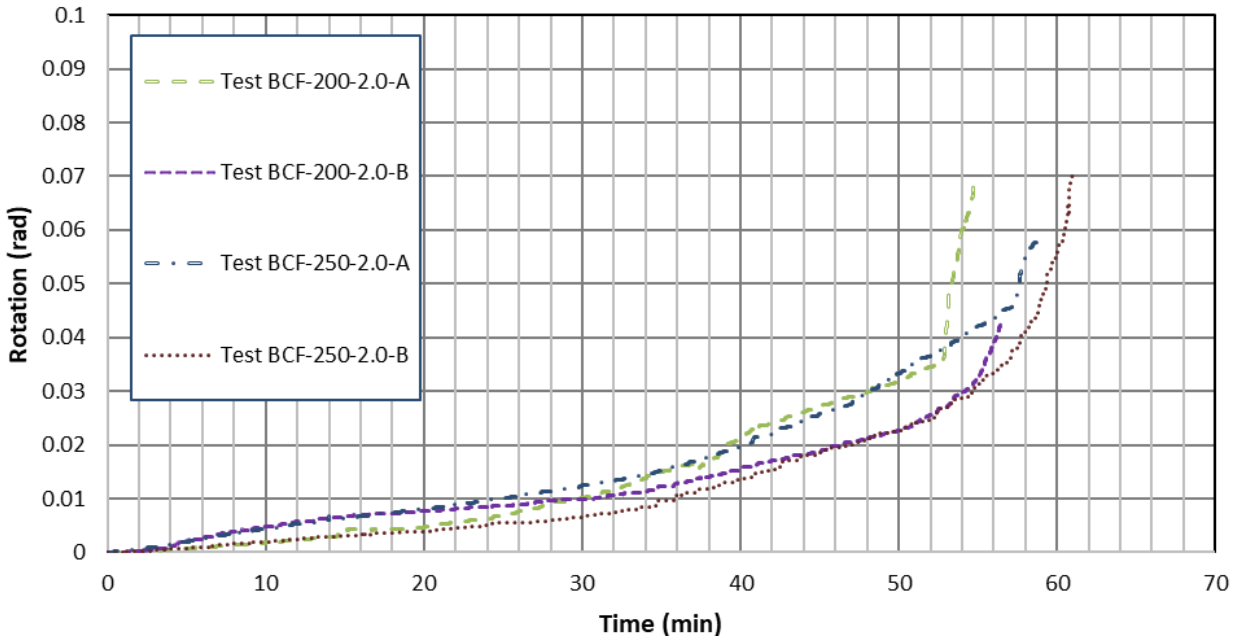

Figure 5.14. Time-rotation relationships for Test-BCF 200-2.0 versus 250-2.0

When comparing configurations Test-BCF 200-1.5 and Test-BCF 200-2.0, the curves do not match well in the last 10 minutes, as shown in Figure 5.15. The configuration Test-BCF 200-1.5 was able to achieve a higher rotation by an average of 0.03 additional rad when compared to Test-BCF 200-2.0. The additional wood cover provided by the smaller washer also added an average of 2.5 minutes of fire resistance time.

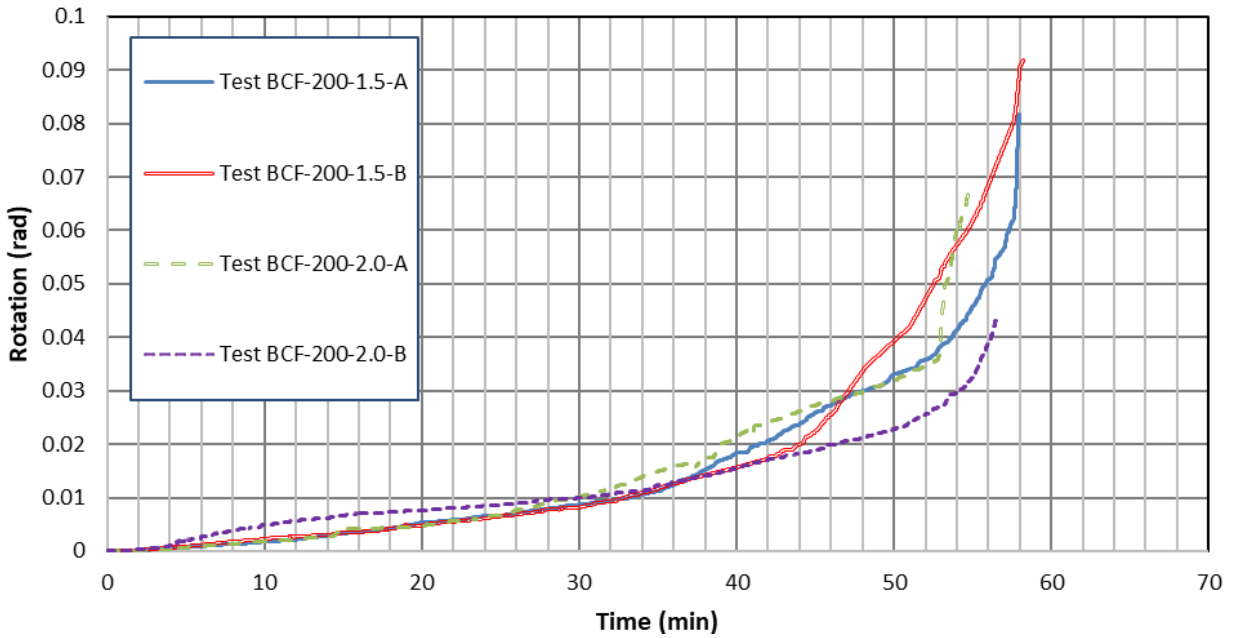

Figure 5.15. Time-rotation relationships for Test-BCF 200-1.5 versus 200-2.0

The configurations Test-BCF 250-1.5 and Test-BCF 250-2.0 have relatively similar curves except for Test-BCF 250-2.0-A as shown in Figure 5.16. Both configurations had a relatively ductile failure in comparison except the larger washer configuration had a reduced wood cover which weakened the steel rods sooner at the same time as the smaller washer configuration and therefore reduced the load capacity slowly over time upon failure. The configuration Test-BCF 250-1.5 looked like it had a ductile failure with its high rotation, but at the end the wood split abruptly and could no longer gain any load. The gain in rotation capacity was similar to Figure 5.15 at about 0.035 rad when using the smaller washer versus the larger washer. The gain in fire resistance time was small at about only 1.5 minutes, but by extrapolating the lines of the configuration Test-BCF 250-2.0 if the connections could hold the design load for longer, then the fire resistance time would be nearly the same as configuration Test-BCF 250-1.5.

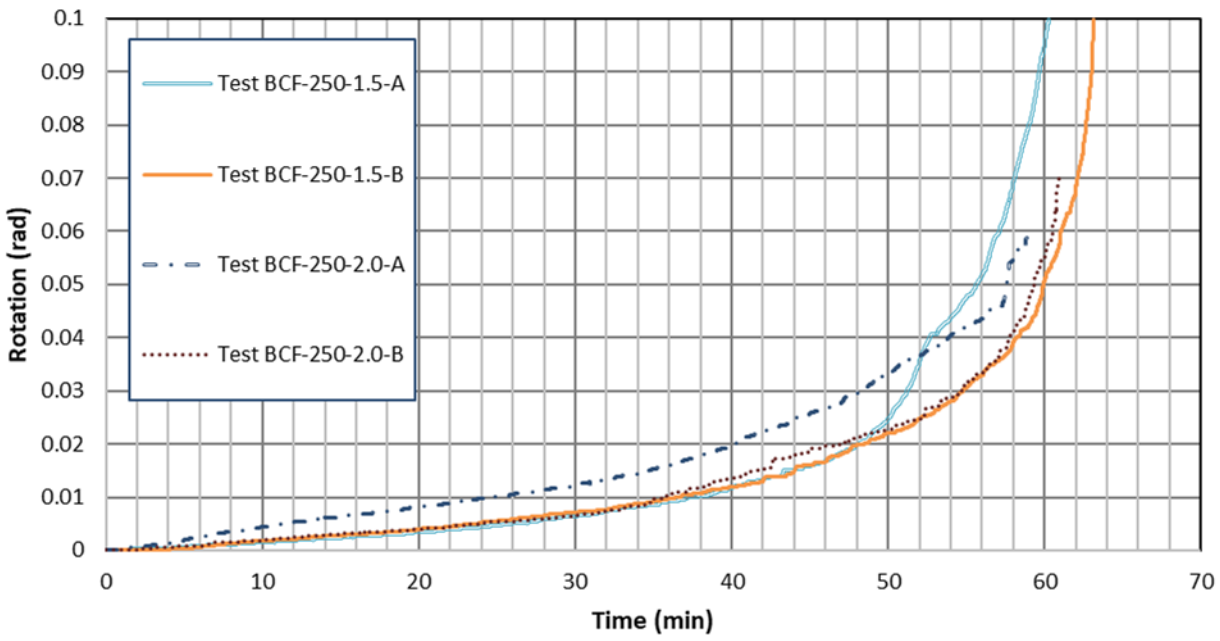

Figure 5.16. Time-rotation relationships for Test-BCF 250-1.5 versus 250-2.0

When comparing the effectiveness of washer size, the smaller washer has additional wood cover and adds about 0.03 rad rotational capacity, but only minimal fire resistance time of about two minutes. Comparing the effectiveness of rod embedment length, the longer embedment length has little effect on the rotational capacity, but it adds an additional four minutes of fire resistance time. When both washer size and embedment length are combined for the best outcome, it can add an average of six additional minutes of fire resistance time.

5.2.3 Time-temperature relationships

All of the connection configurations with the same washer size had their thermocouples data very similar to each other. Shown in Figure 5.17 is the thermocouples data for Test-BCF 200-1.5-A, which was similar to all of the other tests with the 38.1 mm washer. The two thermocouples located on the bottom row in the hole with the nut and washer, thermocouples 3 and 9, were the first to lose their wood cover protection and reached a temperature same as that inside the furnace. No thermocouple reached a temperature above 100°C until just after 30 minutes. Most thermocouples stayed below the 200°C temperature until the end and even then, only about half were above the 300°C temperature which is considered the temperature when wood chars. These temperatures show that the steel components are protected by the wood which allows the connection to hold its design load until the end when there was very little wood remaining of the cross section to resist the applied load.

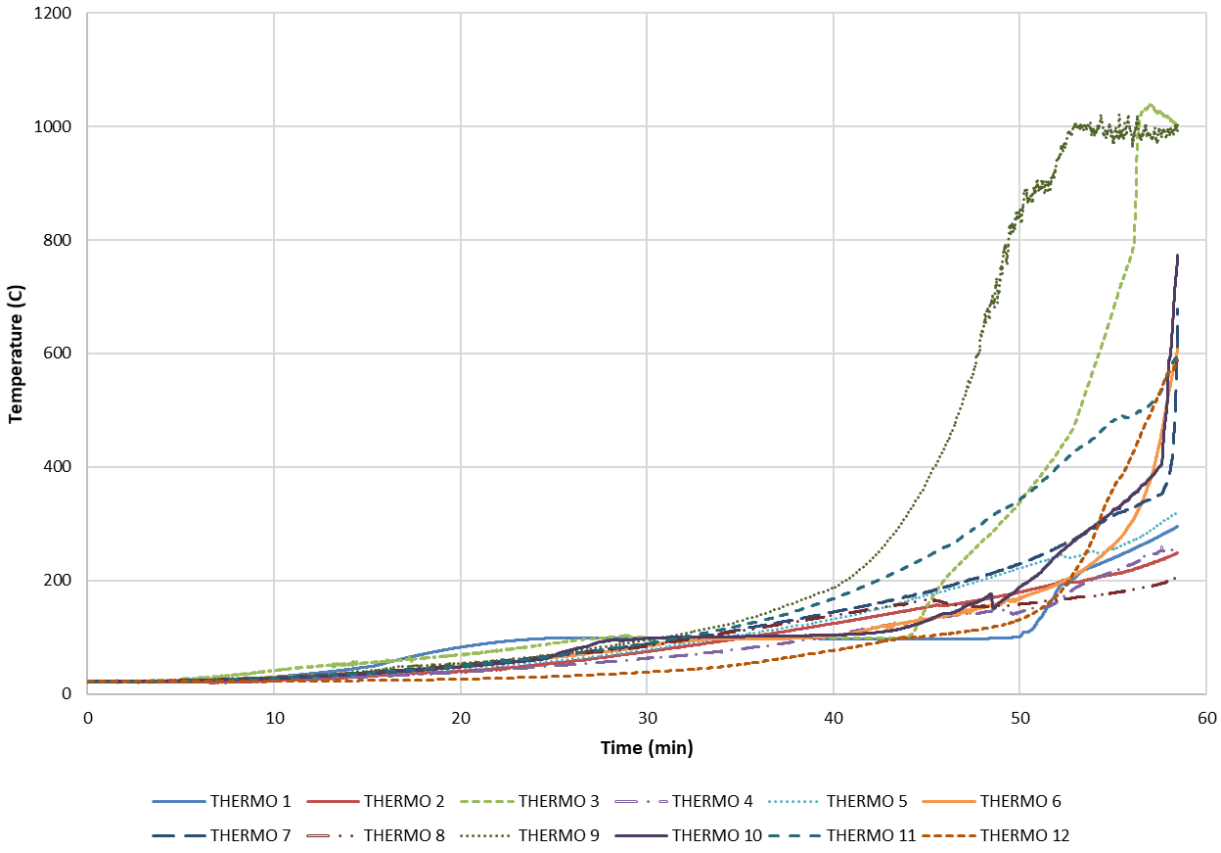

Figure 5.17. Time-temperature relationships for Test-BCF 200-1.5-A

Figure 5.18 shows the first 200°C of Test-BCF 200-1.5-A which reveal an interesting phenomenon happening in the cavities with the steel components. At around the 30-minute mark the thermocouples in the cavities show the temperature holding at 100°C for some length of time before climbing in temperature again. This phenomenon is known as thermo-hydric transfer which occurs when water vapors escaping the wood condense on the steel components and increase the time increment at which the concealed steel components maintain a temperature of 100°C (Samaké et al., 2014) before increasing due to the fire effect. The effect was shown more with the thermocouples in the cavities with the steel rods since the cavities are very small and not as much in the cavities with the nut and washer which have more air space.

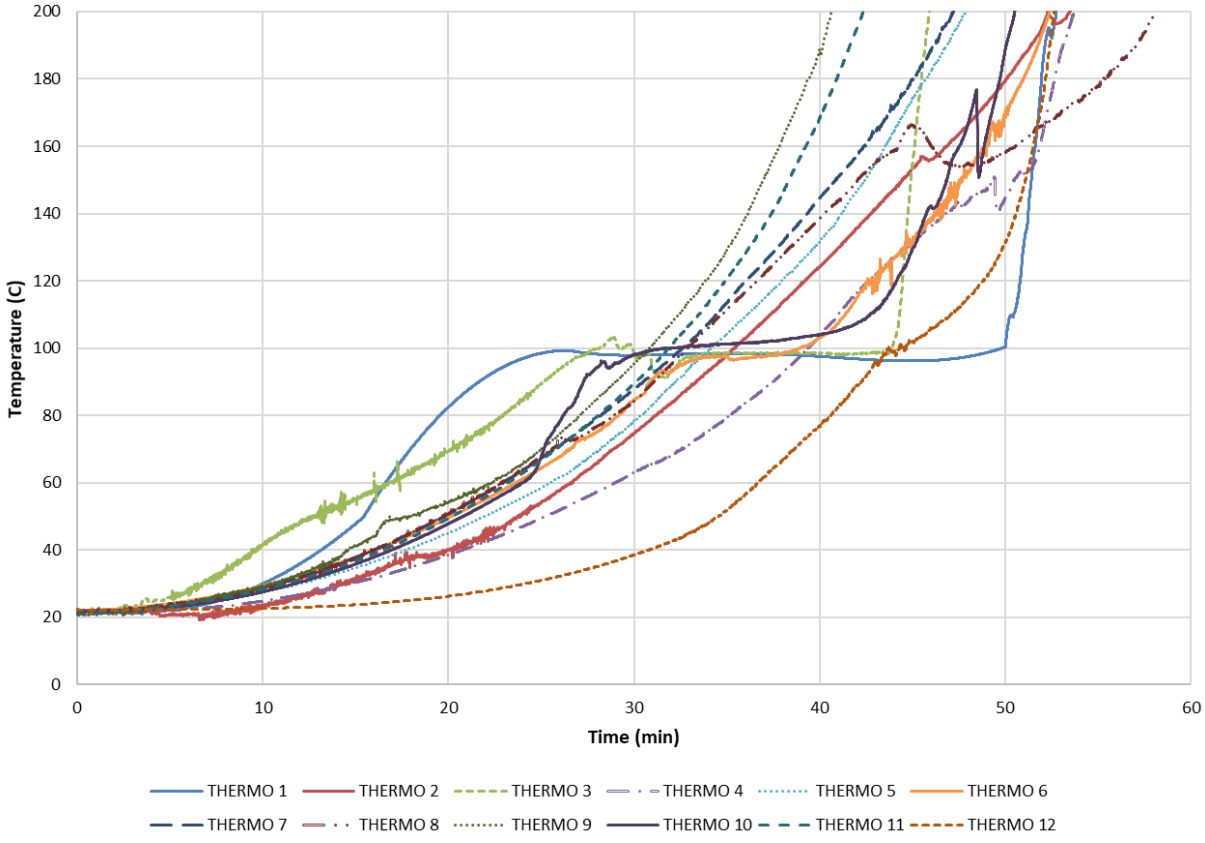

Figure 5.18. Time-temperature relationships for Test-BCF 200-1.5-A, 0-200°C

Focusing on the first three thermocouples show the thermo-hydric transfer well in Figure 5.19. Thermocouple one was located in the top row in the cavity with the nut and washer while thermocouple three was located in the bottom row in the cavity with the nut and washer. Thermocouple three experiences the thermo-hydric transfer less than thermocouple 1 because thermocouple 3 was being heated by the two side and bottom faces of the glulam beam while thermocouple one was only being heated by the two side faces. The protection of the top surface by the slab allows the top steel rod to experience the thermo-hydric transfer for six minutes longer than the bottom rod. Thermocouple 1 stopped experiencing the thermo-hydric transfer at around 50 minutes and thermocouple three stopped experiencing the thermo-hydric transfer at around 44 minutes. Thermocouple 2 was in the center between thermocouple 1 and 3 and since it was not touching any steel components the temperature just increased at a steady rate.

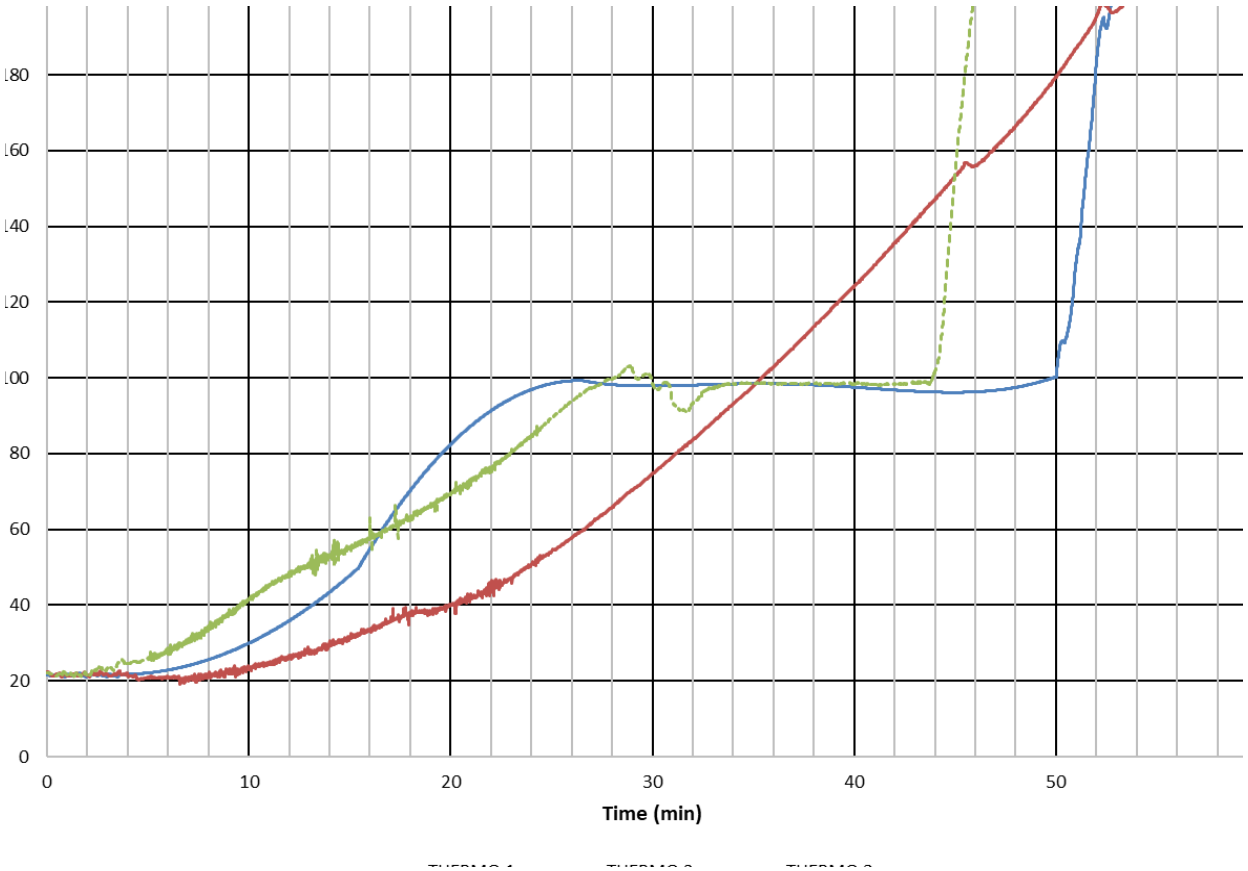

Figure 5.19. Time-temperature relationships for Test-BCF 200-1.5-A, Thermocouple 1, 2, and 3

Shown in Figure 5.20 is the thermocouples data for Test-BCF 200-2.0-A, which was similar to all of the other tests with the 50.8 mm washer. The two thermocouples located on the bottom row in the hole with the nut and washer, thermocouples three and nine, were the first to lose their wood cover protection and reached the temperature inside the furnace similar to the configurations with the 38.1 mm washer. Sometimes the other bottom row thermocouples, 6 and 12, would experience the same trend as thermocouples 3 and 9. Usually, no thermocouples reached above the 100°C temperature until just after 30 minutes similar to the configurations with the 38.1 mm washer. Most thermocouples stayed below the 200°C temperature until about the 45-minute mark, but more than half were above the 300°C temperature at the end, which is considered the temperature when wood chars. These temperatures show that the steel components had less protection from the wood compared to the smaller washer which created more brittle failures since the remaining cross section in less than the configurations with the smaller washer. The lesser wood cover lead to the wood igniting inside the cavities before ultimate failure which decreased the 50.8 mm washer configurations fire resistance time when compared to the 38.1 mm washer configurations.

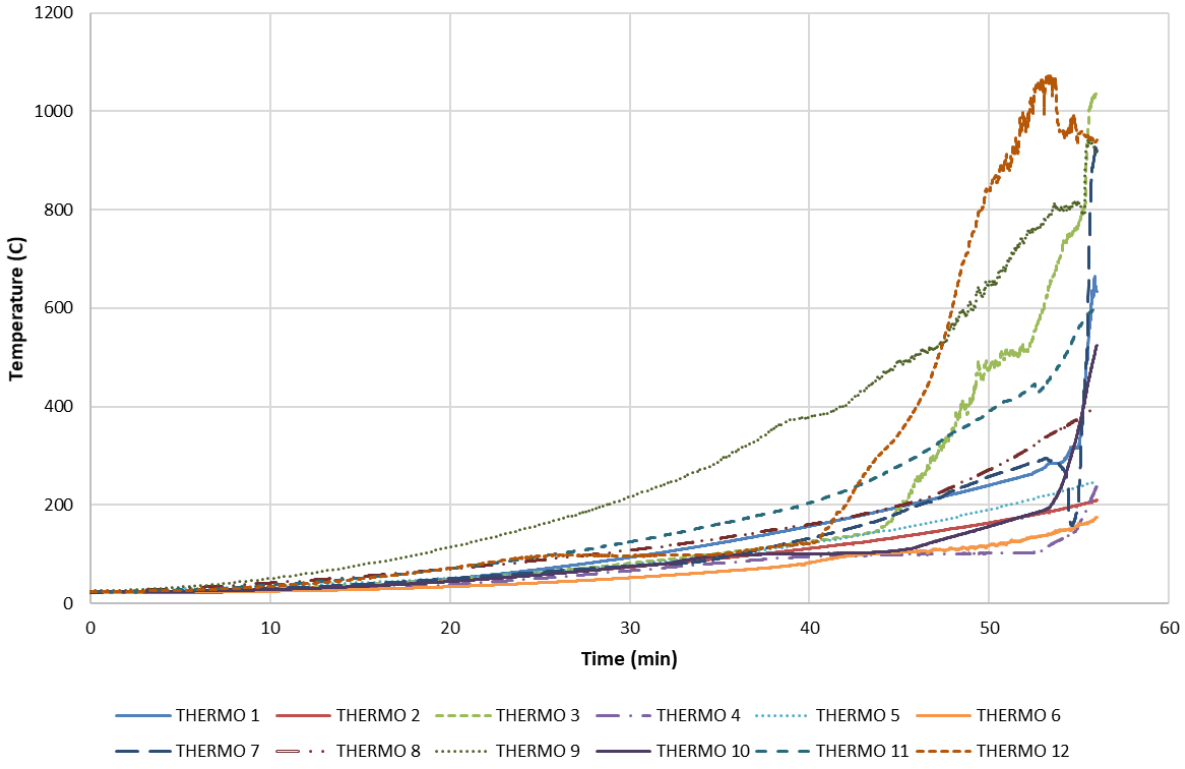

Figure 5.20. Time-temperature relationships for Test-BCF 200-2.0-A

Figure 5.21 shows the first 200°C temperature range of Test-BCF 200-2.0-A, which reveals the same phenomenon happening in the cavities with the steel components as the configurations with the 38.1 mm washer. Similar to the 38.1 mm washer configurations, at around the 30-minute mark the thermocouples in the cavities show the temperature holding at 100°C for some length of time before climbing in temperature again. The thermo-hydric transfer effect was shown more with the thermocouples in the cavities with the steel rods since the cavities are very small and very rarely in the cavities with the nut and washer which have more air space. The air space in the cavities with the nut and washer was much larger in the configurations with the 50.8 mm washer as compared to the configurations with the 38.1 mm washer which explains why the thermo-hydric transfer was rarely noticed.

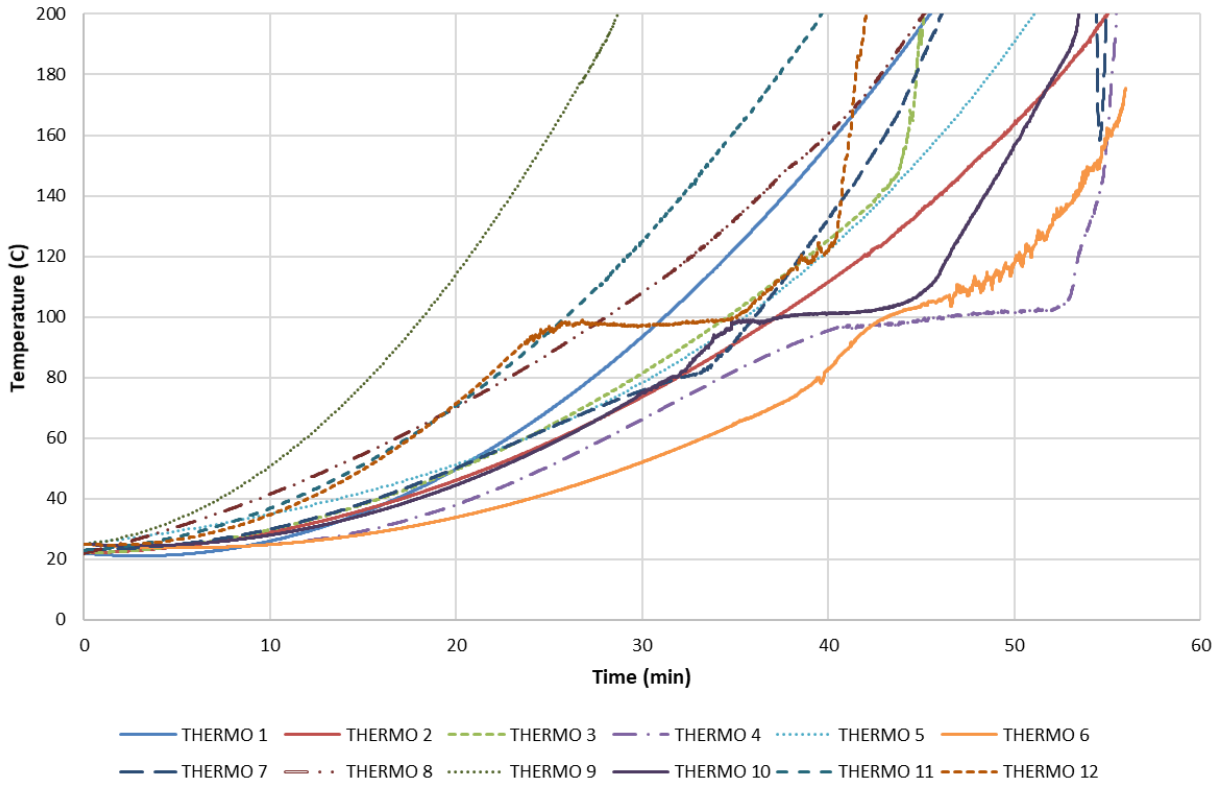

Figure 5.21. Time-temperature relationships for Test-BCF 200-2.0-A, 0-200°C

Focusing on the last three thermocouples show the thermo-hydric transfer well in Figure 5.22. Thermocouple 10 was located in the top row in the cavity with the steel rod while thermocouple 12 was located in the bottom row in the cavity with the steel rod. Thermocouple 12 experiences the thermo-hydric transfer sooner than thermocouple 10 because thermocouple 3 was being heated by the two sides and bottom while thermocouple 1 was only being heated by the two side faces of the beam. The protection of the top surface by the slab allows the top steel rod to experience the thermo-hydric transfer eight minutes later than the bottom rod. Thermocouple 10 stopped experiencing the thermo-hydric transfer at around 43 minutes and thermocouple 12 stopped experiencing the thermo-hydric transfer at around 35 minutes. The difference between when the thermo-hydric transfer ended for the bottom rods of the 38.1 mm and 50.8 mm washer configurations was about nine minutes. The difference in the depth of the washer from the sides of both washer configurations was 6.35 mm and at a char rate of 0.7 mm/min gives nine minutes difference which explains the nine minute difference in the thermo-hydric transfer of the bottom rod. Thermocouple 11 was in the center between thermocouples 10 and 12 and since it was not touching any steel components the temperature just increased at a steady rate.

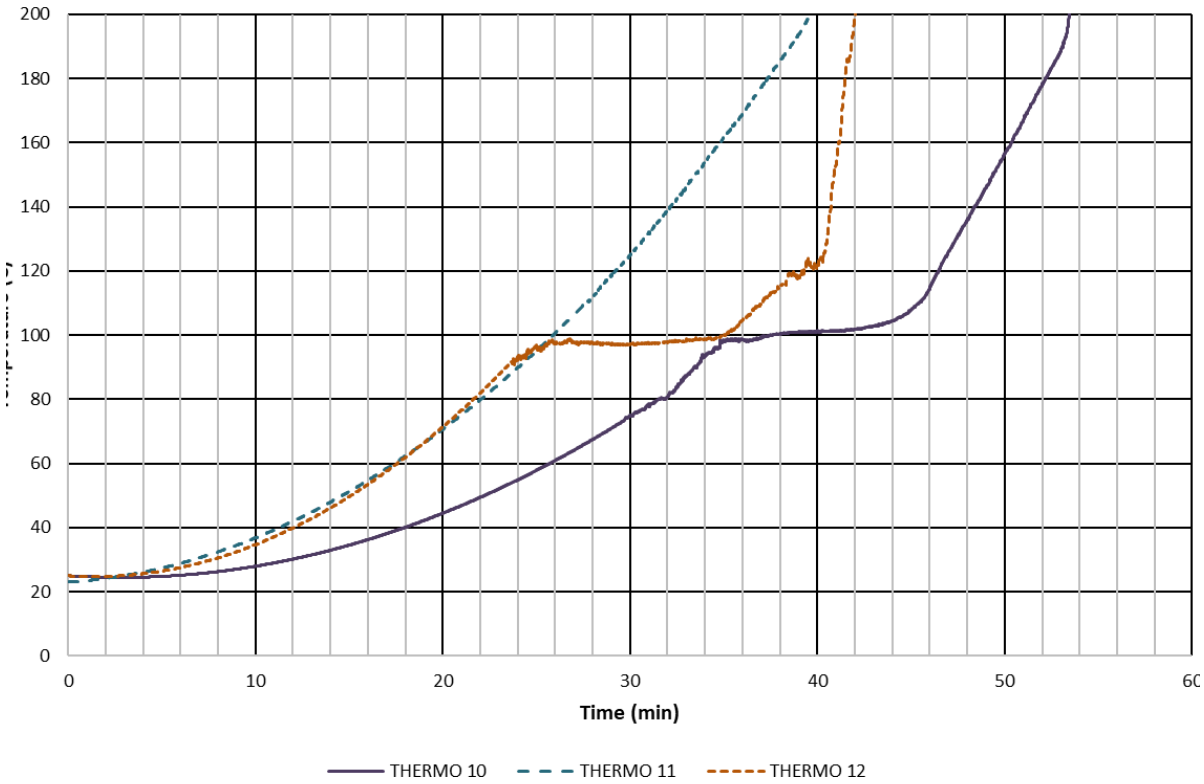

Figure 5.22. Time-temperature relationship for Test-BCF 200-2.0-A, Thermocouple 10, 11, and 12

5.2.4 Summary of test results

Shown in Table 5.2 is a summary of all results including the fire resistance time, rotation, and average fire resistance time for all BCF connection configurations experimentally examined in this study.

Table 5.2. Results summary for all BCF connection configurations tested

Test-BCF ID	Embedment length (mm)	Washer size (mm)	Fire resistance time (min)	Rotation (rad)	Average fire resistance time (min)
200-1.5-A	200	38.1	57.98	0.0818	58.11
200-1.5-B	200	38.1	58.23	0.0917	
200-2.0-A	200	50.8	54.72	0.0686	55.62
200-2.0-B	200	50.8	56.52	0.0431	
250-1.5-A	250	38.1	60.27	0.1000	61.71
250-1.5-B	250	38.1	63.16	0.1000	
250-2.0-A	250	50.8	58.84	0.0587	59.93
250-2.0-B	250	50.8	61.01	0.0702	

The configuration Test-BCF 2.0 was the weakest configuration and experienced the most brittle failure. It had an average rotation of 0.056 rad and an average fire resistance time of 55.6 minutes. By using a 38.1 mm washer, the wood cover is increased, which adds about 0.03 rad of rotation and 2.5 minutes of fire resistance time. The failure is still a sudden brittle failure but has more ductility than with the 50.8 mm washer. By using a 250 mm embedment length instead, the average rotation only increases by about 0.008 rad, but increases the average fire resistance time by 4.3 minutes. The failure still fails close to the same rotation as with the 200 mm embedment length, but the failure was gradual decrease in load over time and not a sudden break. By using both a smaller washer and longer embedment length the ductility increases greatly with an average rotation increase of greater than 0.045 and an increased average fire resistance time of 6.1 minutes.

The smaller washer size increases the wood cover and allows the steel components to be protected from the fire nine minutes longer as shown by the thermocouple data presented in section 5.2.3 of this thesis. The increase in rod embedment length did not show any differences in the thermocouple data as the fire burns the wood at a consistent rate and the rods stay at the same depth into the side of the beam for all configurations. The increase in embedment length increased the shear resistance

of the connection, which gave the connections a longer fire resistance time than the change in the washer size.

5.3 Conclusions

The following conclusions were drawn:

- The 250-mm embedment length connections exhibited a relatively ductile failure mode compared to that of the 200-mm embedment length, which failed mainly due to wood splitting in the fire tests.
- The increase in embedment length changed the failure mode from brittle to ductile but had the smallest increase in rotation capacity when compared to washer size.
- The increased embedment length did increase the fire resistance time more than washer size from an average of four minutes compared to two minutes for the washer size.
- The thermocouples data did show that the washer size has a great effect on the internal temperature of the cross section and protection of the steel components.
- Any fire exposed steel components would cause the beam-to-column connection to fail faster in fire; therefore, the protection from the wood section greatly helps in enhancing the fire resistance of the connection configurations utilized threaded steel rods that were mechanically fastened into the glulam beam sections compared to similar connection configurations with steel plates and fire-exposed bolts.

For a comparison of a simply supported beam with section size of 135 x 314 mm, the moment resistance is 70.5 kN.m and the design load for the connection was 10 kN.m giving the connection an efficiency of about 14%. After an hour of fire, the beam losses 42 mm on each side and the bottom giving a section size of 51 x 272 mm. A simply supported beam after one hour of standard fire exposure would have a moment resistance of about 20 kN.m which gives the connection an increased efficiency to about 50%.

Chapter 6 Conclusions and Recommendations for Future Work

In order to address the growing interest in using glulam and other mass timber products as the primary building material for tall buildings, a greater understanding needs to be acquired for the design of moment-resisting connections at both ambient and elevated temperatures. This thesis presents a new concealed moment-resisting timber connection that can have a more ductile failure than a traditional bolted connection. Previous fire tests conducted with the same glulam type and cross section size but with a slotted cut to accommodate T-stub steel connector and bolts forming wood-steel-wood concealed glulam beam connection subjected to similar design load achieved less than 30 minutes time to failure in standard fire condition (Petrycki and Salem, 2019). The new concealed timber beam connection developed in the study presented in this thesis shows the importance of completely protecting the steel components from fire and allowed the connection to achieve a fire resistance of one hour.

The embedment length of the steel rods and the washer size were the two variables that were examined for their impact on the failure modes and tension capacity of the tension connections, and the moment-resisting capacity of the glulam beam-to-column connections at both ambient and elevated temperatures. The experimental data gathered, and the analyses performed afterwards led to a number of relevant conclusions and recommendations that can be adopted to further enhance the design of mass timber moment-resisting connections.

6.1 Conclusions

6.1.1 Rod pull-out experimental testing

The experimental results and analyses presented in Chapter 3 of this thesis showed that a predictable formula can be achieved for a ductile failure of such connection. The formula shown in Equation 3.1 is highly plausible for pure rod pull-out failures, whereas the formula shown in Equation 3.4 is plausible for wood crushing failures, but more tests need to be performed to confirm their validity. Based on these results, the following conclusion have been made;

1. Keeping a rod embedment length versus a washer size ratio of around 4:1 or 5:1 provides a more predictable failure mode of rod pull-out and a more predictable failure load with the least amount of deviation;

2. Keeping the rod embedment length slightly larger compared to the washer size ratio would keep the failure mode closer to a wood crushing failure which is more consistent, predictable and therefore the next best standard deviation;
3. Having a larger washer size compared to embedment length ratio is not recommended because the failure mode will be closer to a wood splitting failure which is more brittle and unpredictable compared to a wood crushing failure;
4. With an understanding of how the wood section would fail, a connection can be designed so that its metal components would yield before the wood experiences any damage;
5. With the results presented in Chapter 3, the four best configurations could be selected for study as presented in Chapter 4.

6.1.2 Ambient temperature moment-resisting beam-to-column connections testing

The experimental results and analyses presented in Chapter 4 showed that the formulas in Equations 4.1 and 4.2 are plausible for calculating the moment resistance of the glulam beam-to-column connection. However, more tests need to be performed to calculate the bending factor that caused the connection to fail at slightly smaller moment values than that if the top rod was under uniform tension, instead of being subjected to combined tensile and bending forces. Based on these results the following conclusion have been made;

1. Depending on the desired failure, a connection configuration can be designed to promote a steel rod yielding failure which is stronger and predictable, or a wood crushing failure which can provide the connection with a high ductility ratio.
2. The steel rod embedment length affects the strength of the connection slightly negative due to the uneven pressure under the washer at greater lengths but increases the ductility ratio greatly when the failure mode was wood crushing under the washer.
3. The increase in washer size was the largest gain in the connection strength as it increases the area of wood to be crushed and increases the area of wood to resist shear rod pull-out failure.
4. The increase in washer size from 38.1 to 50.8 mm didn't show any ill effect due to the rotation of the connection, but from previous tension tests, as shown in Chapter 3 of this

thesis, a larger washer of 63.5 mm (2.5 inches) was observed to cause splitting in the wood underneath, and therefore should be avoided.

6.1.3 Elevated temperatures moment resisting beam-to-column connections testing

The experimental results and analyses presented in Chapter 5 of this thesis show that a mass timber moment-resisting connection can achieve a ductile failure with a fire resistance time of over one hour. Based on these results, the following conclusions have been drawn;

1. The 250-mm embedment length connections exhibited a relatively ductile failure mode compared to that of the 200-mm embedment length, which failed mainly due to wood splitting in standard fire condition. The increase in the rod embedment length changed the failure mode from brittle to ductile, but had the smallest increase in rotation capacity when compared to washer size;
2. The increased rod embedment length increased the connection fire resistance time more than washer size from an average of four minutes compared to the two minutes due to the increase of the washer size;
3. The thermocouples data showed that the washer size has a great effect on the internal temperature of the cross section and the steel components.

6.2 Recommendations for Future Work

Utilizing the experimental and analytical outcomes of the research study presented in this thesis, it is recommended that for the application of glulam moment-resisting connections, a smaller washer and longer rod embedment length be used to prevent or at least minimize the brittle failure modes. Keeping the failure as wood crushing provides a ductile connection with the most fire protection, while if the failure was rod pull-out then a weaker steel rod should be selected to ensure that the steel rod yields before the connection undergoes a brittle rod pull-out failure.

Future research work should be expanded to investigate the following variables;

1. Multiple glulam cross section sizes to confirm the predicted fire resistance times and possible increase to 1.5-hour fire resistance;

2. Different diameters of the steel rods to see if it affects the strength of the wood using smaller washers;

3. More variations of washer sizes and rod embedment lengths so the transitions from wood crushing to rod pull-out to wood splitting failure can be defined clearer;

4. Applying full design loads instead of the weakest connections design load to see how much the fire resistance time changes;

5. Carving the hole for the nut and washer all the way through the beam to ease fabrication using machinery and then plugging both sides to see if it affects the strength;

6. Utilizing the experimental outcomes of the research study presented in this thesis to validate finite element computer models to simulate the structural behaviour of such novel concealed glulam beam connections under the effect of additional parameters.

References

Andreolli, M., Piazza, M., Tomasi, R., & Zandonini, R. (2011). Ductile moment-resistant steel–timber connections. *Proceedings of the Institution of Civil Engineers-Structures and Buildings*, 164(2): 65-78.

Audebert, M., Dhima, D., Taazount, M., & Bouchaïr, A. (2012). Behavior of dowelled and bolted steel to-timber connections exposed to fire. *Engineering Structures*, 39: 116-125.

Barber, D. (2017). Determination of fire resistance ratings for glulam connectors within US high rise timber buildings. *Fire Safety Journal*, 91: 579-585.

Barillas, E. G. (2014). *Capacity of Connections in Glulam with Single and Multiple Glued in Steel Rods.* Masters thesis, UBC, Vancouver, BC, Canada.

Batchelar, M., & McIntosh, K. (1998). Structural Joints in Glulam. *5th World Conference on Timber Engineering, Montreux, Switzerland*, 1: 289-296.

Bisby, L., Gales, J., & Maluk, C. (2013). A contemporary review of large-scale non-standard structural fire testing. *Fire Science Reviews*, 2(1): 1-27.

Canadian Standards Association. (2013). *CSA G40.20-04/G40.21-13, General Requirements for Rolled or Welded Structural Quality Steel.* Rexdale, Ontario, Canada.

Canadian Standards Association. (2014). *CSA A23.3-14 Design of concrete structures* . Mississauga, ON, Canada.

Canadian Standards Association. (2014). *CSA O86-19, Engineering design in wood.* Mississauga, ON, Canada.

Canadian Standards Association. (2019). *CSA S16-19 Design of steel structures.* Mississauga, ON, Canada.

Canadian Wood Council. (2018). *Wood Design Manual 2017.* Canadian Wood Council, Ottawa, ON, Canada.

Closen, M., & Lam, F. (2012). *Performance of moment resisting self-tapping screw assembly under reverse cyclic load.* 12th World Conference on Timber Engineering, Auckland, New Zealand.

Di Maria, V., D'Andria, L., Muciaccia, G., & Ianakiev, A. (2017). Influence of elevated temperature on glued-in steel rods for timber elements. *Construction and Building Materials*, 147: 457-465.

Fragiacomo, M., & Batchelar, M. (2012). Timber Frame Moment Joints with Glued-In Steel Rods. I: Design. *Journal of Structural Engineering, ASCE*, 138(6): 789-801.

Fragiacomo, M., & Batchelar, M. (2012). Timber Frame Moment Joints with Glued-In Steel Rods. II: Experimental Investigation of Long-Term Performance. *Journal of Structural Engineering, ASCE*, 138(6): 802-811.

Gattesco, N., & Toffolo, I. (2004). Experimental study on multiple-bolt steel-to-timber tension joints. *Materials and structures*, 37(2): 129-138.

Gehloff, M., Closen, M., & Lam, F. (2010). *Reduced edge distances in bolted timber moment connections with perpendicular to grain reinforcements.* 11th World Conference on Timber Engineering, Riva Del Garda, Trento, Italy.

Hadjisophocleous, G. V., & Benichou, N. (1999). Performance criteria used in fire safety design. *Automation In Construction*, 8(4): 489-501.

Humbert, J., Lee, S., Park, J., & Park, M. (2014). *Moment resistance of post-and-beam joints with concealed metallic connectors.* In Proceedings of the 13th World Conference on Timber Engineering, WCTE2014, Quebec, Canada.

Hunger, F., Stepinac, M., Rajčić, V., & Kuilen, J. (2016). Pull-compression tests on glued-in metric thread rods parallel to grain in glulam and laminated veneer lumber of different timber species. *European Journal of Wood and Wood Products*, 74(3): 379-391.

Metten, A. W. (2012). *Structural Steel for Canadian Buildings: A Designer's Guide.* Structured Solutions Inc., Vancouver, BC, Canada.

Muciaccia, G. (2017). An experimental approach to determine pull-out strength of single and multiple axially loaded steel rods bonded in glulam parallel to the grain. *Wood Material Science & Engineering*, 14(2): 88-98.

Muñoz, W., Salenikovich, A., Mohammad, M., & Quenneville, P. (2008). Determination of Yield Point and Ductility of Timber. *Materials Science*.

Murty, B., Asiz, A., & Smith, I. (2008). Wood and engineered wood product connections using small steel tube fasteners: An experimental study. *Journal of the Institute of Wood Science*, 18(2), 59-67.

National Research Council of Canada. (2015). *National Building Code of Canada, 14th ed.* National Research Council of Canada, Ottawa, ON, Canada.

Nordic Wood Structures. (2015, March 11). *Design Properties, Nordic Lam: Technical Note S01.* Retrieved from Nordic Structures: http://nordic.ca/data/files/datasheet/file/T-S01_ePropertiesNordicLam.pdf

Nordic Wood Structures. (2015, June 29). *Non-Residential Design Construction Guide: N-C122.* Retrieved from Nordic Structures: http://nordic.ca/data/files/datasheet/file/N-C122NordicLamnon-res.June2015.pdf

Oh, J. (2016). *Timber Moment Connections Using Glued-in Steel Rods.* Masters thesis. UBC, Vancouver, BC, Canada.

Peng, L., Hadjisophocleous, G., Mehaffey, J., & Mohammad, M. (2010). Fire resistance performance of unprotected wood–wood–wood and wood–steel–wood connections: A literature review and new data correlations. *Fire Safety Journal*, 45(6): 392-399.

Petrycki, A., & Salem, O. (2019). Structural fire performance of wood-steel-wood bolted connections with and without perpendicular-to-wood grain reinforcement. *Journal of Structural Fire Engineering*, Emerald Publishing, UK. https://doi.org/10.1108/JSFE-02-2019-0016.

Petrycki, A., & Salem, O. (2020). Structural integrity of bolted glulam frame connections reinforced with self-tapping screws in a column removal scenario. *Journal of Structural*

Engineering, 146(10), ASCE, USA. http://doi.org/10.1061/(ASCE)ST.1943-541X.0002792.

Racher, P., Laplanche, K., Dhima, D., & Bouchaïr, A. (2010). Thermo-mechanical analysis of the fire performance of dowelled timber connection. *Engineering Structures*, 32(4): 1148-1157.

Ramage, M. H., Burridge, H., Busse-Wicher, M., Fereday, G., Reynolds, T., Shah, D. U., Scherman, O. (2017). The wood from the trees: The use of timber in construction. *Renewable and Sustainable Energy Reviews*, 68(1): 333-359.

Samaké, A., Taazount, M., Audebert, P., & Palmili, P. (2014). Thermo-hydric transfer within timber connections under fire exposure: Experimental and numerical investigations. *Applied Thermal Engineering*, 63(1):254-265.

Steiger, R., Gehri, E., & Widmann, R. (2006). Pull-out strength of axially loaded steel rods bonded in glulam parallel to the grain. *Materials and Structures*, 40(1): 69-78.

Tomasi, R., Zandonini, R., Piazza, M., & Andreolli, M. (2008). Ductile End Connections for Glulam Beams. *Structural Engineering International: Journal of the International Association for Bridge and Structural Engineering, IABSE*, 18(3): 290-296.

Wang, M., Song, X., Gu, X., Zhang, Y., & Luo, L. (2015). Rotational behavior of bolted beam-to-column sections with locally cross-laminated glulam. *Journal of Structural Engineering*, 141(4).

Xiong, H., & Liu, Y. (2014). Experimental study of the lateral resistance of bolted Glulam Timber Post and Beam Structural systems. *Journal of Structural Engineering*, 142(4).

Xu, B. H., Bouchaïr, A., & Racher, P. (2015). Mechanical behavior and modeling of dowelled steel-to-timber moment-resisting connections. *Journal of Structural Engineering*, 141(6).